Attaching mechanisms and strategies inspired by the spiders' leg

Final Report

Authors: Alessandro Gasparetto, Renato Vidoni with the cooperation of Vanni Zanotto and Eugenio Brusa
Affiliation: Department of Electrical, Mechanical and Management Engineering of the University of Udine (Italy)

ESA Researcher: Tobias Seidl

Date: January 2008

Contacts:
Alessandro Gasparetto
Tel: +39 0432 558257
Fax: +39 0432 558251
e-mail: gasparetto@uniud.it

Renato Vidoni
Tel: +39 0432 558281
Fax: +39 0432 558251
e-mail: renato.vidoni@uniud.it

Tobias Seidl
Tel: +31(0)715653872
Fax: +31(0)715658018
e-mail: act@esa.int, tobias.seidl@esa.int

Available on the ACT website
http://www.esa.int/act

Ariadna ID: 06/6201
Study Duration: 6 months
Contract Number: 20272/07/NL/HE

Contents

1 Introduction

The task of finding innovative concepts of spider-inspired attaching mechanisms, as well as suitable locomotion strategies for engineering devices, will be tackled in this research.
The spiders' ability of walking and climbing on different surfaces and in different conditions of slope will be very useful if mimicked with the purpose to create robotic prototypes that can explore extra-terrestrial surfaces.

The remarkable progress in manufacturing automation and robotics in the second half of the 20'th century allowed replacement of humans in dangerous, inaccessible working environments.
With the progresses in nanotechnology and microrobotics appeared the possibility of creating autonomous miniature structures used for a wide range of tasks which could not be realized prior, like the use of robots in securing land-mined areas, inspection of large mechanical structures that present hazard (e.g. electric poles), exploration of narrow and inaccessible environments like underwater structures, industrial pipes or outer-space exploration.
Exploration in these non-structured environments required robots along with low mass, high motion capabilities, climbing abilities and embedded decision elements. The autonomous working capacity, without any linkage to a mother-structure, and a very low energy consumption, are two of the most important requirements to satisfy in order to develop such a devices.
Different types of locomotion have been attempted in order to allow all-surface locomotion, but some of the methods, like air-suction and electromagnets, presented the disadvantage of very limited autonomy because of the power supplies needed in order to work, along with the limitations introduced by the surfaces that these mechanical structures were able to run over and by the lacking of atmosphere. So, the attention turned to biological creatures that were able to climb fast and run over various types of surfaces in unstructured environments and in different weather conditions.
Replicating these creatures, like spiders, lizards (especially gecko lizards) or insects was no easy task because the manufacturing procedures were not available. Moreover the locomotion techniques used were not fully understood and advanced researches needed undergone using modern measuring and observation equipments. The techniques used by the insects, spiders and reptiles include the use of claws to grasp on the asperities of the surface, the use of wet adhesives, in the case of some flying insects, the use of dry adhesives in the case of the gecko lizard, or the mixed use of claws and dry adhesives, like in the case of the spiders. The first one method, the claws, is used by the animal for interlocking with the asperities of the surface. The second one, the adhesion forces, appears between the environment and the hairs present on the limbs of the insects. For the further development of wall climbing robots the spider locomotion modalities are of most interest, given the actual manufacturing and research possibilities, so the locomotion of these creatures will be subject of study.

2 Overview of the project

Development in 4 phases:

1. **Survey on attaching mechanisms and on locomotion strategies in spiders and engineering prototypes.**
2. **Engineering specifications and requirements for the design of an artificial mechanism mimicking the spiders behaviour.**
3. **Mechanical/Elastic model of the adhesion system of the spider**
4. **Kinematic model of the spider system**

3 Phase 1: Survey

Survey on attaching mechanisms and on locomotion strategies in spiders and engineering prototypes

3.1 The spider characteristics and behavior (biological aspect)

3.1.1 Spider anatomy

Most insects have three body parts. Spiders and other arachnids have only two major body parts, as shown in Fig. 1. The anterior part is called the cephalothorax or prosoma, and the posterior part is called abdomen, or opisthosoma.
Spiders have eight legs attached to the cephalothorax and each pair of legs is numbered I, II, III and IV from anterior to posterior. Each leg is composed out of seven segments: coxa or basal segment, the trochanter, femur, patella, tibia, metatarsus and tarsus (Fig. 1).
In some spider families the tarsus ends in two claws, in others it ends in three claws, depending on the adaptation to the environment and hunting technique.
The front appendages are called pedipalps and have only six segments: coxa, trochanter, femur, patella, tibia and tarsus.
Different types of hairs (setae) and spines (macrosetae) are present on the legs. Also, long hairs are present called trichobothria and these hairs are used as sensory units and they originate in sockets with multiple nerve endings. These hairs are extremely sensitive to air currents and to vibrations, compensating for the extremely poor eye sight of some spiders thus helping them hunt. Different types of hairs and bristles are found on the legs, depending on the different taxa, as adaptation to the environment and climbing or hunting techniques.
For example, the spiders in the family *Theridiidae* are called "comb-footed spiders" because of the appearance of the bristles that they have on the ventral side of the tarsus (Fig. 2).
The spider's body does not have veins or arteries to conduct the blood, a liquid called haemolymph runs through the open spaces in the body.
The spider does not use muscles to pull tendons and actuate the legs, instead the prosoma pumps pressurized fluid into chambers into the joints of the legs, and these chambers expand causing the angle between the two leg segments to modify, though having the same effect that a tendon being pulled would have. Studying the way that spiders use their legs to move forward it is possible to say that the 2 anterior legs are used to pull in towards the body while climbing, 2 pairs of lateral legs who travel upwards and then pull in and laterally while climbing and the last pair is placed at the rear and used for climbing balance and pushing. These considerations are only true for spiders capable to climb.
Because of the variety of environments where spiders live (on the water and under the water, caves, trees, on the ground) there is a very large number of spider species with very different adaptations to the environment.
In this paper the spiders capable of walking inclined and climb are taken into consideration.
With these different adaptations arthropods walk over demanding terrain much more effectively than any existing autonomous robot. Spiders use distributed neu-

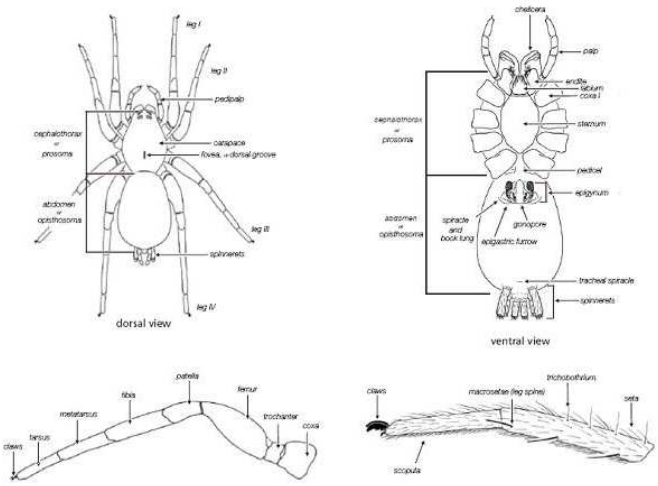

Figure 1: Spider Anatomy

Figure 2: Spider bristles

ral feedback for precise stepping in order to deal with unstructured environments [1].

3.2 Research on attaching mechanisms and experimental evidences

3.2.1 Introduction

In order to be able to climb various surfaces the spiders use two types of different attaching mechanisms: the claws and the hairs.

As regards as the claws such a mechanisms are used for two major operations:

- locomotion, used during climbing rough hard surfaces (stone) or soft surfaces (tree bark, leaves)
- web building, used to spin the silk threads or walk on the already built web.

Web building spiders have three claws and use the claw in the middle to grasp the silk threads.
Jumping spiders and generally spiders that do not use webs to capture the prey do not need specialized claws to spin the silk threads.

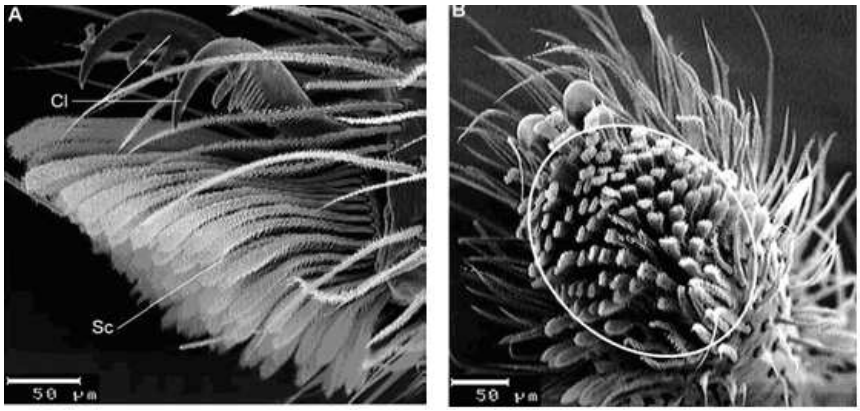

Figure 3: SEM micrograph of the tarsus of *E. arcuata* from Kesel et al.[3, 4]. (A) Lateral view of the tarsal adhesive structures of *E. arcuata*, showing : claws (Cl) and the scopula (Sc). (B) Ventral view of the scopula; the differentiation into single setae is clearly visible. The plotted oval is used to estimate the scopula area.

Therefore there are spiders that do not have claws at the termination of the tarsus for the reason mentioned above and because there are spiders who lack the climbing abilities or, for the small spiders (body dimensions around 1-2 mm) the attachment is realized via dry adhesives and leg spines directly.

Considering the micro-nano hairs on the spider limbs, they allow the spider to attach to a lot of different kind of surfaces thanks to the intermolecular attraction forces between the spider's hairs and the climbing surface (tree bark, rock, stucco, metal, glass or plastics); no matter if the surface is wet or with irregularities.
As a consequence matching these two different attaching mechanisms, such amazing animals are able to cling to almost all the surfaces.

How spiders and gecko lizards attach and detach from smooth, vertical surfaces or walk on ceiling are one of the most fascinating topics of the bio-mimesis.
In order to go deep into such an argument the hierarchy and the characteristics of the attaching devices have to be described.
The evidence of the molecular adhesion forces, also known as Van der Waals forces are presented onwards for some particular species of arachnids and lizards.

3.2.2 Tarsal structure and hierarchy of the attaching elements

In nature there are a lot of different species and in [3, 4] the jumping spider *E. arcuata* has been studied and observed.
Like in other spiders, as presented in Fig. 3, the tarsus of the *E. arcuata* is both covered with hierarchic setal structures used for adhesion on any type of surfaces, and provided with two claws for rough surfaces.
The claws are used because, as shown in [5], the dry adhesives fail to generate enough attachment force if the surface has pronounced irregularities. Using Atomic Force Microscopy on specimens of *E. arcuata* it has been determined that all the eight feet are covered by a tarsal scopula equipped with setae.
The setae present on *E. arcuata* are ramified structures, this type of structure is

also known as a hierarchical structure. The ramifications or terminal branches are called setulae, each of these setulae has a flattened tip called spatula in order to maximize the contact area to the substrate.
It has been determined for *E. arcuata* an estimated 624.000 setulae achieving a mean contact area of around $1.7 \cdot 10^5 nm^2$ [3, 4], thus making a total contact area of approximately $1.06 \cdot 10^{11} nm^2$.
From the AFM analysis it results that a single setula creates an attachment force of $38.12nN$, leading to a total adhesive force of $2.38 \cdot 10^{-2} N$.
Considering that this type of spiders have a mean body mass of 15.1 mg, the spider *E. arcuata* can produce an adhesion force to sustain 160 times its body weight.
Such a safety factor is more than reassuring and considering the fact that these hair structures are also self-cleaning, the spider can be able to climb the substrates in any condition and in safety.
It has to be said that the safety factor mentioned is achieved by the spider while staying with all feet attached. Even though the spider will not have all the feet attached at the same time the resulting safety factor will be more than enough to provide full support and climb reliability.

3.2.3 Experimental evidence. Results: Scanning Electron Microscopy

Thanks to the Scanning Electron Microscopy (SEM) the hierarchical structure of the spider attaching mechanisms can be shown and studied. Images taken via electron microscopy are presented in Fig. 3, 4, 5. Using SEM measurements on *E. arcuata* no other attachment structures were found. In addition to the claws, a tuft-like scopula was found ventrally placed in respect to the claws, representing the dry adhesive structures. The term "dry adhesive" refers to the fact that adhesion is generated without the secretion of any liquid, as in the adhesive mechanisms used by other insects.
Before dry adhesion could be experimentally proved, scientists formulated different theories in order to explain the adhesion of the spiders and lizards. Common for these theories was that lizards and spiders produce a liquid to help adhesion via capillarity. Images of hair structures present on *E. arcuata* obtained via SEM are presented in Fig. 4, 5. From these figures it is possible to understand that the end of the setula is flattened and forms a "sail-like structure". The area of such a structure is about $1.7 \cdot 10^5 nm^2$ and the mean setulae density becomes $2.1 setulae/\mu m^2$. Considering that each scopula has an estimated area of $0.037 mm^2$ the number of contacts of a single foot becomes of 78000 setulae $((0.037 mm^2) \cdot (2.1 \cdot 10^6 setulae/\mu m^2))$.
The same *E. arcuata* tarsus structure can be found in a lot of spider species. Niederegger and Gorb in [6] studied two different species of spiders: the bird spider *Apholopelma seemanni* $(17.9 \pm 3.0g)$ and the hunting spider *Cupiennius salei* $(3.3 \pm 1.0g)$. Both these species are able to climb a lot of surfaces included the smooth glass surfaces. The first one cannot adhere to smooth glass surfaces inclined over 90° whereas the second one can walk on ceilings.
Both these species have an attaching mechanism structure similar to the *E. arcuata*. Fig. 6 and 7 show in detail the hierarchical structure of the tarsus and pretarsus of these spiders. Looking at the dimensions of the attaching elements, the setulae are $2 - 4\mu m$ long and $0.1 - 0.3\mu m$ wide. The spatulae of the bird spider are about $0.013 \pm 0.02 \mu m^2$ while the ones of the hunting spider are about $0.30 \pm 0.05 \mu m^2$. The lowest level elements (setae) are long several hundred of micrometers. In Fig. 8 are shown the tarsal magnifications of further different spiders in order to underline the typical hierarchical structure of the attaching mechanisms.
In Table.1 are expounded the main data of the three considered spiders.

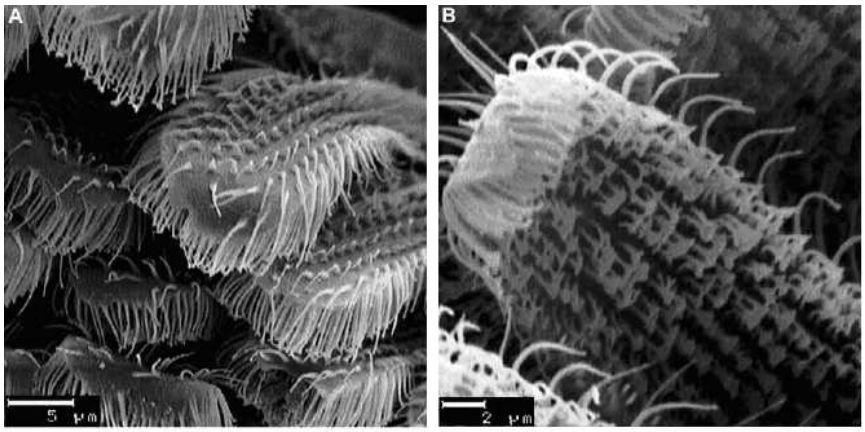

Figure 4: Hierarchical structure of spider dry adhesives attaching mechanisms performed with SEM from Kesel et al. [3, 4]. (A) Each seta is covered by numerous setulae, which are tapered on the seta's dorsal side. (B) On the seta's ventral side, the setulae density is noticeably higher. Here, setulae are broadened towards their ends, forming a sail-like shape.

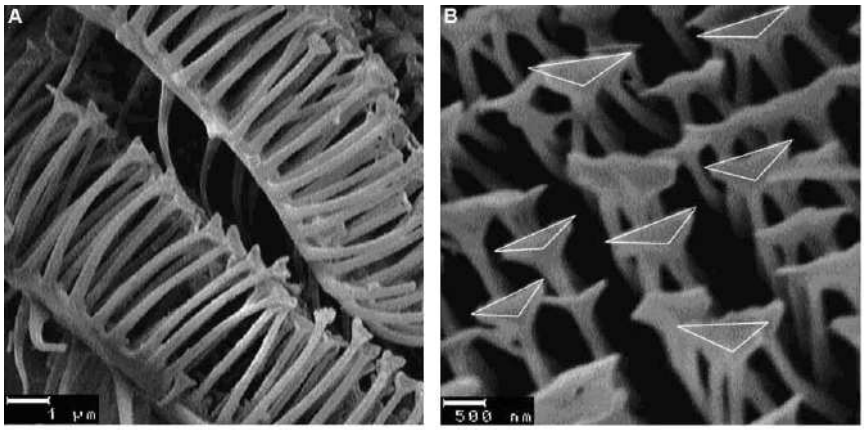

Figure 5: Hierarchical structure of spider dry adhesives attaching mechanisms performed with SEM from Kesel et al. [3, 4]. (A) The terminal setulae broadening represents the contact point between the spider and the substrate. (B) A setulae density of $1.5 \cdot setulae \cdot m^{-2}$ can be calculated from the above figure.

Spider	Spatulae like end	Setulae	Setae	Weight
E. arcuata	$0.17 \pm 0.034 \mu m^2$	$2.1 \pm 1.0 set./\mu m^2$	100-300 μm (l) 25-35 μm (w)	15.1 mg
C. salei	$0.13 \pm 0.02 \mu m^2$	$2 - 4 \mu m$ (l) $0.1 - 0.3 \mu m$(w)	n·100 μm(l)	3.3 ± 1.0g
A. seemanni	$0.30 \pm 0.05 \mu m^2$	$2 - 4 \mu m$ (l) $0.1 - 0.3 \mu m$ (w)	n·100 μm(l)	17.9 ± 3.0g

Table 1: Main dimensions and data of the three considered spiders (l= long, w = wide).

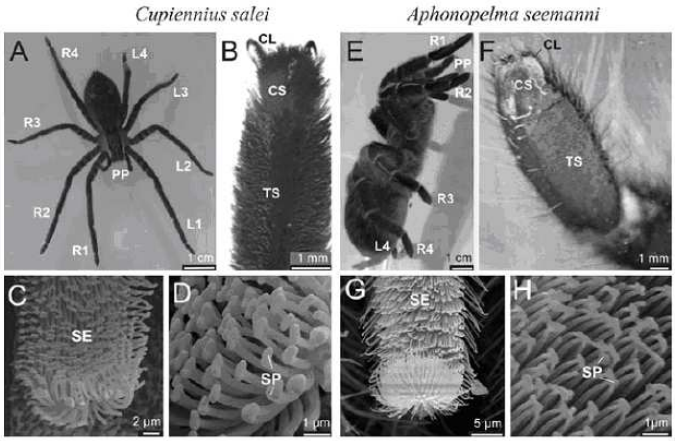

Figure 6: Spider species studied in Niederegger and Gorb [6]: (A-D) *C. salei*; (E-H) *A. seemanni*. (A, E) Spiders resting on a tilted glass plate. (B, F) Claws, pretarsal scopula (claw scopula), and tarsal scopula in contact with the glass surface viewed in a binocular microscope. (C, G) Tip of a single seta, SEM. (D, H) Microtrichia with spatulae at their tips, SEM. CL claws, CS claw scopula, L1-L4 left legs from the front to back, PP pedipalps, R1-R4 right legs from the front to back, SE seta, SP spatulae, TS tarsal scopula.

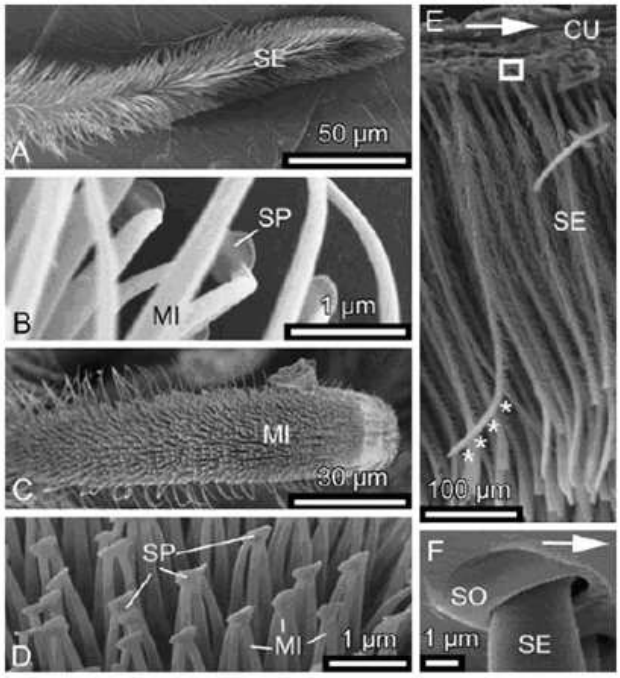

Figure 7: Setae of *A. seemanni* from Niederegger and Gorb [6]. (A) Seta attached to the glass surface by its distal side, cryo SEM. (B) Spatulae in contact with the glass surface, cryo-SEM. (C,D) Ventral view of the seta after being frozen in contact with the glass cover slip (some spatulae are stuck together), cryo-SEM. (E) Orientation of the setae within the tarsal scopula, SEM. (F) Socket of a seta, SEM. Arrows indicate distal direction; asterisks indicate distal surface of the seta covered with spatula-bearing microtrichia. CU cuticula, MI microtrichia, SE seta, SO socket.

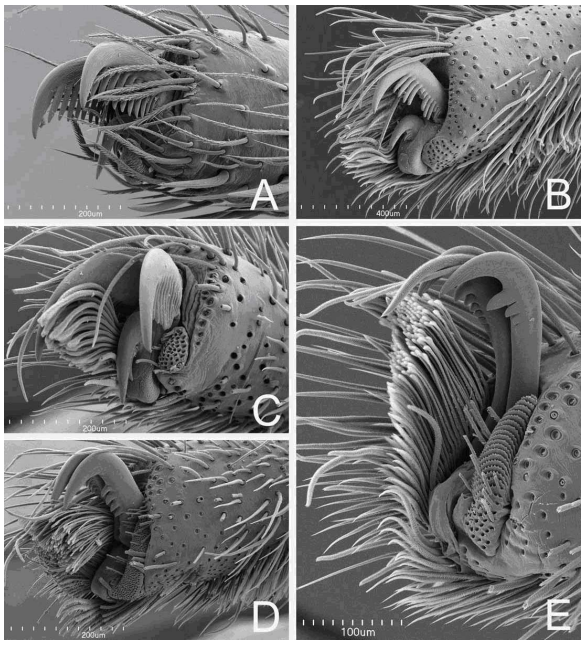

Figure 8: From [7] Female left tarsi I. Hairs of scopula or claw tuft on near side have been removed from B-E. (A) *Nicodemus mainae* from Coalseam Park, Western Australia, Australia. (B) *Tengella radiata* from Guanacaste, Costa Rica. (C) *Psechrus argentatus* from Cape Vogel Peninsula, Papua New Guinea. (D) *Zoropsis rufipes* from Tenerife, Canary Islands. (E) *Acanthoctenus* cf. *spinipes* from Loreto, Peru. Scale bars: A, C, D = 200m, B = 400 μm, E = 100μm.

3.2.4 Experimental evidence. Results: Atomic Force Measurement

In order to determine adhesion forces and to visualize the micro-adhesive structures of the species *E. arcuata* a number of specimens were collected and Scanning Electron Microscopy along with Atomic Force Microscopy measurements were executed by A. B. Kesel et al. [3, 4]
As regards as the Atomic Force Microscopy technique, a force measurement device is used in order to measure the adhesive force of setular structures. This procedure is highly appropriate for the measurement of van der Waals forces.
The measurements must be executed soon after the capture of the spiders, avoiding deterioration of the setular structures or the modification of their physical characteristics.
For the measurements, a cantilever beam was brought into contact with the setular structures, pressed to make contact and after that the setular structures were slowly retracted. During the retraction the cantilever beam of the AFM deformed until detachment. Knowing the elasticity of the beam and measuring its deflection using a laser, the forces that produce the deformation can be calculated.
In this particular case, the forces producing the deformation of the beam can be interpreted as the Van der Waals forces that appear between the setular structures and the flat surface of the AFM cantilever beam.
The experimental results are plotted eloquently into Fig. 9. The value measured at contact break-off represents the adhesive force thus, the mean adhesion resulted 38.12 nN per setula.
Considering an estimation of 78·000 setulae per scopula, a foot can produce a force

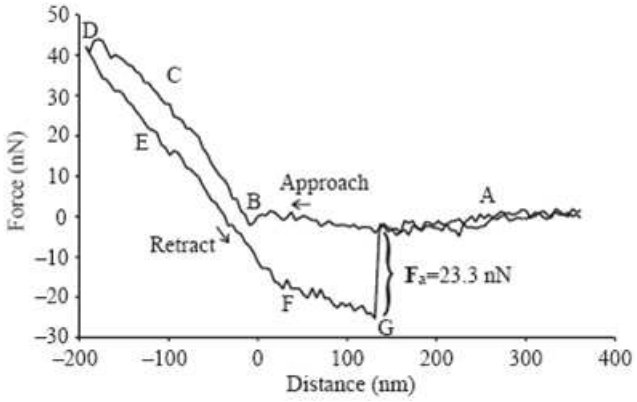

Figure 9: Registration of a force-distance curve recorded on a single setula from Kesel et al. [3, 4]. Reference points are: (A) Probe not in contact with sample. (B) Contact between probe and sample is established. (C) The sample is indented by the probe with a defined force. (D) Turning point (F=maximum), retraction begins. (E) During retraction, the force between the probe and the sample decreases. (F) Due to adhesive forces, the probe remains in contact with the sample during retraction. (G) Contact abruptly breaks off ('pull-off' event).

of $2.97 \cdot 10^{-3}$N. For all eight feet attached, a force of $2.38 \cdot 10^{-2}$N and a tenacity of $2.24 \cdot 10^{5}\text{N}/m^2$ result from the calculations, enough to sustain, as previously cited, 160 times the spider's weight. Measuring the tenacity not normally but parallel to the adhesion surface, due to the friction forces, the tenacity has significantly higher values. Looking at other biological systems it is demonstrated that the adhesion

Material	Force of adhesion (mean [nN])	N
Glass	1315.50	20
Epoxide	443.72	19
Setulae	38.12	45

Table 2: Adhesive forces taken from force-distance curves

increases when not only a normal load but also a parallel load is applied [8, **?**]. Niederegger and Gorb in [**?**, 9] gave an experimental evidence of such an adhesive phenomenon measuring the friction and adhesion forces under different approaching loads and movements.
They measured a very low adhesive force when the final leg segments of *A. seemanni* and *C.salei* were loaded perpendicularly to a glass surface and retracted back without other movements but, during pulling (proximally oscillation) and pushing (distally oscillation) they recorded different behaviors.
The friction force remained quite unchanged with respect to the initial loading value during pulling. In pushing it strongly rose (Fig. 10). Considering the Fig. 10(D) the correlation between the friction force and the normal force is demonstrated. Due to the asymmetric characteristics of the spider's setae, the recorded friction force in pushing and pulling are considerably different (Fig. 10(C,D)).
As a final consideration it is possible to suppose that also in spiders, in order to establish an intimate contact between the attaching elements and the surface, not only a normal preload but also a parallel sliding movement is necessary.

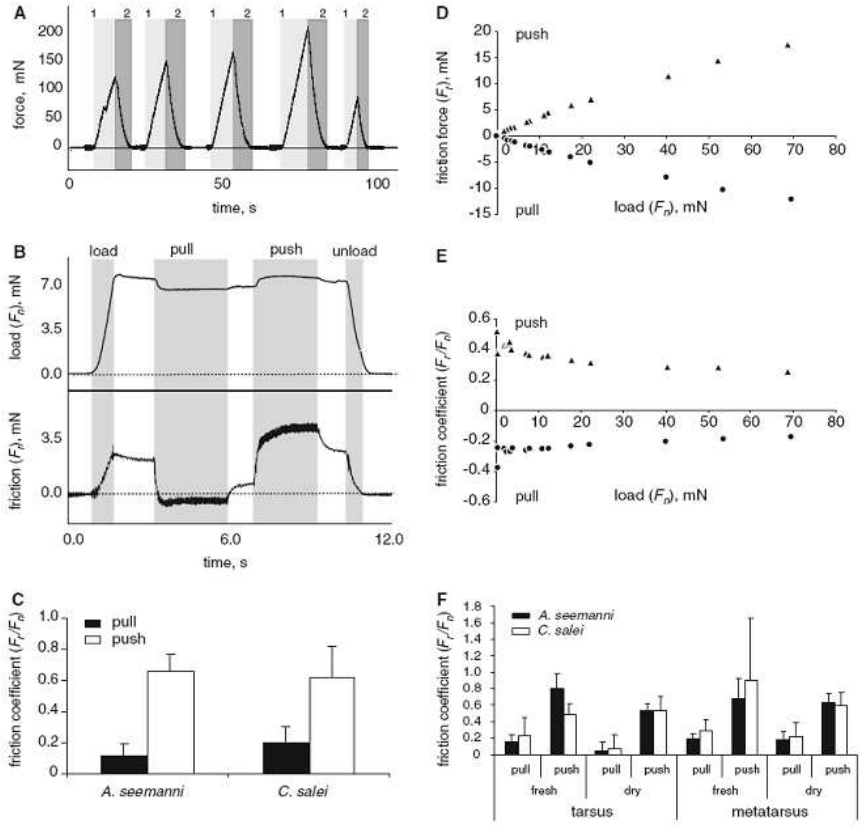

Figure 10: Force measurements from [**?**]. (A) *C. salei*, fresh tarsus, typical recording of adhesive force. The leg was pressed against the glass surface (loading process, 1-light grey area) and retracted (unloading process, 2-dark grey area). (B) *C. salei*, fresh tarsus, typical friction force recording. The leg was loaded against the glass surface (load), pulled (pull), pushed (push), and retracted from the surface (unload). (C) Comparison of the friction coefficient during pushing and pulling in both species. (D) *C. salei*, fresh tarsus, friction force versus normal load during leg pushing and pulling. (E) *C. salei*, fresh tarsus, friction coefficient during leg pushing and pulling. (F) Comparison of friction coefficients at pulling and pushing in fresh and dry tarsi and metatarsi in both species.

3.2.5 Climbing mechanisms used by gecko lizards

The spiders are not the only creatures that use the principles of the dry adhesion for locomotion in their natural environments. Some lizards, like the gecko, use similar or more complicated structures.
Research on these attaching mechanisms represents a step forward towards developing autonomous climbing robots. The gecko uses ramified adhesive structures like the ones present on the spiders. The complicate nature of the adhesive structure used by the gecko refers to the macro-configuration of the feet.
The principles of attachment and detachment are somewhat similar and they will be presented and evaluated in detail further in the paper.
One of the most amazing and studied geckos is the *Tokay Gecko (Gecko Gecko)* attaining lengths of approximately 0.3-0.4 m and 0.2-0.3 m for males and females, respectively, which can walk and climb on a variety of surfaces.

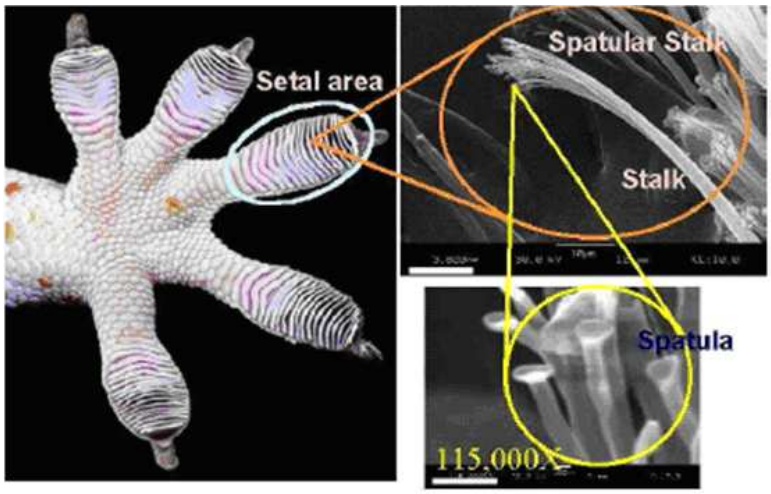

Figure 11: *Tokay gecko* foot-hair images from Sitti and Fearing [10]: gecko foot bottom view (left image); zooming into one of the stalks (right upper image, bar indicates 10micron), and zooming into spatulae and spatular stalks at the end of a stalk under SEM (right lower image, bar indicates 300nm).

In a Gecko toe pad can be identified a complex fibrillar structure constituted of: the lamellae (scansors), the setal branches that have multiple split ends and a final spatular nanostructure.
Referring to the *Tokay Gecko* (weight from 50-300g), as presented in Fig. 11, 12, 13, [8, 10, 11, 12], the first level is constituted of the lamellae, soft ridges that are 1-2 mm in length located on the attachment pads (toes). As final extension of these lamellae there are the setae: curved hairs that in theirs ends split in multiple spatulae elements whose terminal-end is a thin, triangular element.
All the setae are oriented and distributed in a similar manner on the scansors. A single setae of the *Tokay Gecko* is 5-10μm in diameter and 30-130μm in length [13]. Each seta splits at its tip into 100-1000 spatulae elements with a diameter of 0.1-0.2μm. Each spatula can be described as a stalk of 2-5μm in length and 0.1-0.2μm in width with a thin, roughly triangular end (0.2-0.3μm width, 0.5μm in length and 0.01μm in thickness [14, 15]).
In nature there are a lot of species of geckos with different morphological variations at the different levels of the attaching devices but most of the results and of the studies are been done on the *Tokay Gecko*.
For the adhesive structures of the gecko, the adhesion force achieved can be as high as 10N per square centimeter of adhesive structure. Indeed Autumn and Peattie [14] discovered that the two front feet of the gecko can produce 20.1N of force parallel to the surface with a pad area of $2.27mm^2$. Considering that there are about 3600 tetrads of setae/mm^2 a single seta can be an average force of 6.2μN.
As regards as the approach and the dynamics of the attach it is demonstrated that the adhesion occurs only along the axis of the toe and that the angle of the setal shaft is important in the adhesion. In particular a small normal preload force yields a shear force of 40μN and, combining this force with a parallel displacement (pulling) of 5μm the shear force can become 200μN.
The adhesive area of the gecko is much larger that the one of the spider especially because of the large weight of the gecko. Images of the gecko's feet are shown in Fig. 11, 12, 13.

In Table 3 are related the experimental adhesion measures of different works. The

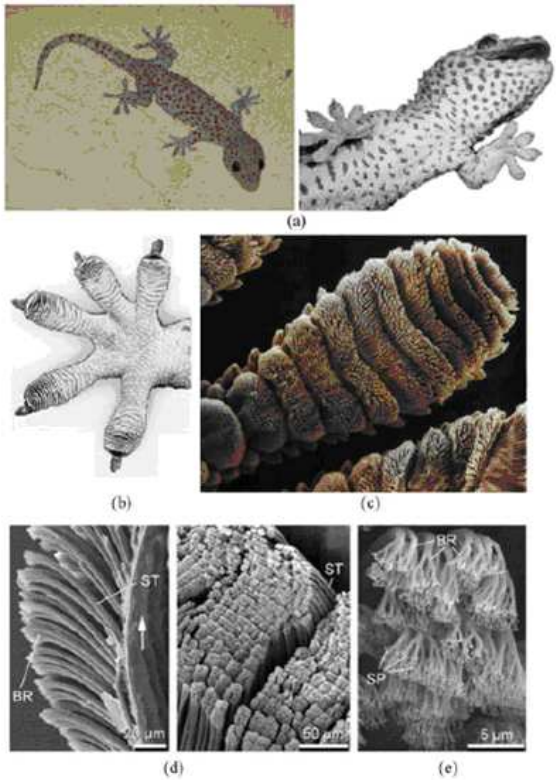

Figure 12: Photographs of a *Tokay gecko*. (a) The hierarchical structures of a gecko foot; photographs of (b) a gecko foot and (c) a gecko toe. Each toe contains hundreds of thousands of seta and each seta contains hundreds of spatulae. (d) SEM micrographs of the seta and (e) spatulae, ST: seta; SP: spatulae; BR: branch.

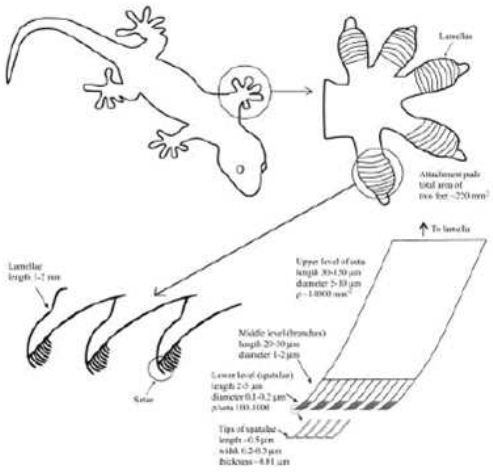

Figure 13: Schematic drawings of a *Tokay gecko*. The overall body, one foot, a cross-sectional view of the lamellae, and an individual seta.

Scale	Mode	Area	Force
Single Spatula [16]	Adhesion	0.02 μm^2	10 nN
Single Seta [8]	Adhesion	43.6 μm^2	20 μN
Single Seta [14]	Adhesion	43.6 μm^2	40 μN
Setal Seta [8]	Friction	43.6 μm^2	200μN
Single Array [17]	Friction	0.99 mm^2	0.37 N
Single Toe [17]	Friction	0.19 cm^2	4.3 N
Single Foot [14]	Friction	0.22 cm^2	20.4 N

Table 3: Experimental measured forces of geckos' attaching elements.

geckos' mechanism of adhesion and the theoretical and experimental evaluation of the strength of adhesion are treated in [5, 8, 13, 15, 18].
Thanks to the dimensions and to the quite simple kinematics of the gecko lizards recently there is a great interest among the scientific community to understand and reproduce the climbing abilities of the gecko feet in order to apply such results in new materials and elements integrated in robot prototypes.

3.2.6 Attachment devices

Attachment systems in spiders, lizards and insects have similar structures.
These microstructures are depicted in Fig. 14 presented by Arzt et al. [15]. From this picture it is possible to understand how as the size (mass) of the creature increases, as the radius of the terminal attachment elements decreases. As a consequence, the density of the last level of attachment elements increases with the mass of the body. In Fig. 15 it is possible to see that geckos have the highest

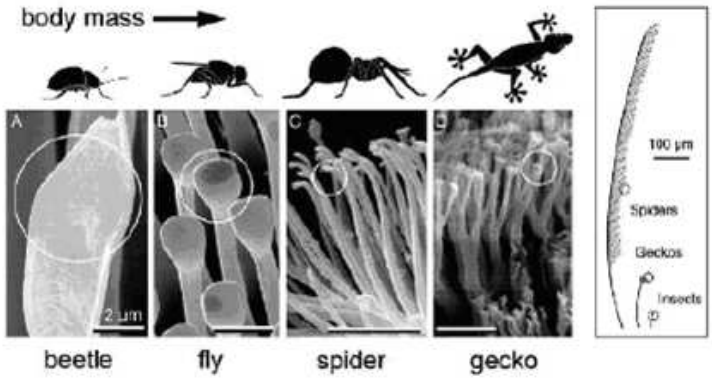

Figure 14: Body mass vs dimension of the terminal attaching elements from Artz et al. [15].

body mass and the greatest density of terminal elements whereas spiders, flies and beetles have a lower density of terminal attachment and larger attachment pads. As regards as the three species previously considered (Tab.1) some considerations have to be made. Both the *A. seemanni* and *C. salei*, a bird spider and a hunting spider respectively, fit the mass-contacts curve.
The *E. arcuata*, a jumping spider, does not fit the curve and its body mass is

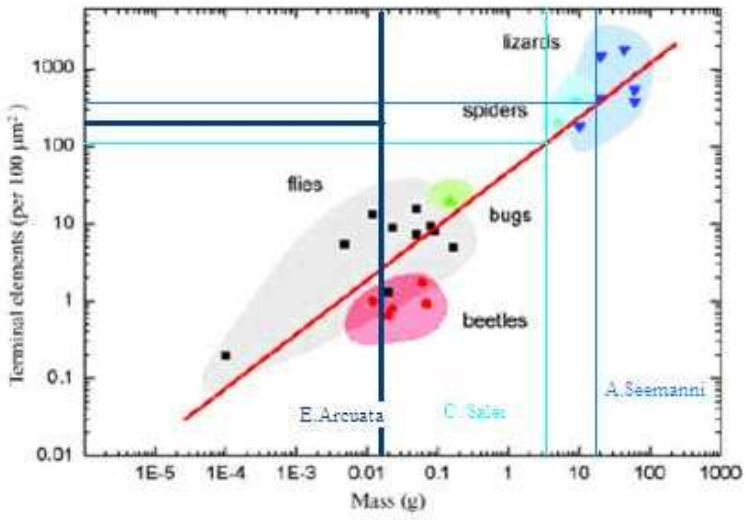

Figure 15: Review of the mass vs density of the final elements (Na) and master curve diagram: (log(Na) = 13.8 + 0.699log(m), R = 0.919 = correlation coeff. (Artz et al. [15]))

largely smaller with respect to the one showed in the curve. Being the number of contacts inner the range of the other spiders it is supposable the the nature has adapted this spider in order to allow to better survive. Indeed the jumping condition between different surfaces asks for an optimal adhesion and a possible solution is the augmentation of the safety factor. Such an increase can be developed in different ways: reducing the radius of the terminal elements preserving the mass or reducing the mass preserving the dimension of the contacts. It seems that the *E. arcuata* chose the second way.
Moreover the position of the setulae between the *E. arcuata* and the other two species is different. In *E. arcuata* the scopula is in the tip of the tarsus while in the other two spiders it is over the entire tarsus. Such a condition is probably related to the different natural behaviors: *E. arcuata* is a jumping spider and then needs different and suitable adaptations.

An experimental evidence of the adhesion enhancement due to the increasing of the density of the surface contact points, i.e. due to the division of the contact area is given, starting from these results and from the JKR theory, by Peressadko and Gorb in [19].
They measured the adhesion on a glass surface both of smooth samples and a structured sample (Fig. 16) obtained by "moulding of the template with a two-compound polymer polyvinylsiloxane (PVS)". The material properties of the PVS can be summarized as: E = 2.5 - 3MPa, highly hydrophobic material and surface energy $\gamma = 16.1 mJ/m^2$. Two series of experiments were made: in the first adhesion of both samples was measured during unloading after that the sample had been brought in contact with the flat glass surface; in the second series the convex surface of various cylinders was used as a contact surface. In the first case the structured samples pointed out 2-4 times higher tenacity with respect to the smooth ones at loads under the buckling condition. With loads in the range of 100-500mN the average tenacity was measured as $7.89 \pm 0.43 mN/mm^2$ for the flat PVS sample and $32.4 \pm 5.71 mN/mm^2$ for the other.
In the second series of experiments the results showed that at curvatures of the

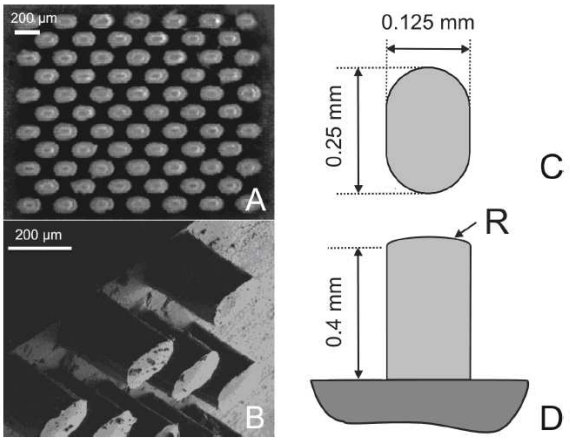

Figure 16: PVS structured sample. (A) Entire sample. (B) Single pins. (C)–(D) Dimensions of the single pin.

glass surface between 40-120m^{-1}, the adhesion of the structured PVS sample was considerably higher with respect to the flat one, and that for high ($> 120m^{-1}$) and low ($< 40m^{-1}$) curvatures of the glass surface, adhesion of the flat was much higher than that of the structured sample. Hence, it can be said that the multiple contact structure of the attachment pads increases the contact area on natural surfaces and, as a consequence, enhances the adhesion.

3.3 Analysis of self cleaning properties

In nature both spiders and geckos have the ability to maintain the terminal ends of their feet clean.
Natural contaminants (dirt and dust) as well as man-made pollutants are unavoidable and have the potential to interfere with the clinging ability of geckos and spiders.
The particles found in the air consist of particulates that are typically less than 10μm in diameter while those found on the ground can often be larger. In particular Geckos and spiders seem to not groom their feet like beetles and surely do not secrete sticky fluids in order to remove adhering dirty particles but they maintain their ability to cling surfaces and retain their adhesive properties.

Shah and Sitti in [20] suggest that the self-cleaning phenomenon is caused by the so called “lotus effect”.
The thin fibers of the attaching elements reduce the surface making contact with the water droplets. In such a manner the droplets cannot make good contact and roll off carrying out the dirt particles. Hence these adhesives have to be super-hydrophobic and the self-cleaning property has to be deeply related to the water (humidity).
Superhydrophobic materials can be viewed as self-cleaning materials because drops slide taking with them the dirty particles. The hierarchical nature of the spider and gecko attachment systems probably creates the superhydrophobic condition as recently explained by Pugno in [22] but the real reason why the spiders and geckos feet are clean both in wet and dry conditions is still not entirely clear.

So far, the best result in the self-cleaning explanation problem can be considered the one carried out by Hansen and Autumn in 2005 [17].
They tested the hypothesis that gecko setae become cleaner with repeated use: a self-cleaning phenomenon. They applied 2.5μm radius silica-alumina ceramic micro spheres to dirty gecko setal arrays. They demonstrate that a significant share of the particles are removed after 5 steps with respect to the initial condition. As depicted in Fig. 17 after only 4 steps the foot is clean enough to support its weight. Considering contact mechanics and modeling the interaction energy between a

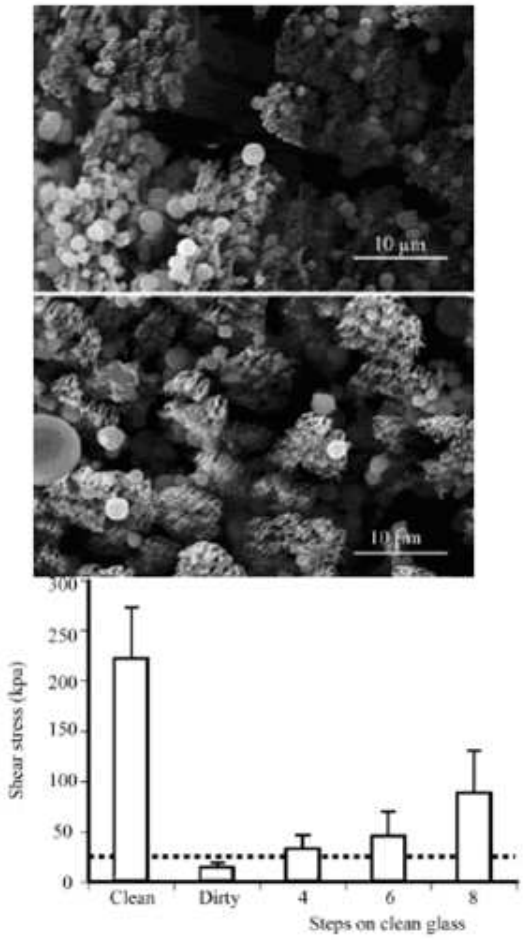

Figure 17: (first) SEM images of spatulae (up) after dirtying with microspheres and (down) after five simulated steps. (second) Mean shear stress exerted by a gecko on a surface after dirtying. The dotted line represents sufficient recovery to support body weight by a single toe (Hansen and Autumn [17]).

dust particle and a wall and a spatulae as in Fig. 18 it is possible to give some explanation to the self cleaning process.
Assuming the spatulae as curved surfaces with spherical shape at the interface, and then as flexible strips, they evaluated the attraction force between dirt (spherical) and wall (planar) and between the same particle to a number of spatulae. Referring to the paper, being the interaction between the wall and a dust spherical particle expressible as (Van der Waals forces):

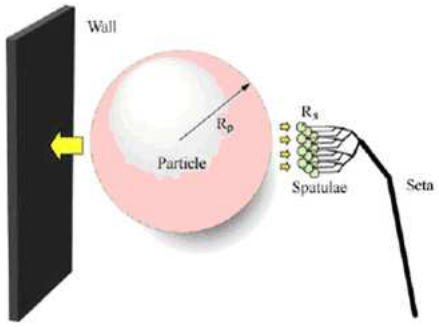

Figure 18: Model of interactions between gecko spatulae of radius R_s, a spherical dirt particle of radius R_p, and a planar wall that enable self cleaning [17].

$$W_{pw} = \frac{-A_{pw} \cdot R_p}{6 \cdot D_{pw}}$$

where: p = particle; w = wall; A = Hamaker constant; R_p = radius of the particle; D_{pw} = wall-particle distance., the interaction energy between a spherical dust particle and a spatula, s, assuming that the spatula tip is spherical, becomes:

$$W_{ps} = \frac{-A_{ps} \cdot R_p \cdot R_s}{6 \cdot D_{ps} \cdot (R_p + R_s)}$$

By defining N as the ratio of the two interaction energies, it can be expressed as:

$$N = \frac{W_{pw}}{W_{ps}} = (1 + \frac{R_p}{R_s}) \cdot \frac{A_{pw} \cdot D_{ps}}{A_{ps} \cdot D_{pw}}$$

In energetic equilibrium the sum of the energy of the spatulae attached to the dirt particle is equal to the energy interaction between the dirt particle and the wall. Reasonably, can be supposed that on every step approximately half particles remain attached on the surface and half on the spatulae.
Hence, when the energy required to separate a particle from the wall is greater than that required to separate it from a spatula, self-cleaning occurs.
For example, if Rp = 2.5μm and Rs = 0.1μm, self cleaning will occur as long as no more than 26 spatulae are attached to the dust particle at one time, assuming similar Hamaker constants and gap distances. The maximum number of spatulae in contact with a particle for self-cleaning, is tabulated in Table 4. It can be seen that very small particles ($< 0.5\mu$m diameter) do not come into contact with enough spatulae to adhere. Due to the curvature of larger particles relative to the planar field of the spatulae, very few spatulae are able to come into contact with the particle.
As Hansen and Autumn concluded, self-cleaning should occur for all spherical spatulae interacting with all spherical particles.
Persson in [21] disagrees with Hansen and Autumn and suggests a "dynamic" explanation: the self-cleaning property is due to minute lateral movements of the toe pads. In such a manner the gecko would scratch away the particles (Fig. 19). These lateral movements are suggested to be in the opposite direction with respect to the one that allows the enhancement of the overall adhesion of the gecko toe pad (that results in strong bonding to the substrate). While the toe pad is already squeezed against the substrate such a lateral movements can allow to scratch away the dirty particles attached to the toe pad. As a conclusion it is possible to say

Radius of particle (μm)	Max.n. of spatulae in contact with particle	Area of sphere (μm^2)	spatulae available	% needed to adhere
0.1	2	0.03	0.25	804
0.5	6	0.79	6.2	96
1	11	3	25	44
2.5	26	19	156	17
5	51	79	622	8
10	101	314	2488	4
20	201	1257	9952	2

Table 4: Self cleaning. Max num of spatulae that can be in contact with a contaminant particle (spatula radius, R_s =0.1μm).

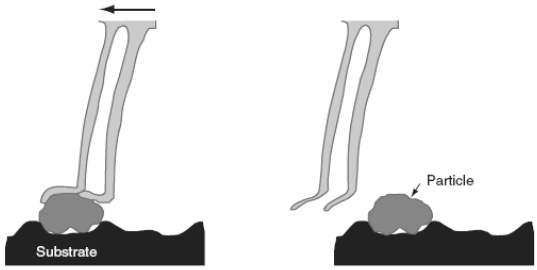

Figure 19: Hypothesis of self-cleaning movements (from Persson [21])

that the energetic explanation seems to be the the best one hypothesis because it can explain the self-cleaning effect in all the working conditions (i.e. wet and dry). Moreover not only the lotus-effect can be viewed as a system that enhances the self-cleaning abilities in wet conditions but also an energetic phenomenon between the dirt particles, the setulae and the water droplets.

3.4 Adhesive mechanisms

So far in order to explain the spider and gecko adhesion the researchers have considered that at least two different types of forces are involved.
Van der Waals forces and capillarity forces are the sources of the adhesion of geckos and spiders. Moreover, a possible nanointerlocking force could have a role in the cobweb gripping for the spiders.

3.4.1 Van der Waals Forces

The Van der Waals forces are weak in comparison to other forces and are always present regardless of separation and effective from large separations ($50nm$) down to atomic separation ($0.3nm$). The van der Waals force per unit area between two parallel surfaces with distance $d < 30$nm can be calculated with the subsequent:

$$f_{VdW}/Area[N/m^2] = \frac{A}{6 \cdot \pi \cdot d^3}$$

where A, the Hamaker constant (typical values $10^{-19} \div 10^{-20}$ J), is assumed as 10^{-19} J. Considering that the surface area of a gecko spatula is $2 \cdot 10^{-14} m^2$ [14] and d = 0.6nm the equation gives a force for a single spatula of $f_{VdW} = 0.3\mu$N. Being 100-1000 spatulae per seta the adhesive force of a single seta becomes 30-300μN similar to the values measured by Autumn and al. in [8, 23].
Arzt et al.[15] assumed the spatulae as cylinders that end with a hemispherical tips of radius R. Defining the adhesion force as (JKR theory):

$$f_a = -\frac{3}{2}\pi\gamma R$$

and assuming γ = surface energy per unit area (expected value 50mJ/m^2) and R =100nm, the adhesive force of a single spatula is predicted to be 0.02μN. For a lower value of the Hamaker constant (10^{-20}J), the adhesive force of a single spatula is comparable to that obtained using the surface energy approach.
Looking now at the characteristics of the *E.arcuata*, remembering that the mean area of a setula is 10^5nm^2, if the tip of a setula is assumed as a curved segment of a sphere (R is the setula tip equivalent radius), the Van der Waals forces can be calculated as:

$$f_{VdW}[N] = \frac{A \cdot R}{6 \cdot d^2}$$

as successfully made by Autumn and Peattie [14].
If R = 0.1-0.2 μm, for A = $10^{-19} \div 10^{-20}$J the estimated Van der Waals (VdW) force for a single setula is $f_{VdW}[N]$ = 1.85-370 nN comparable with the measured results of Kesel et al. [3, 4] of 38.12 nN.
Considering an *E. arcuata* setula radius of R = 0.2 μm and an A = 10^{-19}J, the result is $f_{VdW}[N] = 37nN$, very close to the experimental one.

3.4.2 Capillary forces

In the past the capillary forces were been assumed to be the reason of the adhesion of geckos and spiders but the lack of secretion fluids and of experimental evidences

made this idea less attractive and probable.
In spiders' literature while VdW forces are considered the main adhesion forces, there are no experimental evidences that prove or confute the capillary forces like an adhesion force for the spiders.
In gecko lizards such forces have been yet evaluated.
Autumn et al. [23] demonstrate that the principle adhesion force in gecko is the Van der Waals force. They proved that the highly hydrophobic toes of the *Tokay geckos* adhere both on strongly hydrophobic and strongly hydrophilic, polarizable surfaces in a similar manner.
Experimental results demonstrate that while the VdW force is necessary for the adhesion of the gecko, capillary forces can be only an enhancement.
Following this idea Huber et al. [16] measured the adhesion force of a single spatula in different atmospheric conditions and surface chemistries.
Considering that the gecko does not secrete any fluid the idea was that if there is a capillary effect then it is due to the humidity and to the ambient conditions.
The results confirm the hypothesis: an augmentation of the humidity increases the overall adhesion force. This behavior suggests that an influence on adhesion forces can be exerted by water layers between geckos' spatulae and the substrate.
From another point of view the authors proved that the increasing of the hydrophilicity of the substrates enhances the adhesion. In this case the results, as the authors underline, are more correct with respect to the work of Autumn et al. [23] thanks to the different experimental materials and methods.
A work that confirms these results can be found in [24]. Starting from the considerations that capillary forces can be avoided only with measurements in a liquid or in a completely dry vacuum ambient and that in nature the relative humidity is at least 10%, the authors suggest that the capillary force does not have a secondary role in geckos' adhesion but gives the dominant contribution. In order to demonstrate such an idea experimental tests have been made (more details on materials and methods in the cited paper) by the authors.
First of all, an interaction force measurement between the cantilever-gecko (a fresh single gecko toe from a spiny tailed *house gecko* glued to a magnetic sample plate of an AFM equipped with a tip less cantilever) and silicon cantilevers with different properties (1st hydrophilic 30°, 2nd hydrophobic 110°) showed higher forces (11.8nN) in the 1st test condition with respect to the 2nd ones (4.9nN) suggesting that capillary forces can have an important role in the adhesion.
A subsequent measurement was taken changing the relative humidity of the ambient. Such a test showed that decreasing the relative humidity decreases the adhesion force and vice versa; moreover immersing the sample in the water gave an adhesion force less than the 20% of the original value.
From this analysis can be reasonably assumed that the VdW forces are the dominant forces in the "dry adhesives" systems and the capillary forces enhance the overall adhesion of the system.

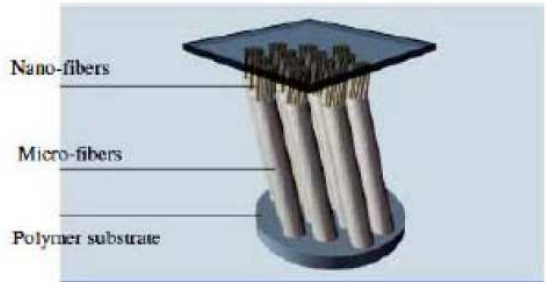

Figure 20: Ramified structures

3.5 Studies and materials for mimicking the attachment elements

In order to manufacture working prototypes based on animals and insects it is necessary to overcome the obstacles presented by the mimicry of the micro and nano structures that these creatures use for attachment.
As described earlier, spiders and geckos use both claws and setal structures for attachment. Manufacturing claws and spines does not represent a challenge with the available technologies.
The major challenge is represented by replication of the second and more complicated attachment structures used: the setal and setular structures. Mimicking dry adhesive structures is an initiative that tries to make available to robots the perfect attachment mechanism: no power required to maintain attachment, no dependence upon gravitational forces to realize attachment, no wear, availability on any surface regardless of issues related to surface roughness or friction coefficient and also very light weight (providing robots with claws means that the additional weight of the claws will influence the overall weight of the robot, in a field where weight is a major factor).
The setular structures have some important characteristics that represent the main obstacle in the way of developing dry adhesive structures:

- micro and nano scale dimensions
- ramified structure
- hydrophobicity

With progresses in nanotechnologies in recent years dimension obstacles have been removed, the main two problems still to discuss remain the possibilities to manufacture ramified adhesive structures and hydrophobic structures. As we see in figure 20, the synthetic fibers must have a ramified structure in order to maximize the contact area. The micro-fibers act as a compliant support structure for the adhesive nano-fibers, minimizing the bunching probabilities that would lead to fibers getting tangled with each other and unable to make contact with the substrate.
Dimensions required for the synthetic fibers are of approximately 100-400nm in diameter for the setulae with slightly larger dimensions at the free end.
Basic requirements for the synthetic hairs are:

- the possibility to manufacture structures with fiber diameters ranging 3-10μm and 50-500nm;
- the fibers must have a high density in order to ensure that the contact area is maximized;
- the fibers must be stiff enough and with a suitable distance one to another in order to ensure that no bunching occurs;
- the material for the fibers must have a high tensile strength and must have properties close to the β-keratin structures used by the spiders/geckos (Young modulus of 1-15 GPa);
- compliance to repeated deformation needed to ensure adaptation to the surface roughness.

Regarding the first requirement in the list above, it has to be remembered that the values for the dimensions of the setae and setulae are a function of body mass.
Considering the fact that the contact between the spatula and the asperity (for a general case of a surface with a certain asperity) is a contact theoretically acknowledged as similar to that of a hemisphere and a flat surface, it is possible to see that a setular termination, or spatula, no matter how large or small, for small deformations during contact, will give a similar contact area. This being said it is possible to see that a large number of setulae leads to a large contact area. The bigger the contact area the bigger the adhesion force capable, so heavier the creature.
Also, there is a certain attachment probability; this would lead to an even greater number of setulae required.
So, when trying to replicate dry adhesive structures a general rule is to try an ensure a high density of hairs without bunching. This can be done ensuring a suitable stiffness for the fibers.
Recent research in the field of nanotubes suggests that nanotubes are even better when bunched, so many of the considerations above are valid for polymers.

Hydrophobicity is generally regarded as the angle between a tangent to the surface of a drop of liquid (water) and a flat surface, tangent from the first point of contact liquid - material. This property describes the measure in which a certain material attracts small particles to it's surface.
Regarding dry adhesives, hydrophobicity is very important because, if the nano-hairs accumulate particles of any sort on their surface than the adhesive structure will become unusable after a certain number of usage cycles.
The adhesive structures found in nature are super-hydrophobic, the polymeric hairs are not (polymide is hydrophilic). This problem must be taken into account also in the case of carbon nanotubes because the nanotubes have a high quantity of surface energy.
In this direction research is still under way; the general idea is to manufacture the setal structures from materials with approximately the same properties of the hairs found in nature.
The attempts to replicate nano-hair go in two major directions:

- using polymers poured into different kind of templates, like membranes, indexed wax, etc.;

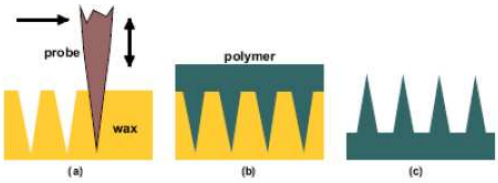

Figure 21: Synthetic hair fabrication by the Method I: (a) Indenting a wax surface using a micro/nano-fabricated probe nanotip, (b) molding it with a polymer, and (c) separating the polymer from the wax by peeling

- using multiwalled carbon nanotubes grown through Chemical Vapor Deposition on different substrates.

3.5.1 Fibers from polymers using pouring forms

In this case the challenge is to use an already available template or construct one, in the shape of a surface with nanometer size holes and high density. The surface with holes would represent the negative of the hairs, molten polymers is poured into the negative and after it is cured, the support material (negative) is chemically dissolved with various solvents who would not attack the polymers, peeled, or, in the case in which wax is used as a negative, simply melted.
Experimental techniques used and results using polymers are presented.

Nanorobotic Imprinting
For this first method, adopted by Metin Sitti et al. [10, 25, 26], the support material is wax, and the experiment tries to create holes of small diameter using an AFM probe with exact dimensions of the nano-hairs desired (tip of apex radius 10-20nm, and 15nm height), as illustrated in Fig. 21.
Indenting the wax, the exact template presented in figure 21(a) resulted, as it can be seen using SEM analysis.
After pouring the polymer in the wax structure and after the polymer cured, the sacrificial wax template was removed, and the results are visible in Fig. 21(b). The materials used in this experiment were: silicone rubber with 0.57 MPa Young's modulus and polyester resin. It is known fact that the natural beta-keratin structures have the elastic modulus of 1-15 GPa, so obviously silicone rubber is not the way to go. Other materials with higher stiffness could be used in this case, polyester is proposed, with a Young modulus of about 0.85 GPa, much more appropriate than silicone rubber.

Parallel Fabrication
This experiment uses an already available template in the form if a membrane with high density nano-pores into which molten polymers would be poured. The membranes used in the experiment were alumina and polycarbonate membranes with different ranges of diameter of the pores density.
The first part of the experiment used an alumina membrane, pores of 60nm in length and 200nm diameter, high ratio. Results obtained are available in Fig. 22, the hairs were too dense and got tangled up. The experiment showed that molding polymers under vacuum on a membrane is feasible, although proper membranes should be

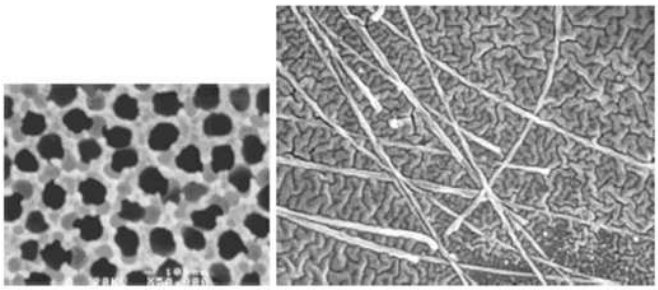

Figure 22: SEM images of (a) alumina membrane with 200nm diameter pores (left image), (b) molded silicone rubber nano-hairs with 200nm diameter, 60nm total length, and about 100 nm spacing between hair bases (right image)).

used for optimum results. A common problem that appeared while trying to pour molten polymer into nano-size holes was the difficulty of the polymer to fill the small spaces due to internal viscosity and drag. This problem could be solved by pouring the polymers with vacuum and it gets worst as size decreases. In order to stop the hairs from sticking to each other the density of the hairs needed to be decreased and also the length, so polycarbonate membranes with random pore orientation were used. Experimental results using rubber can be viewed in Figure 23. The hairs in Fig. 23 have rather large diameters for dry adhesives, so further work is still required for this method.

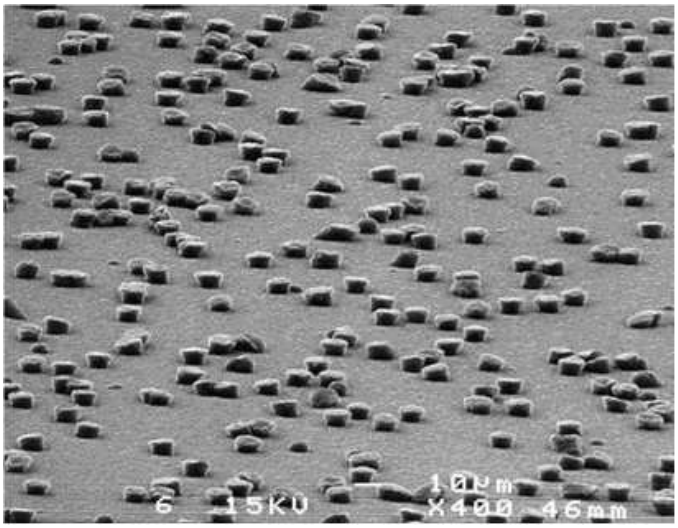

Figure 23: SEM micrograph of molded rubber hairs with about 6 micrometer diameter, 6μm length, and $5 \cdot 10^4$ pores/cm^2 density.

Fiber fabrication using commercially available components
This method uses commercially available membranes which can have pores of 0.02-20μm in diameter, 5μm thickness, and nanopore density of 105-108 pores/cm^2 according to Sitti and Fearing [25]. There are two types of available membranes: alumina, with high density pores and directional uniformity, and polycarbonate, with lower density but random pore orientation. The membrane is attached to a support substrate, polymers are poured under vacuum and results are visible in Fig.

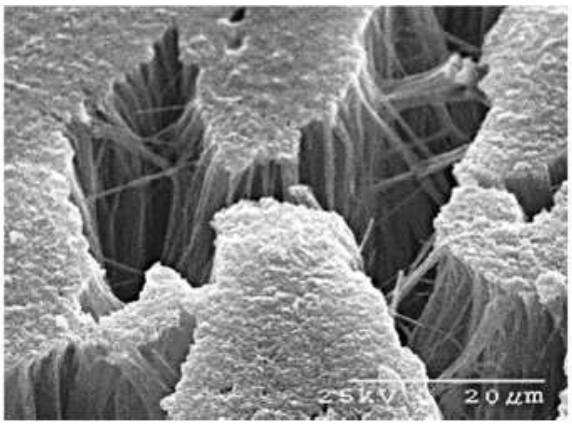

Figure 24: 200nm diameter high aspect ratio polymer nanofibers

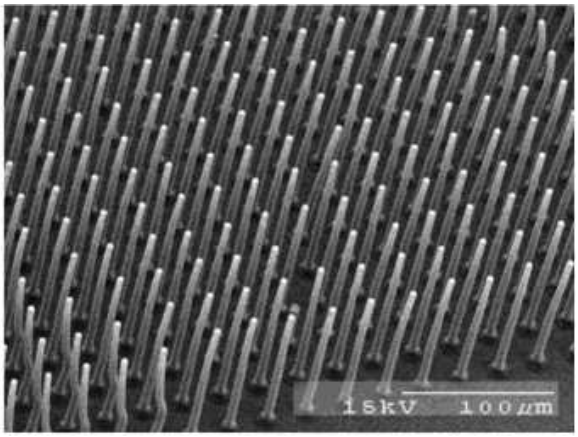

Figure 25: $4\mu m$ diameter polymer micro-fibers.

24. As it can be seen in the image, the fibers bunch together due to the superfluous length and very high density. This problem could be solved by using adequate membranes. The material used in this case is PDMS (polydimethyl siloxane).

Fiber fabrication using PDMS
This method also uses PDMS as material for the hair, but uses a manufactures membrane. The patterning method uses silicon as a base material, and the pores are created using photolithography. Also, a deep reactive ion etch is used to realize a negative mold. To ensure that the hairs come completely out of the template and that they don not break because the high friction during peeling a layer of fluorocarbon is deposited.
During the pouring process vacuum is used as usually, and 4μm diameter fibers show a very uniform structure seen in Fig. 25 are obtained. A previous problem was the breaking of the fibers due to increased drag during peeling, this issue is solved using this method, although photolithography is much more expensive than using commercially available membranes.

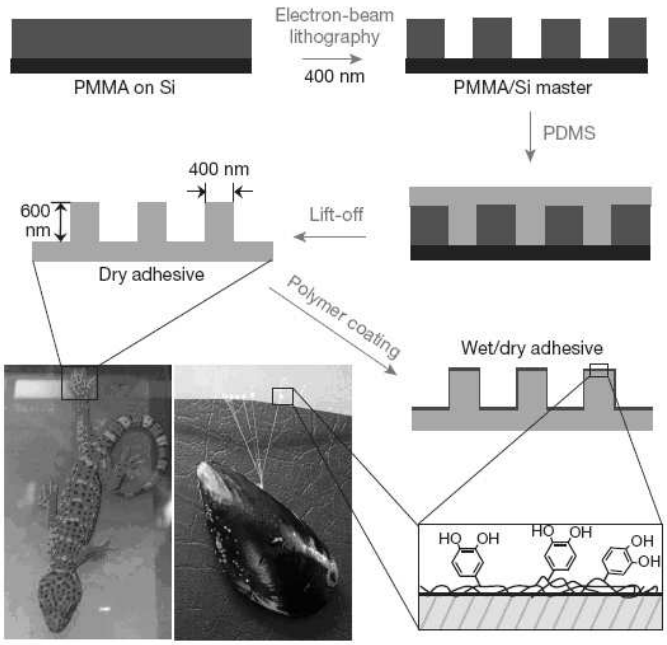

Figure 26: Design and fabrication of wet/dry hybrid nanoadhesive [31].

3.5.2 Adhesive inspired by mussels and geckos

Recently some researchers of Evanston, Illinois, [31] studied the abilities of the attaching mechanisms of the geckos and of the mussels and developed a novel adhesive that exploits the geckos' dry adhesive capabilities and the wet mussels' adhesive properties. Really the bio-inspired geckos adhesives until now does not reach the real geckos' abilities both in adhesion force and in maintenance of adhesion with repetitive use. Moreover the adhesion is function of the humidity and under water lowers considerably. As regards as the mussels, these creatures are able to cling on wet surfaces with the secretion of particular adhesive proteins containing the DOPA (cathecolic amino acid 3,4-dihydroxy-L-phenylalanine) which permits a strong interfacial adhesion strength.
The result (Fig. 26), as the authors say, consists in "an array of nanoscale pillars coated with a thin mussel-mimetic polymer film". Experimental tests confirm the goodness of the idea. The adhesion force increases linearly with the number of pillars in contact with the substrate and for a single pillar the results show an enhance of the adhesive force of 3 times with respect to the geckos' ones in air and 14-15 times in water. Considering the ability to maintain the adhesive capabilities with repetitive use, this novel adhesive maintains almost all the adhesive force (85% in wet and 98% in dry conditions, n° of cycles 1100) after thousands of cycles. This novel adhesive is an important step in the purpose to reproduce a bio-mimetic system that can walk on a variety of surfaces, with a repetitive use and with a small power consuming.

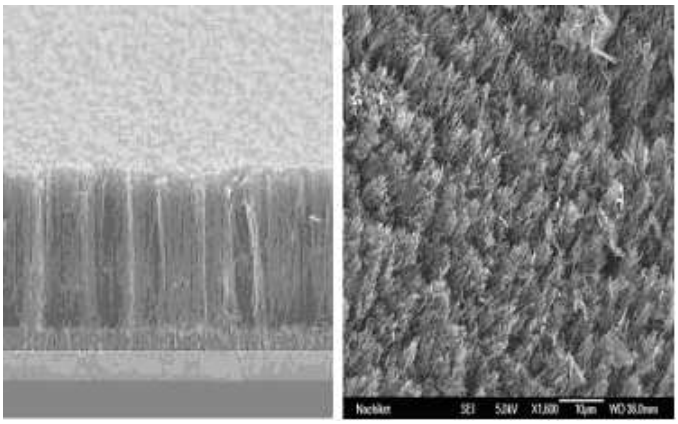

Figure 27: Scanning electron microscope images of vertically aligned multiwalled carbon nanotube structures: (left) grown on silicon by chemical vapor deposition (65 μm long), (right) transferred into a PMMA matrix and then exposed on the surface (25 μm) after solvent etching with a rate of 0.5 μm per min.

3.5.3 Manufacturing artificial hairs from carbon nanotubes

The problem using polymers is that the fibers are too dense and not stiff enough, so they stick to one another rather than the substrate. This makes it impossible for the artificial setulae to make contact to the substrate and realize adhesion. The solution would be to make the fibers less dense, but in this case the adhesion forces needed are not realized. So, an idea was to try and use fibers manufactured from carbon nanotubes and see if the attachment forces could increase even though fibers are bunched.

The carbon tubes are particular structures with electrical and mechanical properties that fascinated ever since they could be measured. Some of the electrical properties are: superconductors, low electric resistance, transport currents up to 1000 times higher than copper. As mechanical properties can be mentioned: tensile strength up to 100 times that of steel, elastic behavior, superior heat conductivity.
The dimensions for the nanotubes start from 0.6-1.8nm, that is why the carbon tubes are better known as carbon nanotubes. The carbon nanotubes are basically sheets of carbon atoms (bonded together in hexagonal structures) rolled to form a tube, with the free ends overlapped, as it can be seen in Fig. 28.

The nanotube presented in Fig. 28 above is a Single-Walled Carbon Nanotube (SWNT). The electric and mechanical properties presented above by comparison are only available for this type of nanotube. The other type of nanotubes, the Multi-Walled Carbon Nanotubes (MWNT) is a collection of coaxial nanotubes, with single tubes held together by Van der Waals forces [28]. There are different methods to obtain nanotubes as described in [29]. In [27] the nanotubes were produced via Chemical Vapor Deposition and the experimental results were very encouraging. The carbon nanotubes bunched together, but because of the combination between Van der Waals forces and energy dissipation during the deformation and elongation of the nanotubes the force/area is much greater than the estimated value of a seta. The carbon nanotubes have extreme high strength and good compliance, flexibility under stress, so they are highly recommended, if available.

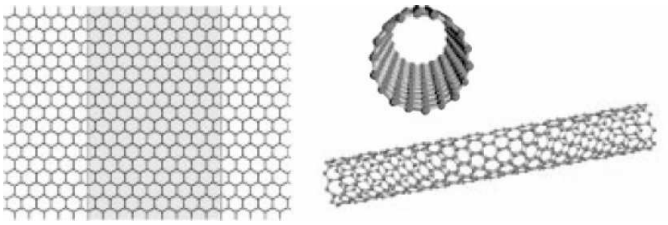

Figure 28: Sheet of carbon atoms and SWNT.

Betul Yurdumakan et al. [27] in their experiments use thick 10-20nm and long of around 65μm nanotubes. The results can be seen in Fig. 27, and the experimental evidences undergone in his work show good results.

Possible biomimetic applications
The domains of application for the CNT are endless: electronics, medicine, chemistry, electrics, etc.
There are two possibilities for the use of the carbon fibers to manufacture attachment systems:

- spine manufacturing
- dry adhesive manufacturing.

In order to manufacture spines it is possible to say that the nanotubes are too elastic, so they should be embedded into a supportive polymeric structure. Because of the covalent bonds they should be resistant to wear. Using the CNT to manufacture the dry adhesives seems promising. It seems that the carbon nanotubes (especially MWNT) produce surface energy when deformed. This increases the superficial energy of the nanotubes making them attach better to the substrate, but also attracts small particles present in the vicinity leading to a contamination of the dry adhesives [30].
From another point of view, considering that the (super)hydrophobicity seems to be intimately related to the so called "lotus-effect", the road of the carbon nanotubes seems to be very promising in a bio-mimetic perspective.

3.6 Advanced manufacturing techniques: SDM

Conventional manufacturing techniques use assembling methods in order to create multipart systems.
The parts are joined together using fasteners and seals and, usually, these connectors are subject to great stress and wear resulting in failure of the whole assembly. The component parts of the assembly are manufactured usually using standard manufacturing methods which use a homogeneous material block shaped by material removal, forged or cast, also requiring at some point material removal. Applying traditional manufacturing techniques in robotics is fast and cheap, but reliability problems tend to occur, especially as the dimensions tend to shrink. Manufacturing small and micro-robots is delicate and requires a different technique that would be able to create a compact structure, light and feasible. Developments in rapid prototyping techniques, also known as Solid Freeform Fabrication came as an answer to the problems encountered by the shrinking robots.
Observing the insects and animals it is possible to see that they use materials of different stiffness bonded together to make a compliant, yet strong and light structure. In order to build reliable and compliant structures the new available technologies must be used in order to create composite structures, structures using different materials bonded together and embedded structures.
All this is possible using the SDM (Shape Deposition Manufacturing).
Combining hard and soft materials the creation of joints that replicate the biological structures used by the animals, especially the joints of the roaches and spiders which represent the object of our study, is possible.
Embedding components and joining materials with different characteristics is only half the task, the difficult part is to make the joints reliable, strong and feasible enough to withstand a large number of usage cycles and also, the embedded components must work without failing, compromising the whole structure. Some embedded components, like motors, electromagnets or electronics usually produce large amounts of heat while working, and if this heat is not efficiently evacuated the motor or electronic device could fail. Failure is a hazard and in the case of the conventional assembly systems, the component can be replaced and the system works without repercussions. For SDM the replacement of a component is generally not possible, so measures have to be taken in order to minimize to the maximum any possibility of failure. Shape Deposition Manufacturing is one of the Solid Freeform Fabrication methods. SFF is a class of rapid prototyping techniques that decomposes CAD models into thin 2 dimensional slices and superimposes these slices in order to obtain the part. This class of methods relies on material deposition (layers) rather than material removal from a starting block of material, like the conventional manufacturing methods.
The layers can be created using various methods (laser cutting, lithography, particle deposition, etc) and the slices are bonded together thru adhesion or cohesion forces. In order to avoid a stair-like final aspect of the part the layers need to be very thin, a very expensive and time consuming process. Moreover, the layers will be from one material, which means that this class of methods cannot be used to produce working parts (the fact that the layers have to be glued together, like in the case of some SFF procedures makes it even more difficult). So, given the drawbacks associated with the conventional SFF methods it results that a new method had to emerge in order to allow working parts and assemblies to be produced.
This new procedure is SDM. The difference between SDM and the other methods is that SDM decomposes the part into primitives which can be manufactured using repeated material deposition and material removal, like we can see in Fig. 29. We can see that the process is a succession of deposition and machining stages. Process

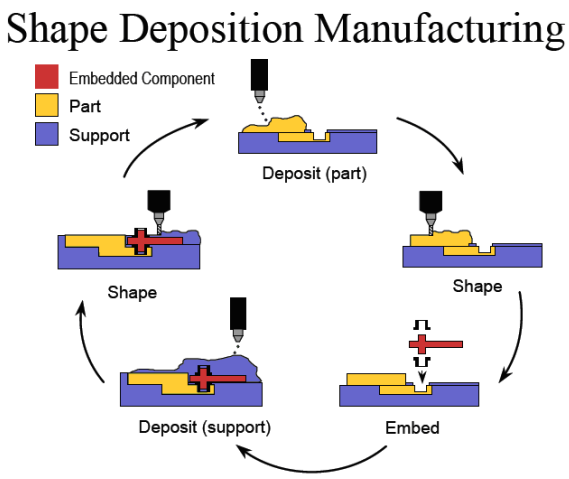

Figure 29: a

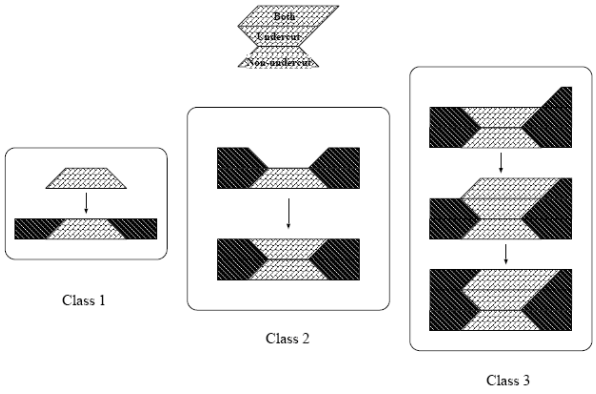

Figure 30: Primary shapes in SDM [49]

planning for SDM is the stage that takes the computerized model of the part, it decomposes the model into primitive realizable parts and defines the manufacturing operations needed.
Designing the CAD model is a simple task which can be done in a reasonable amount of time; the problems can appear when trying to decompose the part into primitives. It can be easy and fast for simple parts or very difficult and time consuming for others. It is obvious then that fast algorithms capable to decompose the part need to be developed for the method to be applicable.
The primitives in SDM are, according to [49] divided in three classes:

- class 1 has non-undercut features
- class 2 has undercut features
- class 3 is a combination of 1 and 2

Explanations for the classes and features are in Fig. 30. The class 1 features are machined by material deposition followed by material removal. Class 2 uses sacrificial material which is first deposited than machined to support the base material. Class 3 is a combination of both; the primitive in this case will be manufactured

combining and applying the methods from class 1 and 2 repetitively.
The materials that can be used are metals and plastics, with the difference that for metals different deposition techniques are involved, and that after the deposition a stress relief operation needs to be executed. For polymers all the considerations above are available, mentioning the fact that the contact surface between different materials has to be as big as possible, like in Fig 31(a), in order to ensure proper adhesion, so that the joint will not fail under repeated stress. The forces that keep the different elements together are adhesion forces that appear when one molten polymer is poured into a form containing a solid one. Molecules of the molten polymer fill the spaces created by the imperfections in the solid polymer. Also, because of the vicinity of the molecules, Van der Waals contact forces can be invoked.

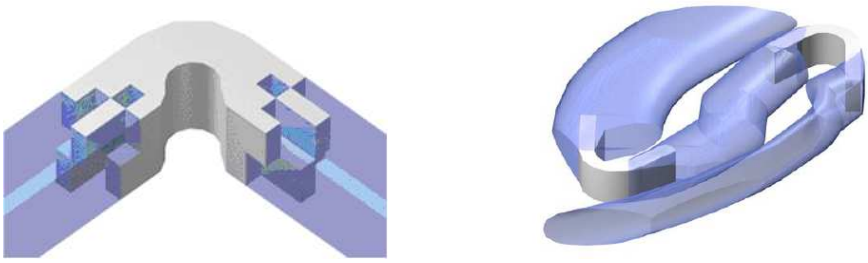

(a) (b)

Figure 31: Bonding section between hard (blue) and soft (white) polymers

If the two materials are incompatible for bonding additional adhesives could be added on the surfaces of the solid material. If metals are to be incorporated into polymeric structures we have to study the adhesion between the specific metal and polymer used, so that the structure does not disintegrate under stress. When metals are combined thru SDM usually the molten metal added over the machined surface melts the superficial layers of the support metal, molecules are bonded together strongly so the danger of disintegration is minimum (it depends off course on the metals, it is considered that a combination of copper with steel is ideal [50]). In this case we can consider cohesion (internal) forces. However, in the case of the polymers, usually the added molten polymer does not melt the surface of the support material; no cohesion forces are present so adhesion between the two surfaces has to keep them in place. Usually, the attachment between 2 surfaces is achieved in 2 ways:

- force
- form

We have seen that between metals forces present are enough to hold them together, but where the forces present are too small we have to consider various contact surfaces that would give enough strength to the joint. This is very important, especially because the robots created thru SDM would be used in surgical and space applications, so if one joint cease it could be a disaster. Using SDM it is possible to:

- combine different materials in order to realize structures with varying mechanical characteristics, replacing fasteners and bearings (Fig. 32(a)).

- embed sensors, actuators, tendons, electronics into the robot's parts, making the structure much lighter and compact (Fig. 32(b)).

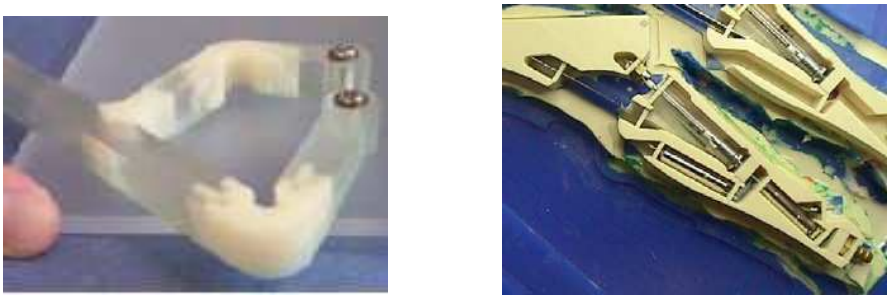

(a) (b)

Figure 32: SDM prototypes

As drawbacks we can mention the fact that the process is time-consuming, for a SDM structure being needed up to 30 hours of highly trained labor. Also, actuators and electronic parts disperse heat, embedding them into heat insulating material could be a failure cause so sacrificial material needs to be placed around the actuator or chips, and later removed in order to give some space. Moving parts have to be also surrounded by sacrificial material (easy melting wax or substances that can be etched away chemically).
A very important drawback is represented by the failure of one component, in a classic assembly a broken part is removed and replaced, but with SDM embedding everything is hard even to diagnose, so the whole assembly needs replacing. SDM allows any shape for a component, so this means that every component in an assembly needs to be designed, which could be time consuming. However, this can be avoided by building libraries with template components. The machines used are cutting mills, so the machined surfaces will have a certain roughness, this means that soft polymers will be necessarily cast, because surface imperfections are the source of fatigue failure.
This being said, if a CNC mill machine, the required components, a CAD program are available and a specific robot design is in mind, any structure can be realized without being limited by the commercially available components. Simulations on a virtual model have to be done before prototyping for obvious reasons. The SDM domain is very vast, so considerations on process planning, design space and so on could be expressed, but this is not the purpose of the present paper.
The process is closely analyzed in [49, 50, 51], so almost any question regarding it should have an answer.

3.7 Survey on bio-inspired climbing robots

There are some specific applications that require special vehicles to be used, where traditional vehicles or man cannot work, or there is a matter of safety involved. These applications can refer to inspection, repair, cleaning and exploration of high-rise buildings, storage tanks and pipes for petroleum industries, nuclear power plants, space vehicles, de-mining operations, surgery.
Some of these applications require climb possibilities on any kind of surface, high autonomy, high maneuverability and robustness. Size is also very important; robots developed for surgery have to be produced using the latest in nanotechnology.
The present chapter is focused on the robots inspired or related to the spiders.
So, the "spider-like" robots can go in two different directions:

- robots imitating the spider body structure and locomotion;
- robots imitating the attaching techniques used by the spider, which consists in the use of claws and micro-hairs on a non-spider structure.

3.7.1 Robots imitating the spider body structure and locomotion

These are walking robots created in an attempt to recreate the spider locomotion. These robots are comprised of a central plate, a body, and a certain number of limbs, from 4, the cheaper, less-complicated robots, to 6 (Fig. 33(a)) or 8 legged robots (Fig. 33(b)). In order to be able to imitate the locomotion of the

(a) (b)

Figure 33: 6 legged (a) and 8 legged (b) spider robots prototypes.

spider these robots use articulated mechanisms that require a certain number of components. Interesting only the locomotion, the total weight of the structure is not a constraint and is high in these prototypes (depending off course on the materials used for the elements). Also the overall energetic consumption is a limiting factor, and the amount of actuators needed to move the robot must be the less as possible. These robots have a restricted autonomy or no autonomy at all, being forced to function with an umbilical cord. These robots are also characterized by a lack of compactness of the structure and trying to apply the climbing mechanisms of the natural spider (the claws and hairs) to these structures would be very difficult because the contact points with the environment are small or not suitable, and the weight of the structure is many times higher than that of the actual spider. These being said, the common characteristic of these robots is

the lack of climbing possibilities due to the specific construction of the structure. Moreover the walk speed of these robots is further to improve, a high walking speed necessitating a very high energetic effort. So, in order to create autonomous climbing robots used for the desired operations the dry adhesion principles coupled with the use of spines/claws on conventional wheeled or crawling under-actuated structures have been used. However, there could be a solution to the over-actuation of the structures which is in future development, and consists in the mimicking of the natural spider actuation.
Indeed the spiders do not use tendons or muscles for all the joints, but they use a sort of dilatation chambers. A mechanical system taking advantage of this method has been prototyped by C. Menon et al. and it is closely described in [32]. This system replaces the conventionally used joints with hydraulic elastic joints. The central elements of the joint is an elastic chamber that dilates differentially creating an angular movement of the 2 elements to which it is linked. The liquid used to fill the chamber is water. A pump serving the joint pressurizes the water which fills the chamber that expands causing the limb to bend. A position sensor monitors the movement of the joint and feeds the information to a controller which tells the pump to increase or decrease the pressure of the liquid, according to the angle needed to be realized. The closed loop used in his case allows the joint to be closely monitored so precision movements can be realized. Using water instead of a gas means that precision movements can be realized due to the incompressibility of the water, and also, this mechanism can be used in outer-space because water does not expand like a gas would do in the lack of outer pressure. The problem with this system consists in the fact that every joint needs a pipe and a water pump, also it needs a close loop system to continuously monitor the angular position of the joint. A working prototype with similar dimensions to those of a spider has been developed, with some limitations regarding the angle at which the joint can bend. The use of a closed loop to control the joint provides advantages of dealing with leeks or pressure differences created by the lack of external pressure.

3.7.2 Robots imitating the gecko's attaching techniques

There is a high number of robots realized and in development based on this principle, mainly because of the low cost and high autonomy and accessibility achieved.

Three wheg robots
The first robot proposed in [33] has 3 feet per wheg, as seen in Fig 34. Each foot has one degree of freedom being able to remain attached to the substrate for 120° of leg rotation. A spring placed in the joint ensures that the foot will approach the substrate in a correct manner, and that after detachment the foot comes back to a predefined position. This particular robot is able to climb vertical and past vertical surfaces detaching on occasion because of the adhesive pads rather than the robot design. A problem is that both wheels are connected to the same shaft, so the robot lacks the ability to steer. The problem associated with this prototype is that the whegs can only turn in one direction, so the robot cannot walk backwards. If the pads are provided with dry adhesive structures the peeling mechanism would require a stiff spring but the use of a stiff spring would make the attachment more difficult and would create a very disturbing reactive moment. Moreover, the stiff spring would require stronger motors to drive the whegs decreasing the robot's

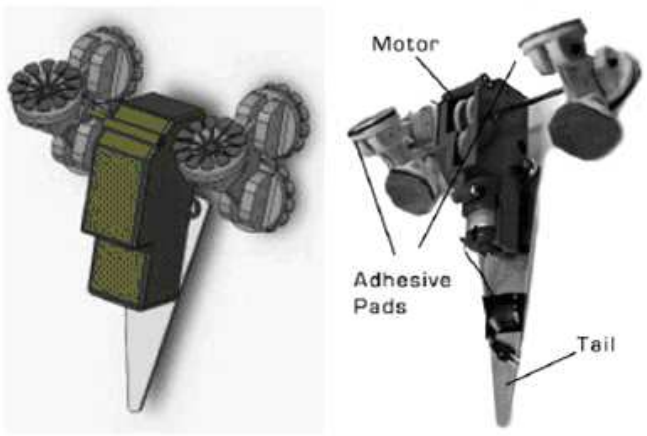

Figure 34: Robot with legged wheels: the CAD design (left image) and the photo of the real prototype (right image).

autonomy. Unless a compliance to tilt the joint of the pad would be introduced this particular design would not allow the robot to steer. As an evolution of this prototypes Murphy et al. [34] developed a similar small-scale climbing robot that can climb and steer in any orientation due to the use of two actuated legs with rotary motion and two passive revolute joints at each foot (Fig. 35). Such a robot can steer at any angle and climb up to 90° slopes with a max speed of 6 cm/s. Another robot, MiniWhegs [35], is a working prototype using the design principles described for the previous robot. The dimensions and weight for the prototype are 100g and is 8.9cm long without the tail. It is estimated that providing the robot with four whegs instead of two would allow full maneuverability and accessibility. As shown in Fig. 36(a), Mini-Whegs is equipped with spines and a adhesive band. In this configuration it cannot climb vertical surfaces. The tail is needed to stop the robot from tilting over due to the reactive moments of the springs and the high distance between the substrate and the center of mass. The robot has spines placed on the pads to make attachment even on rough or soft surfaces. Using spines on the pads brings up issues of spine compliance. Providing the whegs with spines would increase considerably the weight of the wheels and the power needed for the motor.
This robot has a four-bar mechanism (Fig. 36(b)) designed to allow a pair of spines to move independently from the other pair of spines in the search of usable asperities. A certain preload force is required for the adhesive structures used on the pads or if the spines are traveling over a soft substrate, so the preload force for this design is provided by the feet still attached. Another robot of the Mini-Whegs family is presented in [36, 37]. In these works the conventional adhesive feet were fully replaced with a bio-inspired adhesive. With some changes the robot, also if the bio-inspired adhesive shows less tenacity with respect to the conventional ones, become able to climb surfaces up to 90°.

Adhesive belts robots
This robot, presented in [33, 38], is a prototype with adhesive belts, trying to maximize the compactness of the robot along with autonomy. In this configuration the robot can use a single drive motor, going forward or backwards. Tests using adhesive belts manufactured from PDMS and sticky foam showed that the robot

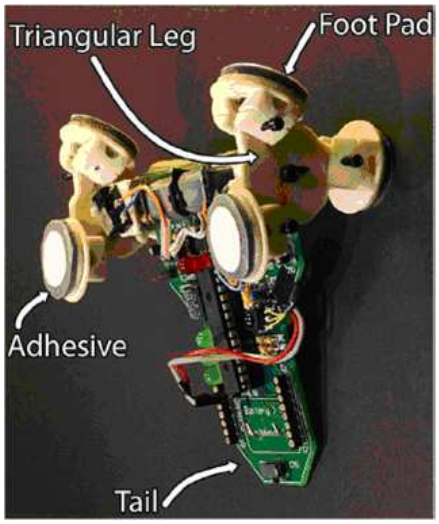

Figure 35: Waalbot: a robot able to navigate on surfaces at any orientation

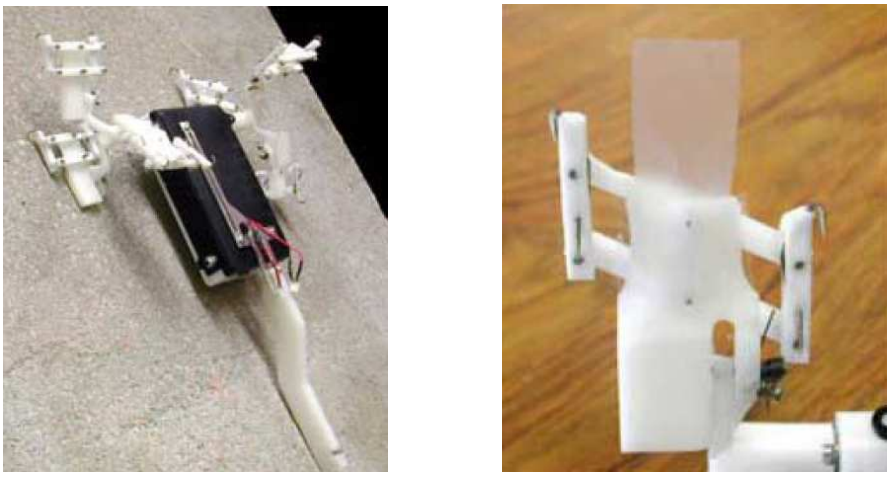

(a) (b)

Figure 36: Mini-Whegs

can climb reliably vertically inclined slopes (Fig.37(a)).
Dry adhesive structures are yet to be developed for this robot. The power efficiency is maximized because the power consumption increases with the increase of the slope. The peel movement for this robot is optimal, a small force being required for peeling, seeing that the peel is continuous. The main problem is steer possibilities; even if every belt would be attached to a separate motor the peel would not be possible because of the tilting motion of the robot that would determine a shear action of the dry adhesive structures. Moreover, the model is built to climb flat surfaces, a surface with ledges and corners would make it impossible for the robot to generate enough adhesion.
The cost of dry adhesives of such size is very important and should not be ignored.
Another belted robot, presented in [39], uses the same principles of the robot presented previously. It is much smaller, has a gravity center very close o the surface and a climb speed of at least 5mm/s (Fig. 37(b)). The weight is low, about 11g, allowing the robot autonomy of around 5 hours for normal climb regimes. For this robot dry adhesives haven't been used, but the design problems from the previous robot remain.

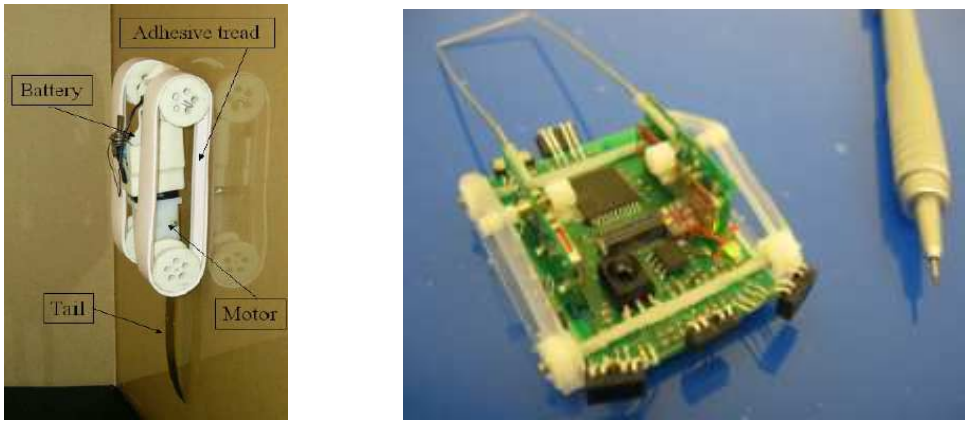

(a) (b)

Figure 37: Belted robots.

Gecko inspired climbing robots
Different Gecko robot prototypes are been developed.
In Fig. 38 is depicted the Geckobot [40, 41]. It uses a four bar mechanism shown in the figure below and a very ingenious peeling mechanism.
The peeling mechanism uses a series of strings attached with one end to the end of an elastic blade supporting the dry adhesives, and with the other end attached to a rotating rod of a motor. Hence when the motor turns, the string is tensioned, the end of the blade pulled upwards and the adhesive peels off the surface.
Considering the overall shape of the robot, it has to be said that there are other projects that, working with the shape and the kinematics of the gecko, propose other gecko robot prototypes with four bar link mechanisms. An example of such a robots can be found in [42].
The state of the art not only in the gecko inspired robots but also in bio-mimetic robots is surely the Stickybot [45].
Such an assertion is due to the fact that this robot climbs on quite smooth surfaces using dry adhesives and a locomotion and an attachment and detachment movements like a real gecko. Stickybot (Fig. 39 has a body constituted of a

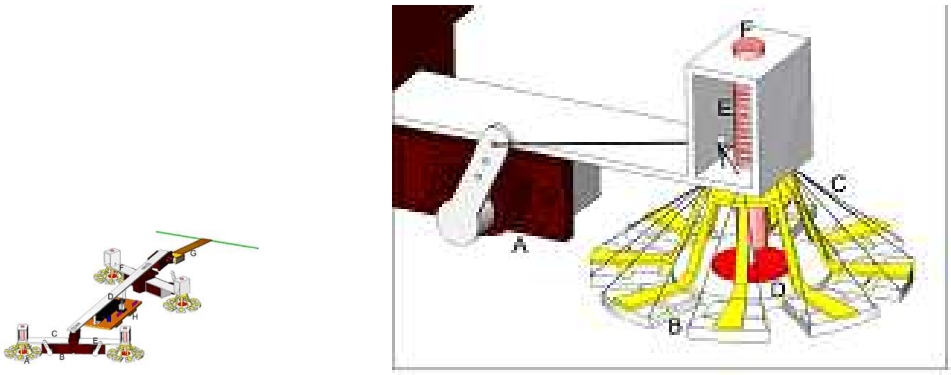

(a) (b)

Figure 38: Geckobot robot.

compliant system with 12 servos and 38 degrees of freedom. Four segmented toes made from two grades of polyurethane constitute each foot and each toe can be actuated in order to approximate the geckos' feet detachment motion: the digital hyperextension. As a real gecko Stickybot has a hierarchical compliant structure (Fig. 39(b)).
Besides the hyperextension, another bio-mimetic concept implemented in this robot is the so-called directional adhesion. Actually in a real gecko there is an enhance of adhesion if a proximal motion is added to a normal preload in the attaching phase. Moreover, as observed and described in [46], adhesion increases with tangential force.
As the authors declare, with such a movements not only the adhesion can be actuated without applying a significant preload but also the detachment requires a low detachment force coupled with a decreasing of the tangential load. Matching these two described principles with an effective force and stability control, allow Stickybot to climb a variety of different surfaces up to 90° (glass, glossy ceramic tile and polished granite).

Climbing robot using compliant microspines
This robot, called SpinyBotII [43, 44], uses an alternating mechanism with three pads supporting the spines 40(a). A motor is used to generate the advance, and a motor for each pad is used for detachment and attachment. At any given moment while moving, the robot hangs attached in three points. A tale acts as a stabilizer to counteract pitching moments acting on the robot in the center of mass. The center of mass is located at 2cm from the wall, and the total weight of the robot is 400g. The climb speed is around 3cm/s and could increase if a stronger motor would be used for the alternating mechanism (Fig. 40(b)).
The robot implements a locomotion inspired by the cockroaches and uses a similar tripod gait. The "pads" or feet of SpyniBot II are presented in Fig. 40(b). The SDM (Surface Deposition Manufacturing) technique had to be used to produce the feet. Each foot has ten identical fingers with two compliant spines. This is an optimal configuration which allows the spines to attach and detach independently. The spines used are 200μm thick and 1.5mm long. A radius of 15μm allows the robot to engage asperities on any surface. The robot is designed exclusively to use spines to grip on asperities so it does not work on very smooth surfaces. Also, it cannot steer and the weight is high especially for the elaborate construction of the out gripping mechanism.
One of the most powerful and amazing bio-inspired robots that can be found in

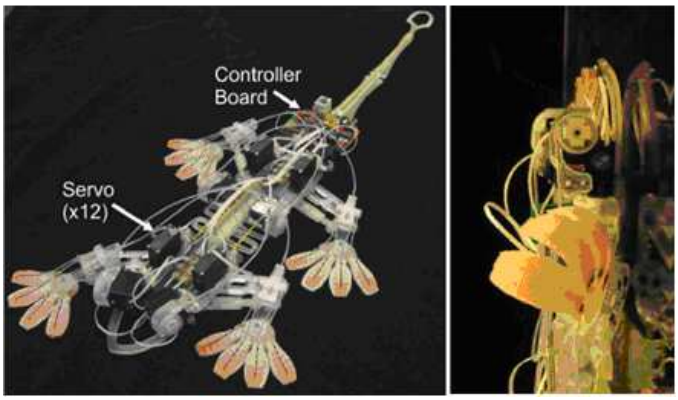

(a)

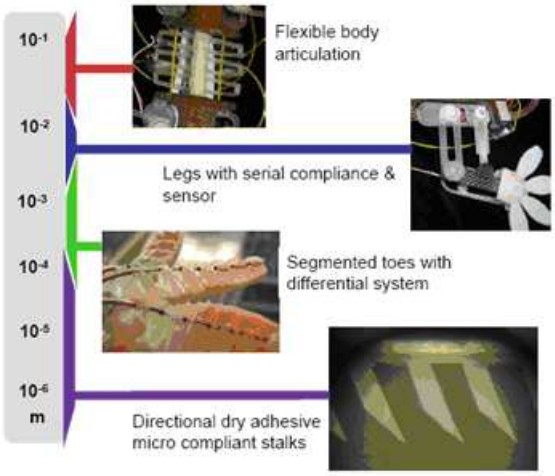

(b)

Figure 39: Stickybot robot.

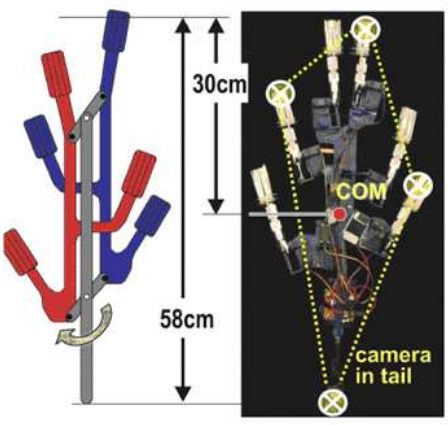

(a)

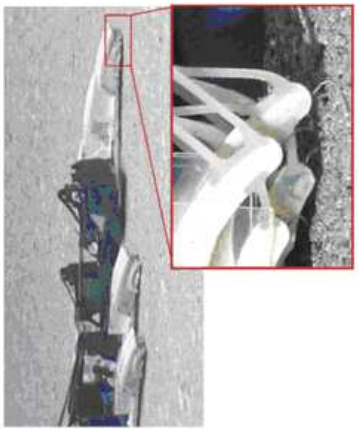

(b)

Figure 40: SpinyBotII robot.

literature is surely the RISE robot. This climbing robot, described in [47, 48] and shown in Fig. 41, is a 25cm, six-legged biologically inspired robot (climbing insect) employing bio-inspired attaching dynamics and micro-spines on the foot structure. Using such a principles the RISE robot is capable of climbing on a large variety of surfaces, using only two actuators per leg. It can adhere and climb on trees, brick and other vertical building surfaces such as stucco (Fig. 41(b)).

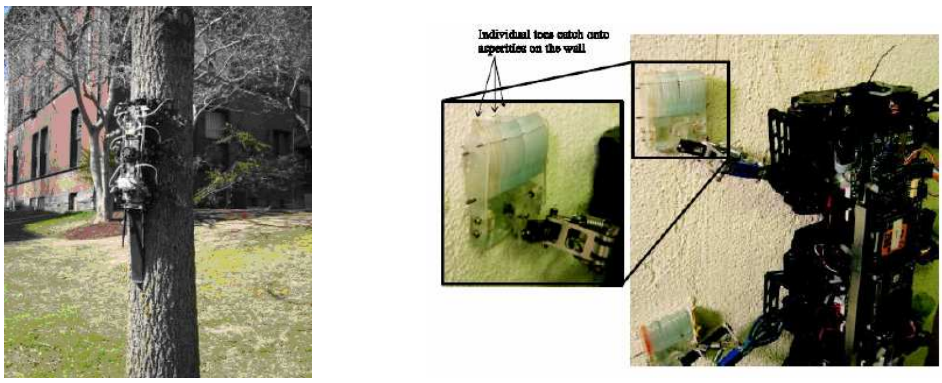

(a) (b)

Figure 41: Rise robot.

4 Phase 2: Requirements of the attaching devices

Mechanical and physical requirements and characteristics of the attaching devices

4.1 Introduction

In order to reproduce and develop a spider model for a future space applications, mechanical and technical directions and constraints have to be carried out.
Hence the biological and experimental results have to be analyzed and transposed into precise and accurate definitions in order to fix the basis for the subsequent analysis and considerations.
In this chapter are evaluated both the spines and the dry adhesive attaching systems in a mechanical perspective.
The spines attaching mechanism is evaluated looking at the climbing factors and at the conditions that allow the adhesion in order to define a suitable approaching condition, a possible way to construct their embedding structure and a correct number of spines per leg in agreement with the load of the system.
The dry adhesive system is analyzed looking at the correct approaching angle and at the dimensions of the elements that have to be reproduced. In particular the anti-bunching condition, related to the geometry of the attaching elements, is evaluated taking into account the results of the previous chapter.

4.2 Spines

Previous attempts of climbing robots tried to use suction cups or electromagnets in order to allow the robots to attach to smooth walls, or sticky tape to allow robots to hang on to glass or very smooth surfaces. These approaches are not appropriate for a robot destined to work in all conditions and all weather, on hard and dusty surfaces like stone, stucco, and brick or on wet and contaminated surfaces. The substrate destined to be climbed will not always be in optimal condition. Taking a close look at insects and animals with climb abilities it can be seen that they employ sticky pads, dry adhesives and claws to grip to wall asperities or penetrate tree bark.
All of these approaches are worthy to be taken into consideration when defining a structure for an autonomous robot. However, the spines and dry adhesives are more adapt to be used for exploration, given the fact that the robot will encounter especially hard and dusty surfaces. The spiders that present climbing abilities and some species of insects make good use of both tarsal claws and adhesive hairs in order to climb the majority of surfaces encountered, regardless of the state of cleanliness, surface roughness of weather conditions. This is a very interesting lead in the pursuit of a robot prototype able to climb any surface in any weather conditions.
If a robot would be designed based on the abilities of spiders, combining the better of the two climbing mechanism, the overall quality of the design would be promising. In that direction we will try to work, defining the main features of a climbing system using spines in order to grip on the asperities of the substrate.
The contact nature between a hard surface and a spine, given the fact that climbing soft surfaces with spines presents no need of advanced contact research, is taken into consideration.

4.2.1 Climbing factors

In order to create a robot that climb a certain surface, inclined or vertical, the spines need to engage the asperities, or bumps encountered on the wall. So, key elements in this process can be considered:

- the climbing substrate;
- the spine/asperity contact;
- the spines used to grip at the surface;
- the spine embedding mechanisms, or the feet.

Considering the first aspect, the climbing substrate, it is desired that the robot will be able to climb different surfaces such as hard, dusty rock and stucco surfaces. For the metallic surfaces there is the option of the magnetic devices, for the soft surfaces can be used penetrating devices.
In order to climb smooth surfaces, a smoothness degree has to be defined, given the fact that certain animals need adhesive structures to climb surfaces like glass or plexy; in the same way, a robot prototype would need adhesive pads to climb very smooth surfaces.
Looking at the surface macroscopically, it is possible to find flat surfaces, quasi-flat surfaces (which can be considered flat and straight on portions) and ledge-like surfaces (the tangent to the surface in consecutive points changes direction abruptly). Microscopically, a surface is a succession of positive and negative features, or bumps and pits. Considering a bump the negative of a pit, a radius r for the average pit can be defined. When using dry adhesives the dimension of the bumps and pits or the state of the surface counts less, adhesion is made anyway in most of the cases, so the surface is defined from the point of view of the spine engagement. In order for a spine to engage such a surface it is necessary that the spine's tip radius r_s to be smaller than the average radius r. Having these radii defined the number of available asperities per length unit can be expected to increase as $1/r_s^2$, and the maximum load for the spine/asperity contact to increase by r_s^2.
In order to be able to construct the gripping elements based on the spines the elements that characterize the contact, such as the spine length, shape, angle of approach to the surface have to be defined. The most convenient materials for the spines are hardened steels, given the overall properties and available manufacturing techniques.
A good analysis of these contact factors is carried out in [44]. The spine used is modeled as a curved beam attached to a robot limb which moves it downwards hoping to attach to an asperity.
The spine radius cannot reach at the bottom of all pits, so the center of the tip describes a trajectory called traced surface. The angle at which the slopes of the asperities in the stroking direction of the spine are inclined is θ. The angle is measured anticlockwise with respect to a direction perpendicular to the wall.
For the asperity to be usable, the angle needs to be larger than a critical usable value called critical angle θ_{min}. The critical angle depends of the angle at which the spines are loaded, called load and the friction coefficient:

$$\theta_{min} = \theta_{load} + arcot(\mu)$$

where:
θ_{load} is the angle at which the feet are loaded in respect to the wall, varying

between 3.5 and 8 degrees in the case of SpinyBot II [43]; μ is the coefficient of friction between the spine material, usually steel and the material of the substrate. The spine swept volume is the volume of the portion of space swept by the spine.
As we can see from the eq. above, the minimum angle is determined by the load angle and the friction coefficient, which is the most important factor. Usually, the friction coefficient of the steel spine with the rock is somewhere between 0.15 – 0.25. The friction coefficient is a very limiting factor for attachment, and an alteration of this coefficient, in the direction of diminishing μ because of the dynamic movement of the spine (when slipping),could lead to an increase of the of θ_{min} over a usable value. An alteration of the friction coefficient through slipping could be prevented by means of restricting the relative speed of the spine gripping the surface, which means that the load cycle of the spines will take more time, restricting the speed of the robot. The alteration of μ through the surface humidity is one factor to consider, because this makes the robot usable only in indoor spaces or outdoor in good weather. The approach angle θ_a, the angle of the spine swept volume, is an independent value in respect to θ_{min} or μ and it is chosen to ensure the engagement of as many asperities as possible, with values ranging between 45 – 85 degrees, the best values being around 65 degrees. The number of usable asperities will depend on the coefficient of friction, and any change made with this respect will alter the total number of grip points, modifying the spine/asperity contact load. As it can

μ	θ_{load}		
	3.5 deg.	5 deg.	8 deg.
0.05	90.7	92.2	95.2
0.075	89.3	90.8	93.8
0.1	87.8	89.3	92.3
0.125	**86.4**	87.9	90.9
0.15	**85.0**	**86.5**	89.5
0.175	**83.6**	**85.1**	88.1
0.2	**82.2**	**83.7**	**86.7**
0.225	**80.9**	**82.4**	**85.4**
0.25	**79.5**	**81.0**	**84.0**
0.275	*78.2*	*79.7*	*82.7*
0.3	*76.8*	*78.3*	*81.3*
0.325	*75.5*	*77.0*	*80.0*
0.35	*74.2*	*75.7*	*78.7*
0.375	*73.0*	*74.5*	*77.5*
0.4	*71.7*	*73.2*	*76.2*

Table 5: Variation of the minimum angle in respect to the friction coefficient and the load angle of the feet (*very good minimum angles, but only possible for high friction*, **usual angles for the usual friction coefficient steel/rock of (0.15 - 0.25)**).

be seen from Fig. 42, for values of the friction coefficient under 0.15 the attachment requires ledge-like asperities, very hard if not impossible to find for most surfaces.
In [44], the authors show can that above a certain tip radius the number of asperities drops quickly and that varying the value of θ_a, the number of asperities per cm changes little, decreasing significantly only for large approach angles, when the spine is almost parallel to the wall.
The number of available asperities is related to the wear of the tip due to repeated usage, starting from 10-15μm for the spines available today and ending with 25-30 μm after a few usage cycles.

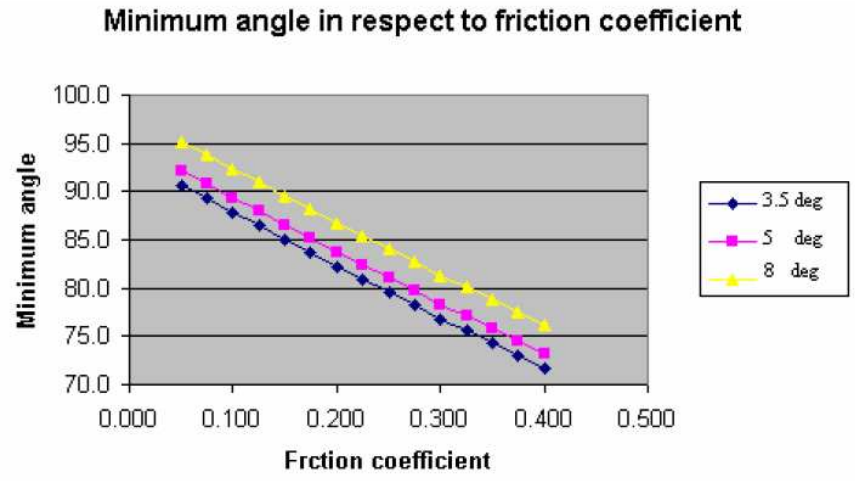

Figure 42: Graphical representation of the variation from Table 5.

This means that the number of asperities per given surface will vary significantly, and that on some surfaces, like polished granite or other smooth surfaces the robot will detach from the surface and fall. Because of this the wear cycle of every spine must be taken into account. The natural spine systems used by spiders and lizards suffer small wear because of the high safety coefficients so the key solution can be the use of hardening treatments for the spine material, correlated with the increase of the safety coefficient. In order to increase the safety coefficient as many spines as possible engaged are required and the whole robot must be as light as possible.

With respect to the spine/asperity contact strength it is possible to say that smaller spines are useful because they maximize the chance to find a usable asperity but, because they are thinner they are also more fragile, so the possibility to fail under load increases. The spine usually fails in one of the three ways:
- the base of the spine breaks or plastically deforms because of the moment produced by the attachment force;
- excessive elastic rotation of the spine due to the increased compliance;
- asperity failure.
Considering a spine of radius r_s, the contact strength will increase by r_s^2, and the number of usable asperities will decrease by $1/r_s^2$. Spine/asperity contact strength tests were done in [43, 44]. The surfaces used can be divided into three categories:
- fragile surfaces. These are usually composite surfaces formed from strong particles linked together by an adhesive like concrete or sandpaper. In this case the asperity failed first by detachment;
- tough surfaces, like granite where the spine failed in the majority of cases;
- surfaces where both spines and asperities failed equally.
Even if the dimensions for the spine shaft diameter allow the engagement, the problem is the spine tip which, because of the act that is very sharp tip it plastically deforms. The compromise in this case is to accept a maximum load force for the spine/asperity contact in order to avoid plastic or elastic deformation of the spine or asperity break-off. As suggested, this force is approximately 1-2 N per spine. So the key is to ensure that as many spines are attached rather than using a small number of strong spines and that the weight is distributed equally between spines. Clearly in order to prevent premature wear the spines need to have a special construction.

Transmitting the robot's weight to the wall and spines integration are two possible problems.
The upward movement of the robot involves a successive number of climb phases that have to be safely realized. Considering the robot in equilibrium attached to the surface, the necessary locomotor movements are:
1. detaching from the substrate;
2. an upward movement of the paws embedding the spines;
3. contacting the substrate with a small force to insure spine contact with the wall surface;
4. a downward movement of the paw slightly pressed in order to ensure that the spines come into contact.
This means that a certain paw-like structure needs to be created to sustain the spines. Because during these phases there are forces acting on the spine's tip, the spine must have a certain compliance when dealing with those forces, in order to avoid bending of the spine from overload or rupture of the spine's shaft. It is preferred that the spine leaps over the asperity and engages the next one instead of breaking and becoming unusable. This means that, in a 2 dimension environment the spine will need to have compliance in two directions, along with a rotational compliance, which would allow the spine to make a small rotation in order to slip off the asperity when overloaded.
This can be achieved in two ways: using compliant spines (elastic) or using a compliant structure for the spine.
The first solution means that curved spines are to be used, because of the curved shape the spine would be able to bend and avoid destruction. This means that a cheaper rigid structure can be used; the main inconvenient is that embedding multiple spines in a rigid structure makes them dependent, so the number of spines engaged at the same time decreases considerably.
In order to prevent all this a straight rigid spine embedded in a compliant structure can be used. Two cases can be defined, according to the compliance level:
- overall compliance, uses a damper and spring to insure vibration management but it's basically a rigid structure that embeds spines. Using compliant spines would allow a certain compliance for the spines along with good vibration management, but still would not allow the spines to work independently.
- independent compliance. This is the most complicated, expensive and evolved type of compliance; each spine is embedded in a rigid structure anchored with elastic damping elements from a hierarchically superior structure. This has the advantage of being able to control the compliance of each spine, and the spines work independently. The general idea behind this type of structure is presented in Fig. 43. The structures presented in Fig. 43 require SDM in order to be able to connect in the same structure materials with different physical characteristics. The compliances needed for an optimal engagement performance have to be defined and confirmed experimentally. Theoretically, for an optimal spine engagement the compliances should be defined for each direction. The y compliance need to have a large value in order to allow the spine to slide over the substrate searching a usable asperity.
The x compliance needs to have a large enough value, in order to allow the spines to take the shape of the substrate (assuming that the substrate is perfectly vertical is wrong), or if a spine rests on the tip of an asperity it should not restrict the other spines to engage asperities. However, this rigidity needs to have a moderate value, because, if the spine engages a hole in the substrate the structure needs to be stiff enough to pull the spine out without needing excessive force.
The rotational compliance of the spine needs to be relatively small, enough to allow the spine to leap over the asperity if overloaded, but not to big to cause premature disengagement.

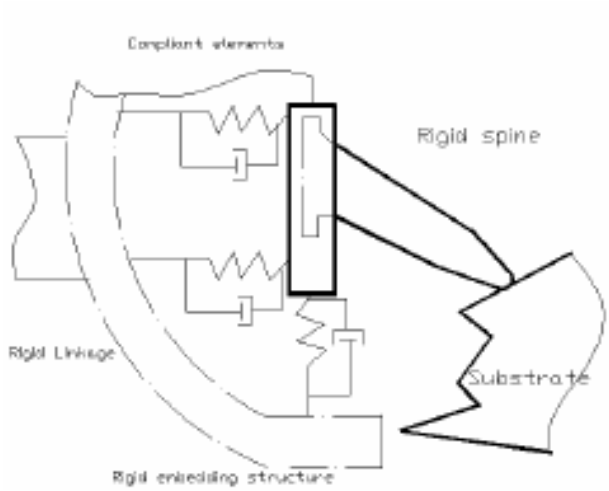

Figure 43: Elastic embedding structure using compliant links

The technologies used to manufacture the support for the spines should satisfy the following demands:
• ensure that as many spines as possible will independently find asperities to attach;
• ensure that the total load is distributed among the spines uniformly.
If the spine failure problem could be solved by carefully selecting the materials, sizes and integrating methods of the spine in the support, these two demands require some complex manufacturing technologies in order to be satisfied, such as SDM, in order to create a compliant structure. As previous cited these structures have been already designed and used for the SpinyBotII [43, 44] and Rise [47, 48] platforms using SDM technologies.

Looking at the climbing surface the spine size can be different in the case of a tree climbing robot in comparison to a wall climbing robot, this introducing the need of creating gripping paws with different number and size of spines. However, being given the fact that the strength of the available materials for the manufacturing of the spines is very high, the number of spines needed by a robot of a certain weight is only decided by the strength of the asperities on the wall to be climbed combined with the weight of the robot.
The overall weight of the robot is also a constraint, deciding the autonomy of the robot and the safety coefficient. Robot structures (claw robots) have been created with weights above 0.4 kg. Accepting a total load per spine of 1.5 N, as previous discussed, the number of spines needed for a specific robot weight is available, taking into consideration also the safety coefficient of the robot.
Assuming a safety coefficient of 3, because a fall from a considerable distance would destroy the robot, the number of spines needed for a certain robot weight can be represented. Considering G as the total weight of the robot and the force needed to be sustained by the robot, M as the mass of the robot, g the gravitational acceleration, S the safety coefficient and the force at the spine/asperity contact as F_{sa} (here 1.5 N), the number of spines n is:

$$n = S \cdot G / F_{sa}$$

The values presented in Fig. 44 are expressed considering an ideal case in which

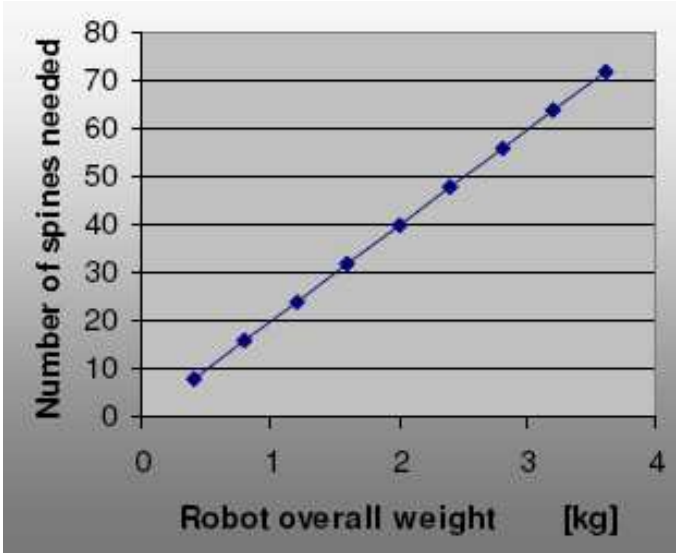

Figure 44: The linear dependency of the weight/number of spines

the spine tip radius is constant, which in reality is not and considering that the radius has a value that allows each particular spine to engage and stay engaged until release. Also, the approach and load angles and the friction coefficient are situated within the optimum intervals.
How many spines are actually necessary to push the robot upward on the substrate? The answer to this question lies within another question: how many legs are actively participating to the sharing of the robot's weight during climb?
Once found the supporting legs in every phase of the locomotion, using the overall weight of the robot combined with the results depicted in Fig. 44, it can be possible to assign a certain number of spines per leg. Analyzing a spider-robot structure (8 legs), it is possible to assume that in a locomotion step the robot moves at most 4 feet at the time, so the whole weight of the structure is loaded onto the attaching mechanisms of 4 feet.
This can be assumed as the critical load case, the case in which the smallest number of legs have to support the weight of the whole robot. The number of legs in contact is four but looking at the spider structure only the hind legs can be able to grip and exploit the spines, so the worst case becomes 2/3 legs. By taking the weight of the robot and correlating it with the number of spines needed the number of spines per foot required is determined. However, there is one overload factor that has not been accounted for in the calculus for the number of spines presented in this chapter, and that factor is inertia. The acceleration's influence on the gravitational force is to be neglected for the actual climbing speeds (e.g. 3cm/sec in SpinyBot II [43, 44]), but in the further development of fast climbing robots, with fast upward strokes the acceleration could have an important value.
Considering an 8 legged structure with a overall weight of 0.5 kg, using Fig. 44, and assuming that all the hind legs have a similar climb role the minimum theoretical number of spines resulted for that weight is around $5\ spines/leg \cdot 8 = 40\ spines$ (for the worst case of two legs; 1,5N/spine; Safety Factor = 3).

4.3 Setulae

In order to mimic the dry adhesives systems of the spider some considerations about the dimensions and the approaching behavior in the attaching and detaching phases must be developed.
Are there an angle and a succession of movements that enhance the adhesion and allow to attach and detach rapidly spiders' and geckos' feet?
Studying a finite element model of a setae Gao [11] made a step forward to answer this question. Two mechanisms of adhesion failure are been characterized depending on the pulling angle: sliding off and detachment. Looking at Fig. 45 it is possible to understand the results. The 30° condition is the limit of the two

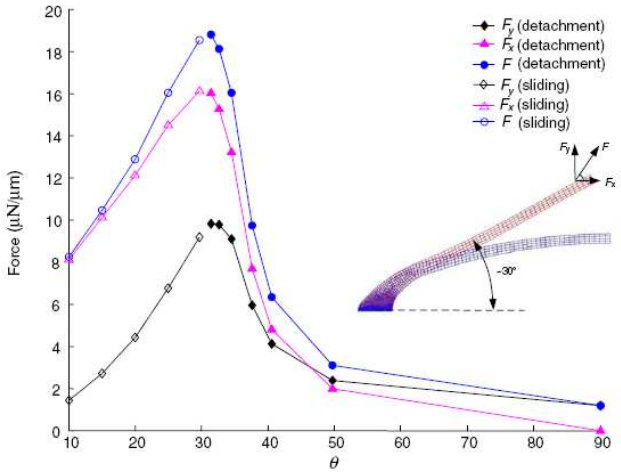

Figure 45: Pull-off force of a single seta vs pulling orientation [11].

conditions: with a smaller angle there is a sliding before detachment; with a larger angle there is detachment as a dominant adhesion failure condition.
It seems that the maximum adhesion condition is around 30° and that in order to maximize the adhesion a pulling phase with 30° is necessary. At angles bigger than 30° a smaller force is necessary for detaching the setae. This suggests that a suitable increasing of the setal angle allows to rapidly detach the setae from the substrate.
In a previous work Autumn [8], working with gecko's setae, pointed out that the detachment can be realized only increasing the setal shaft angle over 30°.

4.4 Anti-bunching conditions

Bunching occurs when different spatulae stick one to another. These microscopical structures have a high density and lateral contact can occur. In a recent study [52] it has been demonstrated that when a lateral adhesion between fibrillar structures occurs, the adhesion force reduces. The majority of the authors model the setae structure as a beam and consider two contiguous beams.
Sitti and Fearing in [26] modeled the setae as parallel fibers with radius R and length L. The minimum spacing Δ_{min} between two fibers is found in:

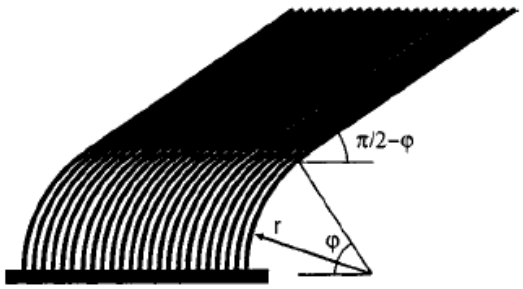

Figure 46: Model of the setae (from Persson [21])

$$\Delta_{min} = \frac{8 \cdot F_0 \cdot L^3}{3 \cdot \pi \cdot R^4 \cdot E}$$

where F_0 is the setae adhesion force and E_p the modulus of a cylindrical cantilever. Looking at the formula, as Sitti and Fearing observed, it is possible to underline as the smaller F_0 the smaller become the radius or the distance between the hairs. Stiffer setae allow greater density. Moreover short, fat hairs give higher allowable densities even if fat hairs are not desirable for adhering to rough surfaces.
Making the L/R ratio explicit, the result is:

$$\frac{L}{R} = \sqrt[3]{\frac{3 \cdot \pi \cdot \Delta \cdot E \cdot R}{8 \cdot F_0}}$$

Persson in [21] modeling the setae as long thin fibers (Fig. 46) works with an energetic approach. Looking at the relation between the elastic energy and the Van der Waals interaction force he finds an upper condensation limit for the ratio L/R. The equilibrium condition is:

$$\frac{L}{R} = (\frac{E \cdot R^{\frac{3}{2}}}{2 \cdot \gamma^* \cdot \Delta^{1/2}})^{\frac{1}{2}} \cdot \phi$$

where ϕ is the angle defined in Fig. 46 and γ^* the change in the surface free energy when two solids make contact. Other authors investigates the bunching and anti-bunching condition.
Recently Spolenack and al. in [53], starting from the Sitti results, models the interaction force with the JKR theory reaching the subsequent condition:

$$R \geq \frac{\gamma^* \cdot h(f)^{1/2}}{E} (\frac{L}{R})^3$$

with:

$$\frac{1}{h(f)} = (\frac{\sqrt{\pi}}{4 \cdot f} - 1)^2$$

and

$$f = \frac{R^2 \cdot \pi}{\Delta^2}$$

Gao in [11] models the spatula as a square cross section cantilever beam (Fig. 47)[1]. Considering that the condensed condition must be instable in order to have an anti-bunching condition, the result, rose from a crack propagation condition, is

[1] the real spatula has something like a rectangular section

clearly very similar to the one found by Sitti:

$$E \geq \frac{8 \cdot \gamma^* \cdot l^4}{3 \cdot \Delta^2 \cdot t^3}$$

where l and t are defined in Fig. 47. Exploiting the formula with respect to the ratio l/t, the result is:

$$\frac{l}{t} = \sqrt[4]{\frac{3 \cdot \Delta^2 \cdot E}{8 \cdot \gamma^* \cdot t}}$$

Substituting the approximative data (kept from the previous analysis): Δ= 0.3-0.7 μm, $\gamma^* = 0.01 - 0.05$ J/m^2, E= 1-4 GPA and as R or t the data of the setae and spatulae it is possible to find the anti-bunching dimensions and ratios depicted in table 6.

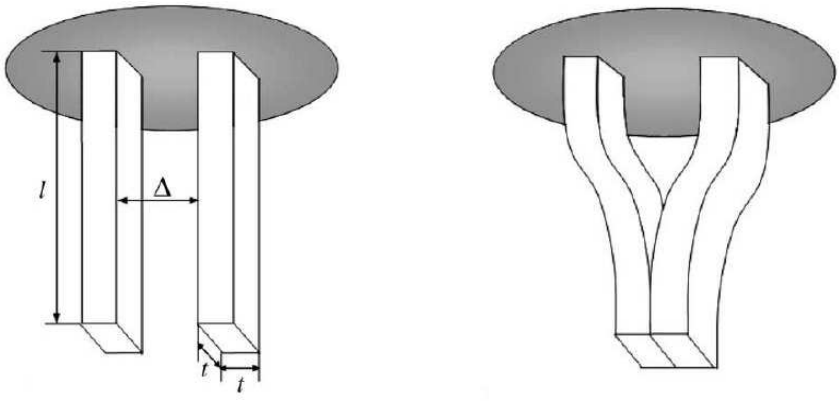

(a) (b)

Figure 47: Model of free and bunched adjacent spatulae

Data :	Δ	F_0	E	γ^*	R (t)
Spatulae			2 GPA	0.01 J/m^2	
Gecko	0.35μm	10 nN			0.1 μm
Spider	0.69μm	40 nN			0.15μm
	Gecko		Spider		
Results	L/R	L_{max}	L/R	L_{max}	
Sitti	25.5	2.6 μm	23.0	3.5 μm	
Persson	103.4	10.4 μm	118.3	17.7μm	
Spolenack	31.1	3.1 μm	42.7	6.4 μm	
Gao	20.7	2.1 μm	26.3	3.9 μm	

Table 6: Anti-bunching conditions

Looking at the biological data the natural setulae have length of about 2 μm and then they match the anti-bunching conditions.
From similar considerations it is possible to fix the dimensions of the fibers and define conditions on the relative distance or on the elastic modulus.
From this results it seems that a hierarchical structure is necessary if the anti-bunching condition and the surface roughness adaptation are desired. Indeed the

unique elasticity and dimensions of the spatulae level do not allow to bend and adhere in a good manner on no-flat surfaces, result that can be reasonably achieved with upper hierarchical levels.

5 Phase 3: Mechanical model and adhesion

Mechanical/Elastic model of the adhesion system of the spider

5.1 Introduction

Spiders and geckos have a hierarchical adhesion structure that give them the ability to adapt to different rough surfaces and create a large real area of contact.

In the previous sections the relation between the dimensions of setae and spatulae, and the overall adhesion has been defined.
Moreover the roughness adaptability, the anti condensation condition and the self-cleaning ability seems to be related to the hierarchy of the attachment systems. On rough surfaces the structure of the setae is an essential mechanisms to produce a high adhesion condition.
Recently Bhushan [54, 55] has demonstrated how, for the gecko, the hierarchical structure increases the contact area on a rough surface and the overall adhesion force. Starting from Bhushan's results and considerations the idea is to compare the adhesion force (from experimental data) and the elastic force stored in the structure, implementing a model that is loaded and unloaded on different rough surfaces. In the unloading phase the hierarchical elastic structure is put away gradually and the adhesion condition is checked for all the setulae elements. If the equivalent elastic energy stored into a setula becomes lower than the adhesion force, this setula is considered detached from the substrate and does not cooperate to the overall elastic force.
In this chapter a spring-based model of the dry adhesive system is analyzed and implemented with the spider dimensions and characteristics in order to answer the subsequent ideas:

- Are the dry adhesive system and spines convenient to maintain a high Safety Factor for any value of surface roughness?
- Is the hierarchical structure of the spider attaching elements necessary for adhering and sustaining the overall system on smooth surfaces?
- Can the variation of the stiffness of the upper hierarchical level of the system (due to a variation of the hydraulic pressure) result in a speed up of the detachment of the tarsus from the substrate?

In order to answer to these questions a first comparison between the spider and gecko system with a one-level model is carried out.

5.2 One-level model

The spatula (gecko)-setula (spider) is considered and modeled as a spring element with a spherical tip element, and all the springs of the same level have the

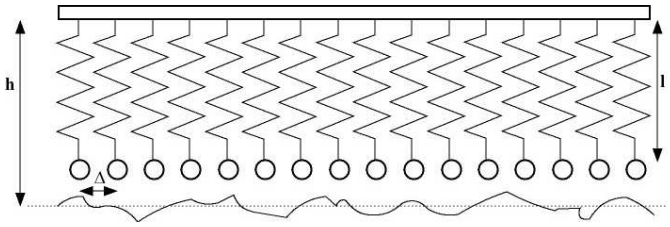

Figure 48: Single level model of the attaching system

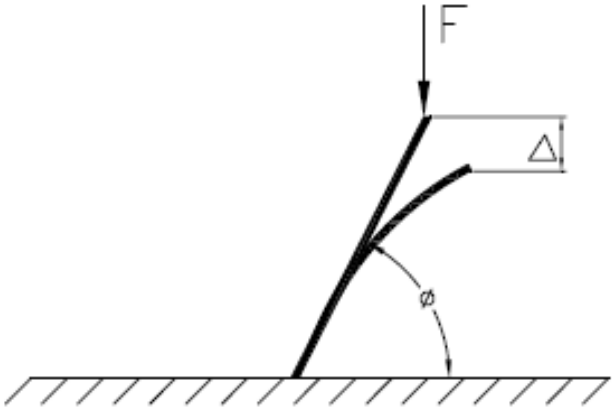

Figure 49: Cantilever model of a setulae-spatulae

same stiffness. The stiffness of every spring is assumed as the bending stiffness of the spatula-setula (Fig. 48). The approaching angle is considered equal to 30° in order to implement the optimal attachment condition and evaluate the maximum adhesion force. In order to deduce the stiffness of the spatula-setula a cantilever beam model is considered (Fig. 49). The applied force F is considered perpendicular to the substrate and can be decomposed in the $F \cdot cos(\theta)$ and $F \cdot sin(\theta)$ responsible of the bending (δ_b) and compressive (δ_c) deformation:

$$\delta_b = \frac{F \cdot cos(\theta) \cdot l^3}{3 \cdot E \cdot I},\ \delta_c = \frac{F \cdot sin(\theta) \cdot l}{A \cdot E}$$

where l is the length, I the moment of inertia ($\pi \cdot R^4/4$), R the radius, A the cross-sectional area ($\pi \cdot R^2$). The total stress becomes:

$$\delta_n = \delta_c \cdot sin(\theta) + \delta_b \cdot cos(\theta) = \frac{F \cdot cos^2(\theta) \cdot l^3}{3 \cdot E \cdot I} + \frac{F \cdot sin^2(\theta) \cdot l}{A \cdot E}$$

The stiffness of a single spatula-setula becomes:

$$k = \frac{\pi \cdot R^2 \cdot E}{l \cdot sin^2(\theta) \cdot (1 + \frac{4 \cdot l^2 \cdot cot^2(\theta)}{3 \cdot R^2})}$$

Considering a Young modulus of 2 GPa (materials such as keratin have Young modulus on the order of a few GPa) the stiffness of the setulae-spatulae can be calculated. Assuming a contact element-surface with the surface asperities modeled with a spherical tip, the interaction force can be evaluated thinking at two spheres. Looking at the JKR model the adhesion force is

$$F_{ad} = \frac{3}{2} \cdot \pi \cdot R_c \cdot E_{ad}$$

	Length	Diameter	K_b [N/m]	Density
Spatulae	2-5 μm	0.1-0.2 μm		100-1000 per setae
(chosen data)	2.5 μm	0.1 μm	0.0025	1.4-14$\cdot 10^6/mm^2$
Setulae	2-4 μm	0.1-0.4μm		
(chosen data)	2.5μm	0.2,0.4μm	0.0015,0.0233	2.1$\cdot 10^6/mm^2$

Table 7: Single level parameters

where R_c is the reduced radius:

$$((1/R_1) + (1/R_2))^{-1}$$

with R_1 and R_2 the radius of the surfaces in contact, here assumed as $R_1 = R_2$. The E_{ad}, the energy of adhesion, can be evaluated as $50 \div 66 mJ/m^2$. Working with the estimated radius of Table.8, the adhesion force becomes very close to the experimental ones both for the gecko and the spider [16, 3].
Looking at Fig. 48 the surface where the springs are mounted is assumed flat and stiff; the distance between the elements Δ, calculated from the density value, is: for the gecko 0.35 μm whereas for the spider 0.69 μm.
Hence, the spring deviation becomes

$$\Delta l = h - l - z$$

where z is the height of the surface profile.
The spring force can be expressed as:

$$F_{el} = -k \cdot \sum_i \Delta l_i \cdot u_i$$

where u_i=1 or 0 in case of contact or not.
In the attaching phase the springs are pushed toward the rough surface until the overall elastic force becomes equal to the weight of the animal.
In the detaching phase the springs are pulled until when the overall force $(F_{el} - F_{ad})$ at the interface becomes equal to 0. The adhesion force is considered as the lowest elastic force that causes the detachment of the system. The adhesion energy is:

$$E_{ad} = \int_{\infty}^{D^-} F_{el}(D) dD$$

D is the distance between the spring base and the contact surface after the detach.
The rough surface is created through a random generation code that assures the RMS amplitude value (σ) of the roughness and the correlation length (β^*). The length scales is assumed as 2000 μm (as in Bhushan [54, 55]), and in order to simulate natural surfaces σ varies between 0-5 μm and β^* is fixed to 200μm. The length scale has been chosen as 2000μm, because it is suitable for the two systems simulation.
Looking at the spider system there are some elements that must be taken into account in the implementation of the model:

- the number of the legs simultaneously in contact with the substrate;
- the load on a single leg;
- the surface area covered by a single leg of the *E.Arcuata* is $1.7 \cdot 10^5$ nm^2, about 1000 times smaller than the one of the gecko; then a scale length of 80 μN can give more accurate results;

Being the length scale 2000μm, the number of possible contacts become:

$$N = l_p/\Delta = 2000/0.69 = 2900$$

The applied load on the legs varies due to the spider specie. Looking at the data of the Table 1 and assuming:

- 4 legs in contact;
- load as the spider weight;
- num. of setulae/mm^2 equal for all the legs;
- 78000 setulae/foot

the force applied on a single setula for the *E.Arcuata* becomes 0.47 nN and the overall load on the considered length scale is 1.36μN.

5.2.1 Results

The first simulation compares the adhesion behavior of the gecko and *E.Arcuata* for different rough surfaces.
In Fig. 50 and in Table 8 are depicted and summarized the results.
For every considered roughness the system is brought near to the surface from a detached condition until when the overall elastic force stored in the system is equal to the load of the spider (i.e. max positive force). After that, the system is moved away until when the overall elastic force stored into the attached elements becomes smaller than the overall adhesion force (i.e. max negative point). Such a value is recorded and used for the evaluation of the safety factor of the system.
In Table 8 F_n is the normalized load force applied on the considered length scale; σ is the RMS roughness of the surface; F_{ad} is the force that have to be applied in order to detach the system from the surface; S.F. is the safety factor of the system. Three cases are evaluated: two for the spider model of the *E. arcuata* (tip radius of 0.1μm and of 0.2μm) and one for the gecko model.

	F_n [μN]	σ [μm]	S.F.	F_{ad} [N]
Spider *E.Arcuata*, 15mg,	1.37	0.01	**80.7**	$1.11 \cdot 10^{-4}$
0.1 μm radius, 3 μm length	1.37	0.1	35.6	$4.88 \cdot 10^{-5}$
k=0.0233	1.37	1	7.5	$1.03 \cdot 10^{-5}$
	1.37	5	**3.8**	$5.24 \cdot 10^{-6}$
Spider *E.Arcuata*, 15mg,	1.37	0.01	**39.9**	$5.46 \cdot 10^{-5}$
0.2 μm radius, 3 μm length	1.37	0.1	6.6	$9.06 \cdot 10^{-6}$
k=0.371	1.37	1	2.2	$3.03 \cdot 10^{-6}$
	1.37	5	**1**	$1.36 \cdot 10^{-6}$
Gecko,	1.6	0.01	**31.3**	$-5.01 \cdot 10^{-5}$
0.1 μm radius, 2.5 μm length	1.6	0.1	6.0	$-9.65 \cdot 10^{-6}$
k=0.0402	1.6	1	2.4	$-3.83 \cdot 10^{-6}$
	1.6	5	0.5	$-8.60 \cdot 10^{-7}$

Table 8: Single level parameters and results.

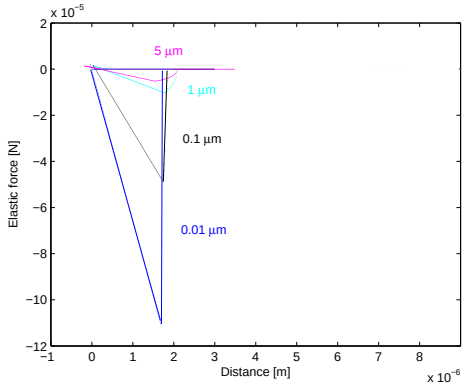

(a)

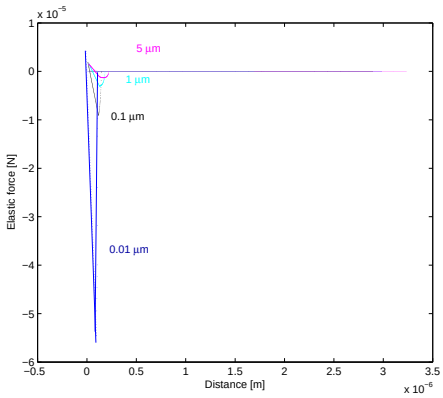

(b)

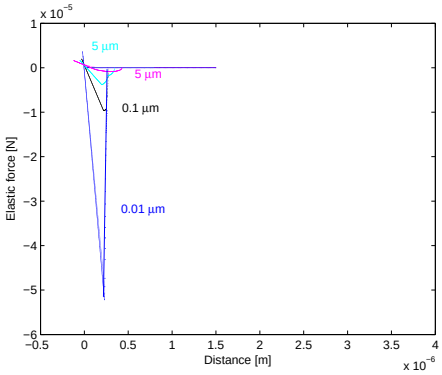

(c)

Figure 50: One level model simulation results: (a) *E. arcuata* with tip radius of 0.1μm. (b) *E. arcuata* with tip radius of 0.2μm. (c) Gecko with tip radius of 0.1μm.

Looking at the results it is possible to underline how the *E.Arcuata* has an optimal adhesion and a high safety factor when loaded on smooth surfaces. The safety factor coefficients of this spider are in the order of the the geckos' results and higher.
Moreover the dry adhesion seems to be possible in high roughness conditions and the safety factor is ≥ 1 also when the surface roughness presents a RMS value of 5 μm. Over this roughness the climbing capabilities can be exploited by the claws. Hence the spider seems to be a very powerful system capable to climb the most of the surfaces.

5.3 Three-level model

In order to analyze the enhancement of adhesion with a hierarchical level structure and go deep into the spiders' abilities a three level spring model has been developed. Looking at the spider systems it is possible to state that:

- the first level is constituted by the setulae with triangular shape tips called spatulae;
- the second level is constituted by the setae;
- the third level can be assumed as the tarsus (cuticolae).

For the data of the first and second level it is possible to refer to the Table 1. In order to define the third level some considerations have to be made.
It is known that the spider can change the pressure into some limbs and joints of the legs in order to actuate and stretch the joints. The spider can change the pressure inner the tarsus and, inflating pressure into the limb can reasonably change the overall stiffness of the cuticle and, as a consequence, of the third hierarchical level. For a better explanation of the principle it is possible to consider an inner tube. When little air is inflated, the outer surface of the tube shows a quite high degree of adaptation to the surface, a good compliance and a big area of contact with the substrate. If the inner tube is filled up, the stiffness increases, thus change the features of the system.
Considering the spiders' adhesion system, this changing of stiffness can result in more or less adhesion.
The attaching mechanisms of the *E.Arcuata* are located on the tip of the tarsus whereas for other spiders they are located over all the inferior side of the tarsus limb. Utilizing the model of the cantilever beam with circular section for the third level of the *E.Arcuata* a hypothetical bending stiffness of the highest level can be found.
The parameters used in the simulations are in Table 9. In Fig. 51 and in Table

Level	Length (μm)	Diameter (μm)	Bending stiffness (N/m)
III Tarsus	1000-5000	100-1000	40-630
II Setae	200	10-16	0.49-3.22
(chosen value)	200	13	1.40
I Spatulae	3	0.2-0.4	0.02-0.37

Table 9: Three level parameters of the *E.Arcuata*.

10 the comparison between a one-level structure and a three-level structure for the

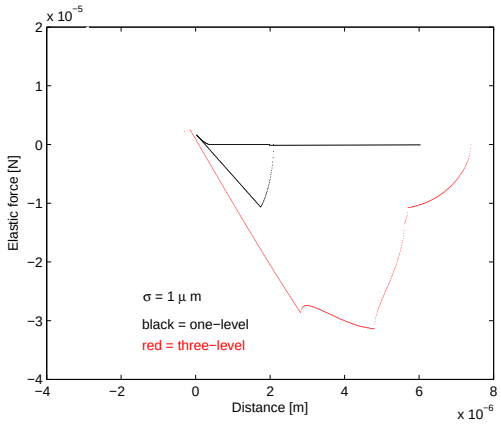

Figure 51: Comparison beetween one and three level systems.

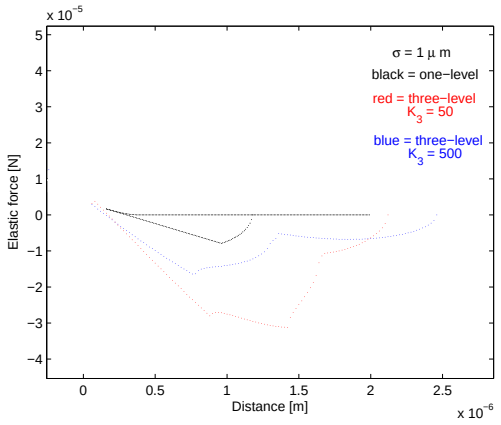

Figure 52: Different stiffness results.

E.arcuata is shown.

	F_n [μN]	σ [μm]	S.F.	F_{ad} [N]
Spider *E.Arcuata*,15mg. K_3=50	1.37	1	22.6	$3.11 \cdot 10^{-5}$
$K_3 = 500$	1.37	1	11.7	$1.6 \cdot 10^{-5}$

Table 10: Three level system results.

The results show that a three level system enhances the overall adhesion of the spider and allows to adhere in a suitable manner also on surfaces with a higher roughness with respect to the one level system.
Hence, a hierarchical level system is recommended in a bio-mimetic perspective in order to develop a system that can adapt on different roughness surfaces with a high degree of safety.

With respect to the variation of the stiffness of the third hierarchical level two different cases have been simulated (Fig. 52). The first one considers a value

of stiffness for the cuticolae hierarchical level kept as K_3= 50 N/m and the second one a stiffer value, K_3 = 500 N/m.
The results show that different stiffness of the first level correspond to different forces of adhesion.
In the evaluated case the overall force of adhesion becomes the half with respect to the first case.
As a conclusion it can be reasonably assumed that a possible fast detaching system, or an acceleration of it, can be made by the spider with a suitable variation of the stiffness of the first hierarchical level, hence with the variation of the inner pressure of the tarsal link.

6 Phase 4: Kinematics

Kinematic model of the spider system

6.1 Spiders' legs analysis and evaluation

6.1.1 Introduction

The spider's leg has seven limbs: coxa, trochanter, femur, patella, tibia, metatarsus and tarsus.
Coxa is the first limb between the body and other limbs. As there are seven limbs in the leg of a spider, there are seven joints to be examined. The overall motion of the joints and limbs could be explained with the comprehensive study of muscular and hydraulic systems. Hydraulic systems are responsible for the movement of some of the limbs rather than muscular systems. Muscular systems of limbs have been studied by various researchers. Those who studied more than one family, found significant differences among the species [56]. However, significant differences of limb lengths (ratios of the limb lengths of individual species) of various spider species, given some examples in appendix A, have been observed during the study. Such differences are expected since spiders have different characteristics of hunting or living conditions, environment and ecology, as well as climate. It has been assumed that joints of various spider species are the same with differing limitations; and these joints are of two types: monocondylar and bi(di)condylar. As Shultz and Sensenig [59, 57, 58] argued, bicondylar joints have one axis of movement and substantial angular movements during locomotion while monocondylar joint have multiple axes of movement and have little movement during locomotion. All the authors, except Parry [56], agree that most of these joints are bicondylar.

6.1.2 Coxa, trochanter and coxa-trochanter joint

Both coxa and trochanter are not measured by the scholars generally as they are extremely short -trochanter being the shortest limb. Parry [56], studying on common British spider *Tegenaria Atrica*, states there are eight muscles connecting coxa to trochanter, and a ninth muscle passing through the joint to insert on the femur. Furthermore, he argues coxa-trochanter joint is the only ball-and-socket joint in a spider leg while Foelix [60] defines the joint as a "saddle joint" being capable of moving forward and backward, adds the joint has a range of movement of 60 degrees in lateral plane (Y-Z plane) and 70 degrees in dorsal plane (X-Y plane) for the wandering spider *Cupiennius*. Fichter and Fichter [61] state the joint has two degrees of freedom, is restricted to a small arc and has limited range of motion. Shultz [59] also comments the joint has significant rotation movements. Hence there are two different views about this joint, either a 3-DOF ball-and-socket or a 2-DOF saddle joint. A ball-and-socket joint and a saddle joint are shown in 53(a),53(b).

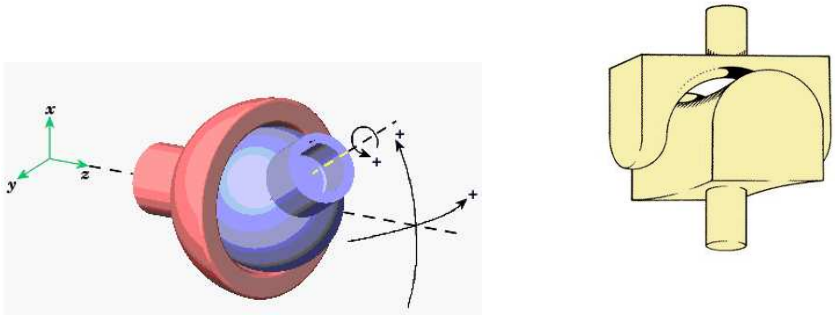

(a) (b)

Figure 53: A ball-and-socket joint with 3 degrees of freedom and a saddle joint with 2 DOFs, limiting the rotation (source: web)

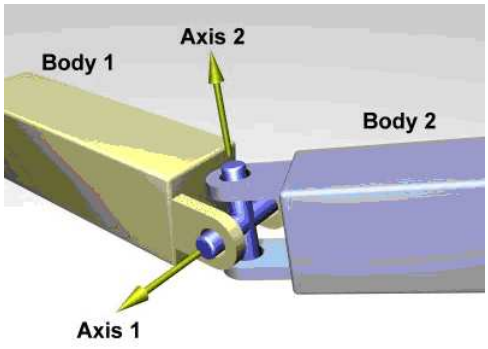

Figure 54: A universal joint with 2 DOFs (source: web)

6.1.3 Femur and trochanter-femur joint

Femur is the longest limb in some of the species, or second longest limb after metatarsus. According to Parry [56], four muscles are responsible for the articulation in trochanter-femur joint and it is the only dicondylic joint - while other authors agree there are more than one dicondylic joints- that limits the movement only in vertical plane because of lateral condyles. Fichter & Fichter [61] also state the joint has one degree of freedom while Foelix [60] agrees and states the range of movement for the joint is 105 degrees only in Y-Z plane.
It is more likely to model this joint as a universal joint with 2-DOF shown in Fig. 54

6.1.4 Patella and femur-patella joint

Patella is relatively small, has a slight concave shape, and is usually measured with tibia. Generally it is the second shortest limb of spiders after trochanter. Parry [56] states the articulation is along a dorsal hinge-line with condyles at each end resulting in the elimination of elevator muscles. There are two pairs of and one single muscle causing flexion. Ellis [62] also states flexor patellae bilobatus muscles produces strong flexion on the joint. However muscles originating on femur are more complex as they are also taking part in the movement of trochanter-femur

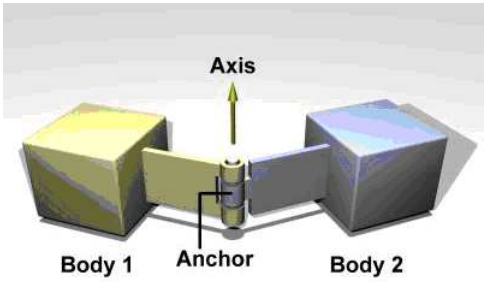

Figure 55: A hinge joint. 1 DOFs (source: web)

joint.
Foelix [60] discusses about the lack of extensor muscles for femur-patella joint that it can only flex. Both Ellis and Foelix agree that extension of the joint is enabled by a hydraulic mechanism. Foelix adds the joint has a range of 160 degrees in Y-Z plane, and Karner [63] gives a range of 60-170 degrees for the first legs and 50-130 degrees for the second legs for *Cupiennius salei*. Foelix agrees with Fichter and Fichter stating the joint has one DOF.
Hence this joint can be modeled as a hinge joint (Fig.55).

6.1.5 Tibia and patella-tibia joint

As mentioned, patella-tibia is usually considered as a unique system and is clearly much longer, mostly longer than femur when considered with patella. Parry [56] argues that this joint is free to move in a horizontal plane only, being capable of more retraction than protraction due to a pair of muscles. Foelix [60] argues the joint has a range of movement in 20 degrees in Y-Z plane and 70 degrees in X-Y plane. Shultz [59] states sun-spider *Eremocosta* has a natural range of motion of 150-90 degrees (60 degrees of motion) and the joint is assumed to be the main contributors to propulsion by the fourth leg of *Eremocosta*. Such a difference in the angles might be because of species studied. Fichter and Fichter [61], probably to simplify the motion in Y-Z direction, state that the joint has one DOF.
It is possible to model this joint aa a hinge joint, or a universal joint with very limited joint on Y-Z axis.

6.1.6 Metatarsus and tibia-metatarsus joint

Depending on the species, metatarsus could be either long- the longest limb - or relatively small - the second or third longest -. As Parry, Ellis and Foelix [60] stated, like femur-patella joint, extensor muscles are lacking for the joint and it is obtained by hydraulic systems. Flexion is provided by muscular systems, that are composed of two pairs of muscles according to Parry [56]. Ellis [62] argues "flexor metatarsi longus" muscles of the joint have the strongest flexor movement. According to Foelix the joint has a range of motion 125 degrees in Y-Z plane and

15 degrees in X-Y plane, where Shultz [59] states the range as 100-160 degrees, a total of 60 degrees of motion. Moreover Karner [63] scales the range as 80 to 170, a total of 90 degrees of movement. Fichter and Fichter [61] again states that the joint has one DOF.
It is also possible to assume this joint as a hinge joint, or a universal joint with very limited motion on X-Y axis, in contrast with patella-tibia joint.

6.1.7 Tarsus and metatarsus-tarsus joint

The tarsus, where the claws are attached, is a fairly short limb of a spider leg. There are no muscles directly associated with the joint and the disposition of the long tendons on metatarsus, originating on tibia, is responsible for the active movement of this joint (as Parry stated). Parry [56] argues the joint has no articular condyle therefore it is a universal one. Foelix argues the joint has 125 degrees of motion in Y-Z plane and 65 degrees of motion in X-Y plane where Shultz [59] ranges the motion of metatarsus-tarsus joint of a sun spider between 240 and 200 degrees. Fichter and Fichter [61] simplify the joint having one DOF.
According with Parry [56], this joint can be regarded as a universal joint.

6.1.8 Limb Lengths

As mentioned, spider legs differ a lot depending on the spider species or their ecology and so on. Therefore it is not plausible to state a longest or shortest limb for all species. Observation of twenty different spider species from Taiwan, North America and Africa made it possible to have a general idea about the rations of limb lengths. Limb lengths and their rations to each other or to other legs are stated in appendix. Although almost all of the ratios vary greatly for the set of reasons stated, two close ratios are found after studying of given number of spiders:
Femur/Patella+tibia ratio is between 0.85 and 1.05.
Femur/Metatarsus+tarsus ratio is between 0.75 and 0.8.

6.1.9 Leg with limit angles and arbitrary positions

In the first figure the lateral view of a spider leg with the ranges of motion for each joint in Y-Z plane is presented (Fig. 56); the angles are estimated from the results of above described. The second figure (Fig. 57) is a simplified dorsal view of a spider leg, dashed arrows show the range of motion and the sketch is based on Foelix' results [60].

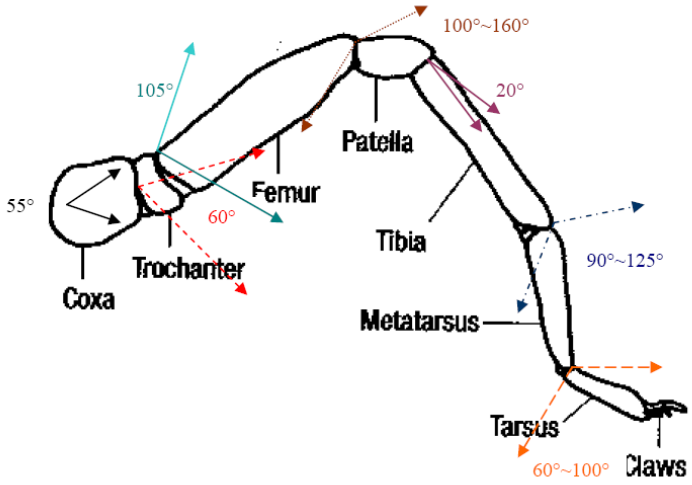

Figure 56: Ranges of motion for joints in Y-Z plane

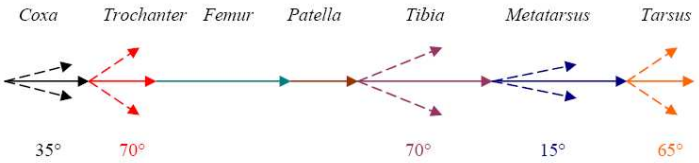

Figure 57: Ranges of motion for joints in X-Y plane

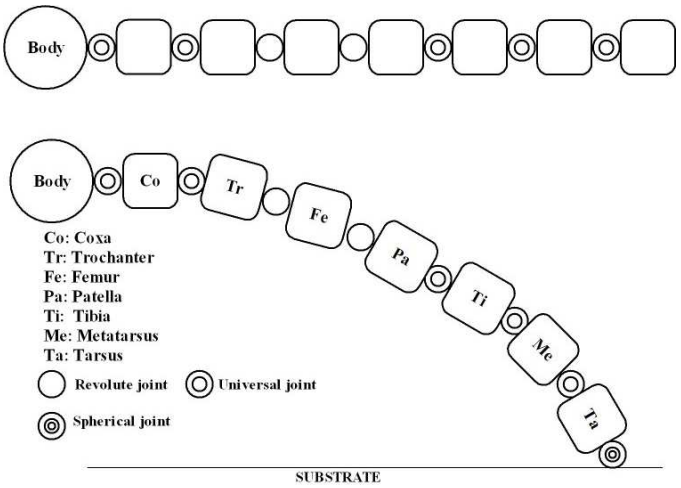

Figure 58: Sketch of the spiders' leg kinematics

6.2 Spider kinematics

6.2.1 Introduction

The ability of the spiders to walk and climb most of the natural and artificial surfaces, to overcome obstacles and change direction in a fast and suitable manner is surely related to their particular structure and shape. As a consequence, in order to better understand how the spider behaves in different environments and external conditions, the kinematics structure must to be evaluated.
Studying and solving the kinematics of the leg of the spider can give more information as regards as the pre-attaching and de-attaching phases. Considering that the adhesion of a single feet depends on the approaching angle of the attachment elements and on the sequence of active movements made by the tarsus and the leg, constraints and directives in order to create a robot prototype become available with the knowledge of the kinematics.
Studying and solving the kinematics of the overall spider can result in important information on the climbing ability because not only the position of the center of mass becomes available but also a comparative study between the position assumed by the spider in the real word and the available inverse kinematics solutions of the system can help to understand the strategies and the decision rules of the spider.

6.2.2 Spiders' mobility

Starting from the results and considerations made in section 6.1, the kinematic chain of a single leg can be represented in the free flight (i.e. leg non in contact with the substrate) as well as in the contact (i.e. leg in contact with the substrate) conditions (Fig. 58). The mobility of all the joints and the degrees of freedom per leg depend on the position and condition of the leg that alter the total number of degrees of freedom.

The mobility equation (Kutzback equation) is:

$$d = 6 \cdot (n-1) - \sum_{i=1}^{j}(6 - f_i)$$

where:

- n = n° of links;
- j = n° of joints;
- f_i = n° of DOF per every joint;
- d = n° of DOF per leg.

In the free flight configuration the spider leg can be viewed as a manipulator with 7 joints (2 of class 1, 5 of class 2) while, when the spiders' leg is in contact with the surface an equivalent additional spherical joint must be considered.
Then, substituting these numbers in the mobility formula, in the free flight case:

$$d = 6 \cdot (8-1) - (4+4+5+5+4+4+4) = 12$$

and in the contact case:

$$d = 6 \cdot (9-1) - (4+4+5+5+4+4+4+3) = 15$$

Looking at the overall spider system, the mobility can be calculated with the Kutzback formula or as made by Fichter and Fichter in [61]:

$$M = 6 \cdot (n-1) - \sum_{i=1}^{j}(6 - f_i) = g \cdot (d-6) + 6$$

where:

- g = number of legs on the substrate;
- d = DOF per leg;

In Tab.(11) are shown the mobility results considering the number of legs in contact (g) and the number of DOF per leg (d). Looking at the results when the DOF per leg is $d > 6$, an increase of the rested legs brings to an augmentation of the overall mobility of the system. If $d < 6$ an increase of the rested legs brings to a reduction of the overall mobility of the system. When $d = 6$ the mobility of the system is 6 in spite of the number of legs in contact with the surface.
In case of mobility = 6 the body of the spider can move in all the directions and with all the orientations. If the position and orientation of the body is defined only a finite number of positions for every link is allowed.
If $M = 0$ at least one leg must be raised up from the substrate in order to move the body, while when $M > 6$ at least one pair can assume infinite values with a body position and orientation defined.
Looking at the mobility of the real spider it is possible to underline that the system has 78 DOF when 8 legs are in contact with the surface and 42 DOF when 4 legs are in contact with the surface. Spiders' legs are used not only for walking but

d	**g**							
	1	2	3	4	5	6	7	8
3	3	0	-3	-6	-9	-12	-15	-18
4	4	2	0	-2	-4	-6	-8	-10
5	5	4	3	2	1	0	-1	-2
6	6	6	6	6	6	6	6	6
7	7	8	9	10	11	12	13	14
8	8	10	12	14	16	18	20	22
9	9	12	15	18	21	24	27	30
10	10	14	18	22	26	30	34	38
11	11	16	21	26	31	36	41	46
12	12	18	24	30	36	42	48	54
13	13	20	27	34	41	48	55	62
14	14	22	30	38	46	54	62	70
15	*15*	*24*	*33*	*42*	*51*	*60*	*69*	*78*

Table 11: Mobility of the system.

also for manipulating objects, capturing prey and sensing the environment. These tasks can justify the complexity of the system that is unimaginable to mimic in a bio-robotic perspective. Due to these considerations a reduction of the complexity of the system has to be made.
The robotic system has to allow the control of the body system and, consequently, must have at least 6 DOF (3 positions, 3 rotations). The number of DOF per leg has to be $d \geq 6$ but the smallest as possible in order to be feasible.
In the previous analysis it emerged that for controlling the adhesion of every leg the approaching angle must be suitably controlled. As a consequence, at least one extra degree of freedom per leg has to be available in order to define and control the approaching angle between the tarsus link and the substrate.
Thus, the DOF per leg have been chosen as 7.

6.2.3 Model

The model of the spider, with the previous considerations, consists in an eight legged structure with a body modeled with a hemispherical element with radius r_{body}.
The legs are radially collocated with respect to the body and with a step between two legs of 45°. The first leg is rotated at 22.5° on the Z axis with respect to the X axis of the body. In such a manner the system is symmetrical and can be viewed as head-less and tail-less (Fig. 59). The legs structure is the same for all the 8 legs.
In order to assure a correct mobility, every leg is defined with 7 DOF in a suitable configuration with three links and three joints.
In Fig. 60 is shown the chosen leg model. Limits for links and joints of the leg model in a first analysis are chosen as those of the corresponding real spider:

- 1^{st} joint. Universal joint with two DOF and limits:
  - θ_1 range = 70°;
  - θ_2 range =105°;
  The 1^{st} revolute joint works on the XY plane;

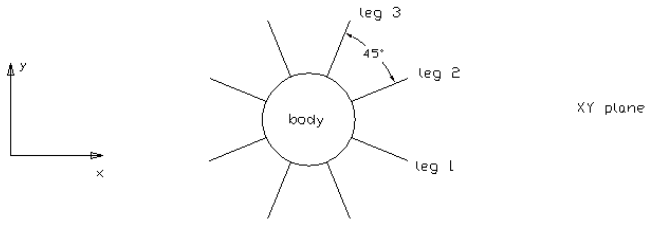

Figure 59: Shape and geometry of the robotic model of the spider.

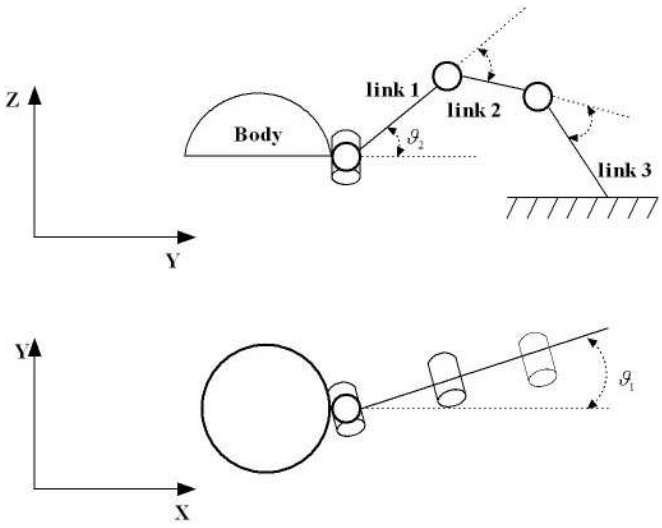

Figure 60: Reduced model of the spider leg.

The 2^{nd} revolute joint works in the YZ plane;

- 2^{nd} joint: revolute joint and limit θ_3 range =160°;
- 3^{rd} joint: revolute joint and limit θ_4 range =115°;
- link 1. Femur:
  - length $len_f = k_1 \cdot len_m$, with $k_1 = 0.75 - 0.8$;
- link 2. Tibia:
  - length $len_t = \frac{(k_1 \cdot len_m)}{k_2}$, with $k_2 = 0.85 - 1.05$;
- link 3. Metatarsus:
  - length len_m (in the model chosen equal to 1).

When the leg is in contact with the surface an additional spherical joint has to be considered in order to properly model the contact condition. Moreover this condition allows to close the kinematics chain and to study the overall kinematics in a correct manner. When the leg system touches the substrate and adheres to it, the contact point becomes a known fixed point, thus creating a closed kinematic chain.

6.2.4 Approaching angle

The approaching angle of the attaching elements must be carefully controlled in the locomotion in order to realize a suitable adhesion.
The idea is to allow to control a bio-mimetic attaching hierarchical structure placed on the tip of the (meta)tarsus link in a suitable manner. Looking at Fig. 61, representing a sketch of a frontal view of a leg, the approaching angle is θ_A.

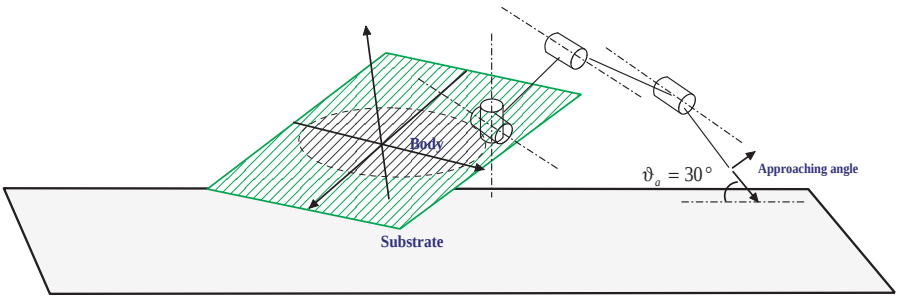

Figure 61: Sketch of the leg-model and of the approaching angle.

6.3 Kinematic analysis

The study of the kinematics of the spider model allows the definition of the conditions to position the body and control the approach angle.

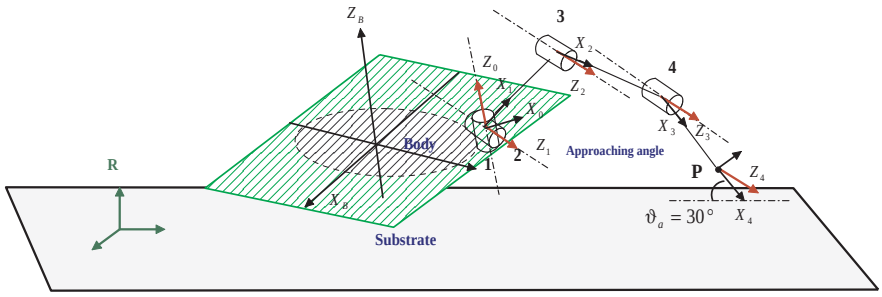

Figure 62: DH coordinate systems of a spider leg.

The coordinate systems are fixed with the Denavit-Hartemberg (DH) convention (Fig. 62, [65]).
The kinematics chain is made by:

- coordinate system R: Reference;
- coordinate system B: located in the middle point of the Body;
- coordinate system 0: located in the middle point of the pair 0;
- coordinate system 1: located in the middle point of the pair 1;
- coordinate system 2: located in the middle point of the pair 2;
- coordinate system 3: located in the middle point of the pair 3;
- coordinate system 4: leg end-effector coordinate system.

The DH parameters starting from the body reference system are represented in Table 12 . Due to the task to satisfy the system can be viewed with different

	d_i	θ_i	a_i	α_i
Body $\rightarrow$ 0	0	θ_0	len_{hip}	0
0 $\rightarrow$ 1	0	θ_1	0	$\frac{\pi}{2}$
1 $\rightarrow$ 2	0	θ_2	len_f	0
2 $\rightarrow$ 3	0	θ_3	len_t	0
3 $\rightarrow$ 4	0	θ_4	len_m	0

Table 12: DH parameters for a spider leg.

approaches. Two possible targets can be defined:

1. Free-flight kinematics: considering the body as fixed, the target is to solve the direct and inverse kinematics problem for the free flight condition of a leg, hence for the open-chain configuration;
2. Contact (Body)-kinematics: considering the position of the contact points between the supporting legs (legs in contact with the substrate) and the substrate as fixed, the target is to solve the direct and inverse kinematics of the system in order to control the position and orientation of the body.

6.3.1 Free-flight kinematics

In this analysis the body position and orientation are known and the purpose is to control the end of the legs.

Direct kinematics

The position of the end-effector is known once defined the values of the revolute pairs. Considering A_i^j as the roto-translation matrix between the joint j and i the direct kinematics equation becomes:

$$\mathbf{A}_4^R = \mathbf{A}_B^R \cdot \mathbf{A}_0^B \cdot \mathbf{A}_1^0 \cdot \mathbf{A}_2^1 \cdot \mathbf{A}_3^2 \cdot \mathbf{A}_4^3$$

The matrix A_B^R is known and the body can be considered as the Base coordinate system. The direct kinematics problem becomes:

$$\mathbf{A}_4^B = \mathbf{A}_0^B \cdot \mathbf{A}_1^0 \cdot \mathbf{A}_2^1 \cdot \mathbf{A}_3^2 \cdot \mathbf{A}_4^3$$

with the θ_0 parameter of the A_0^B fixed and related to the considered leg. Being fixed the relation between the B and 0 coordinate systems, the remaining matrices become [2]:

$$\mathbf{A}_1^0 = \left[\begin{array}{ccc|c} c_1 & 0 & s_1 & 0 \\ s_1 & 0 & -c_1 & 0 \\ 0 & 1 & 0 & 0 \\ \hline 0 & 0 & 0 & 1 \end{array}\right]$$

$$\mathbf{A}_2^1 = \left[\begin{array}{ccc|c} c_2 & -s_2 & 0 & len_f \cdot c_2 \\ s_2 & c_2 & 0 & len_f \cdot s_2 \\ 0 & 0 & 1 & 0 \\ \hline 0 & 0 & 0 & 1 \end{array}\right]$$

$$\mathbf{A}_3^2 = \left[\begin{array}{ccc|c} c_3 & -s_3 & 0 & len_t \cdot c_3 \\ s_3 & c_3 & 0 & len_t \cdot s_3 \\ 0 & 0 & 1 & 0 \\ \hline 0 & 0 & 0 & 1 \end{array}\right]$$

$$\mathbf{A}_4^3 = \left[\begin{array}{ccc|c} c_4 & -s_4 & 0 & len_t \cdot c_4 \\ s_4 & c_4 & 0 & len_t \cdot s_4 \\ 0 & 0 & 1 & 0 \\ \hline 0 & 0 & 0 & 1 \end{array}\right]$$

The rototranslation matrix between the coordinate system 4 and 0 is:

$$\mathbf{T}_4^0 = \mathbf{A}_1^0 \cdot \mathbf{A}_2^1 \cdot \mathbf{A}_3^2 \cdot \mathbf{A}_4^3 = \left[\begin{array}{ccc|c} \mathbf{a}^0 & \mathbf{n}^0 & \mathbf{s}^0 & \mathbf{p}^0 \\ \hline 0 & 0 & 0 & 1 \end{array}\right]$$

where the approaching vector $\mathbf{a}^0$ is related to the X axes of the last coordinate system.

[2] $c_i = cos(\theta_i)$ and $s_i = sin\theta_i$

Inverse kinematics

The inverse kinematics problem solution can be found by looking at the particular configuration of the leg system (Fig. 62). In the body reference system the unique revolute pair that works in the XY plane is the first (θ_1).
Letting $\mathbf{P}$ be:

$$\mathbf{P} = \begin{bmatrix} p_x \\ p_y \\ p_z \\ 1 \end{bmatrix}$$

θ_1 has 2 possible values:

$$\theta_1 = atan2(p_y^0, p_x^0)$$

$$\theta_1 = \pi + atan2(p_y^0, p_x^0)$$

The residual chain is a planar manipulator with three links (Fig. 63).
The $2, 3$ and 4 joints make a dyad and the inverse kinematics can be analytically solved.
Calling $\phi = \theta_1 + \theta_2 + \theta_3$ the overall rotation on the $\mathbf{Z}$ axis of the joint 2 coordinate system, the position of the center of mass of the 4^{th} revolute pair ($\mathbf{P4}$) becomes:

$$\mathbf{P4} = \begin{bmatrix} p4_x \\ p4_y \\ p4_z \\ 1 \end{bmatrix} = \mathbf{p}^0 - len_m \cdot \mathbf{a}^0$$

where $\mathbf{a}^0$ is known once defined the target and the approaching angle. For θ_3 holds:

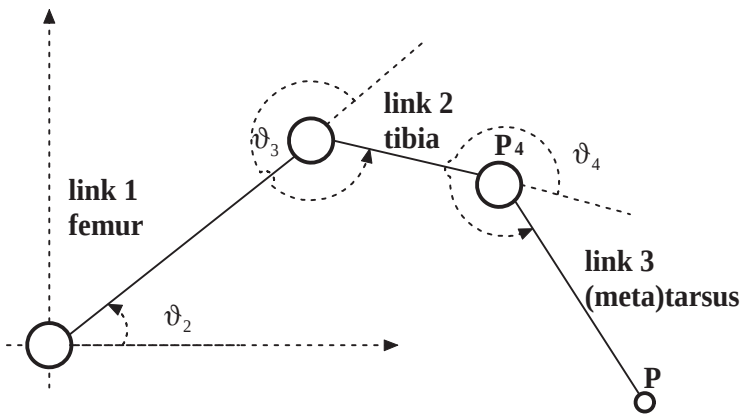

Figure 63: Model of the spider-robot leg.

$$c_3 = \frac{p4_x^2 + p4_y^2 + p4_z^2 - len_f^2 - len_t^2}{2 \cdot len_f \cdot len_t}$$

$$s_3 = \pm\sqrt{1 - c_3^2}$$

and the solutions are:

$$\theta_3 = atan2(s_3, c_3)$$

Once θ_3 has been computed, θ_2 can be found.
With some manipulations two equations in two unknown quantities can be found:

$$c_2 = \frac{(len_f + len_t \cdot c_3) \cdot \sqrt{p4_x^2 + p4_y^2} + len_t \cdot s_3 \cdot p4_z}{p4_x^2 + p4_y^2 + p4_z^2}$$

$$s_2 = \frac{(len_f + len_t \cdot c_3) \cdot p4_z - len_t \cdot s_3 \cdot \sqrt{p4_x^2 + p4_y^2}}{p4_x^2 + p4_y^2 + p4_z^2}$$

and the solution is:

$$\theta_2 = atan2(s_2, c_2)$$

directly linked to the θ_3 solutions. Being:

$$\theta_4 = \phi - \theta_2 - \theta_3$$

for θ_4 there are two solutions. Hence, for the inverse kinematics of this model 4 possible solutions are found.

Singularities

Two types of singularity can be found in the considered kinematics chain:

- **knee**: it occurs when $\theta_3 = 0$ or π, when tibia and femur are aligned.
  In this case one degree of mobility is lost and an arbitrary motion rule on the end-effector cannot be defined;
- **ankle**: it occurs when $p_x = p_y = 0$ that is when the **P** point is on the **Z** axis of the 0 coordinate system.
  With such a condition, infinite solutions can be found for the inverse kinematics problem because for all the possible θ_1 the **P** point is in the same position.

The described singularities can be found by studying the Jacobian **J** of the system because it is related to the:

$$\mathbf{v} = \mathbf{J} \cdot \dot{\mathbf{q}}$$

where **v** is the end-effector velocity vector:

$$\mathbf{v} = \begin{bmatrix} \dot{\mathbf{p}} \\ \omega \end{bmatrix}$$

and $\dot{\mathbf{p}}$ the translation velocity of **P** and ω the angular velocity vector. A singularity occurs when the $det(\mathbf{J}) = 0$ and the $\mathbf{J}^{-1}$ can not be found.
The Jacobian matrix related to the considered leg system is:

$$\begin{aligned} \mathbf{J}(\mathbf{q}) &= \begin{bmatrix} \mathbf{J}_1 & \mathbf{J}_2 & \mathbf{J}_3 & \mathbf{J}_4 \end{bmatrix} \\ &= \begin{bmatrix} \mathbf{z}_0 \times (\mathbf{p} - \mathbf{p}_0) & \mathbf{z}_1 \times (\mathbf{p} - \mathbf{p}_1) & \mathbf{z}_2 \times (\mathbf{p} - \mathbf{p}_2) & \mathbf{z}_3 \times (\mathbf{p} - \mathbf{p}_3) \\ \mathbf{z}_0 & \mathbf{z}_1 & \mathbf{z}_2 & \mathbf{z}_3 \end{bmatrix} \end{aligned}$$

where:

$$\mathbf{p}_0 = \mathbf{p}_1 = \begin{bmatrix} 0 \\ 0 \\ 0 \end{bmatrix}$$

$$\mathbf{p}_2 = \begin{bmatrix} len_f \cdot c_{\theta_2} \cdot c_{\theta_1} len_f \cdot c_{\theta_2} \cdot s_{\theta_1} \\ len_f \cdot s_{\theta_1} \end{bmatrix}$$

$$\mathbf{p}_3 = \begin{bmatrix} (len_t \cdot c_{\theta_2+\theta_3} + len_f \cdot c_{\theta_2}) \cdot c_{\theta_1} \\ (len_t \cdot c_{\theta_2+\theta_3} + len_f \cdot c_{\theta_2}) \cdot s_{\theta_1} \\ len_t \cdot s_{\theta_2+\theta_3} + len_f \cdot s_{\theta_2} \end{bmatrix}$$

$$\mathbf{p} = \begin{bmatrix} (len_m \cdot c_{\theta_2+\theta_3+\theta_4} + len_t \cdot c_{\theta_2+\theta_3} + len_f \cdot c_{\theta_2}) \cdot c_{\theta_1} \\ (len_m \cdot c_{\theta_2+\theta_3+\theta_4} + len_t \cdot c_{\theta_2+\theta_3} + len_f \cdot c_{\theta_2}) \cdot s_{\theta_1} \\ len_m \cdot s_{\theta_2+\theta_3+\theta_4} + len_t \cdot s_{\theta_2+\theta_3} + len_f \cdot s_{\theta_2} \end{bmatrix}$$

$$\mathbf{z}_0 = \begin{bmatrix} 0 \\ 0 \\ 1 \end{bmatrix} \quad \mathbf{z}_1 = \mathbf{z}_2 = \mathbf{z}_3 = \begin{bmatrix} s_{\theta_1} \\ -c_{\theta_1} \\ 0 \end{bmatrix}$$

$$\mathbf{J}_1 = \begin{bmatrix} -s_{\theta_1} \cdot (len_m \cdot c_{\theta_2+\theta_3+\theta_4} + len_t \cdot c_{\theta_2+\theta_3} + len_f \cdot c_{\theta_2}) \\ c_{\theta_1} \cdot (len_m \cdot c_{\theta_2+\theta_3+\theta_4} + len_t \cdot c_{\theta_2+\theta_3} + len_f \cdot c_{\theta_2}) \\ 0 \\ 0 \\ 0 \\ 1 \end{bmatrix}$$

$$\mathbf{J}_2 = \begin{bmatrix} -c_{\theta_1} \cdot (len_m \cdot s_{\theta_2+\theta_3+\theta_4} + len_t \cdot s_{\theta_2+\theta_3} + len_f \cdot s_{\theta_2}) \\ -s_{\theta_1} \cdot (len_m \cdot s_{\theta_2+\theta_3+\theta_4} + len_t \cdot s_{\theta_2+\theta_3} + len_f \cdot s_{\theta_2}) \\ len_m \cdot c_{\theta_2+\theta_3+\theta_4} + len_t \cdot c_{\theta_2+\theta_3} + len_f \cdot c_{\theta_2} \\ s_{\theta_1} \\ -c_{\theta_1} \\ 0 \end{bmatrix}$$

$$\mathbf{J}_3 = \begin{bmatrix} -c_{\theta_1} \cdot (len_m \cdot s_{\theta_2+\theta_3+\theta_4} + len_t \cdot s_{\theta_2+\theta_3}) \\ -s_{\theta_1} \cdot (len_m \cdot s_{\theta_2+\theta_3+\theta_4} + len_t \cdot s_{\theta_2+\theta_3}) \\ len_m \cdot c_{\theta_2+\theta_3+\theta_4} + len_t \cdot c_{\theta_2+\theta_3} \\ s_{\theta_1} \\ -c_{\theta_1} \\ 0 \end{bmatrix}$$

$$\mathbf{J}_4 = \begin{bmatrix} -c_{\theta_1} \cdot len_m \cdot s_{\theta_2+\theta_3+\theta_4} \\ -s_{\theta_1} \cdot len_m \cdot s_{\theta_2+\theta_3+\theta_4} \\ len_m \cdot c_{\theta_2+\theta_3+\theta_4} \\ s_{\theta_1} \\ -c_{\theta_1} \\ 0 \end{bmatrix}$$

It is a 6x4 matrix where the first three lines are related to the linear velocity of the end-effector whereas the other three lines are related to the angular velocity.
From the mobility study there are 4 DOF for this manipulator. The linear velocities and only one angular velocity can be arbitrary imposed.
In order to study the singularities of the system the first three lines and the fifth are chosen. The fifth line is chosen in order to avoid an extra singularity condition arising when the θ_1 equal to $+\frac{\pi}{2}$ or $-\frac{\pi}{2}$.
The determinant of the resulting matrix is:

$$\begin{aligned} Det(\mathbf{J}) &= len_f \cdot len_t \cdot c_{\theta_1} \cdot s_{\theta_3} c_(len_f \cdot c_{\theta_2} + \\ &\quad + len_t \cdot c_{\theta_2+\theta_3} + len_m \cdot c_{\theta_2+\theta_3+\theta_4}) \end{aligned}$$

and the singularities are:

- **knee** for:

$$\theta_3 = 0 \quad \theta_3 = \pi$$

- **ankle**, that occurs when the center of the revolute joint 4 is on z_0:

$$p_x = p_y = 0$$

6.3.2 Working space

An analysis of the working space of a single leg can define limits and abilities of the spider model.
The reachable working space is the space defined by the tip of the leg with any orientation. Looking at the Fig. 63, when the $\theta_3 = \theta_4 = 0$ the farthest points are reached. Turning on the total allowable range of θ_2, the largest circumference arch is defined. Fig. 64 shows the reachable working space with an approaching angle between 20° and 90° and θ_1 fixed. Considering that the optimal approach condition is near 30° and the detachment occurs at bigger angles, in Fig. 65 the two areas related to the optimal approaching angle and optimal detaching angle with respect to a level surface are highlighted. Looking at Fig. 65, only the green area (i.e. optimum angle) assures the adhesion of the leg.
The working area is limited and in order to switch between an adhesion condition to a detaching one, the unique way seems to be an enhance of the body height. However, such a condition is surely not advisable.
The imposed joint limits are the limits of the real spider joints but they do not take into account the reductions applied to the model. Hence in order to study and model in a correct manner the leg system, the joint limits have to be relaxed considering the coupling of consecutive elements. The coxa-trochanter and the trochanter-femur joints are coupled into an unique joint and then, looking at Fig. 56, θ_2 can be limited between ±90° with an overall angle of 180°. The θ_3 angle represents the fusion of the femur-patella and patella-tibia joints and can be limited at $+10°, -150°$ with an overall angle of 190°. Such a limit is further relaxed on ±150 in order to allow to reach both the configurations depicted in Fig. 66. The θ_4 angle is the fusion of the tibia-metatarsus and metatarsus-tarsus joints and it can be limited to ±115° with an overall angle of 230°.

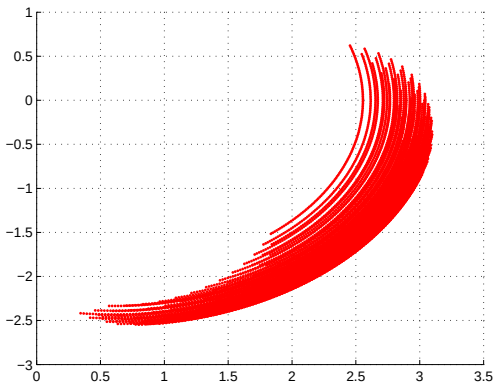

Figure 64: Working space of the spider-robot leg ([0,0] is the center of the revolute pair 1).

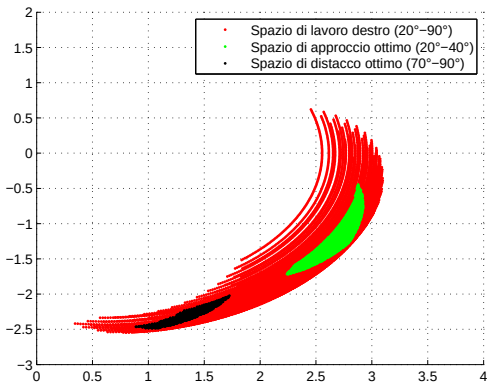

Figure 65: Dexterity analysis of the spider-robot leg ([0,0] is the center of the revolute pair 1).

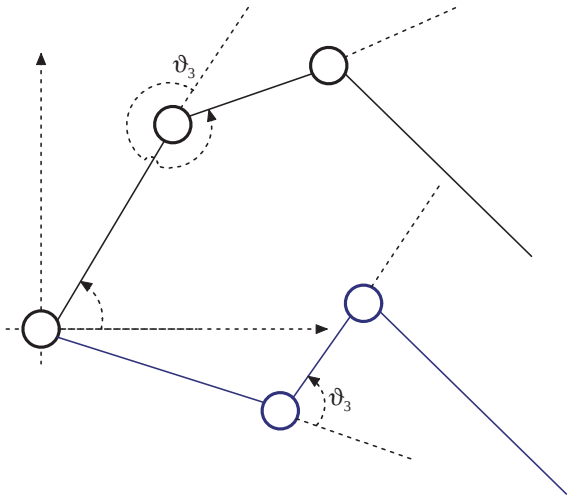

Figure 66: Allowed configurations.

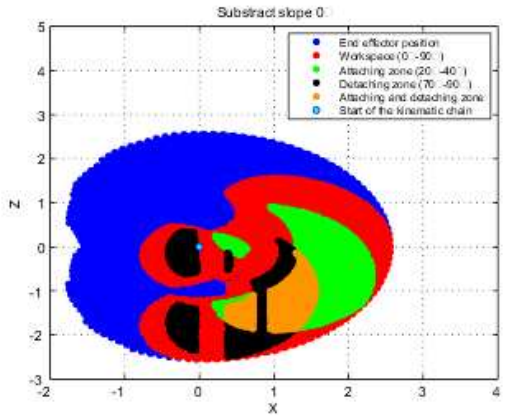

Figure 67: Dexterity of the spider-leg model with the new limits ([0,0] is the center of the revolute pair 1).

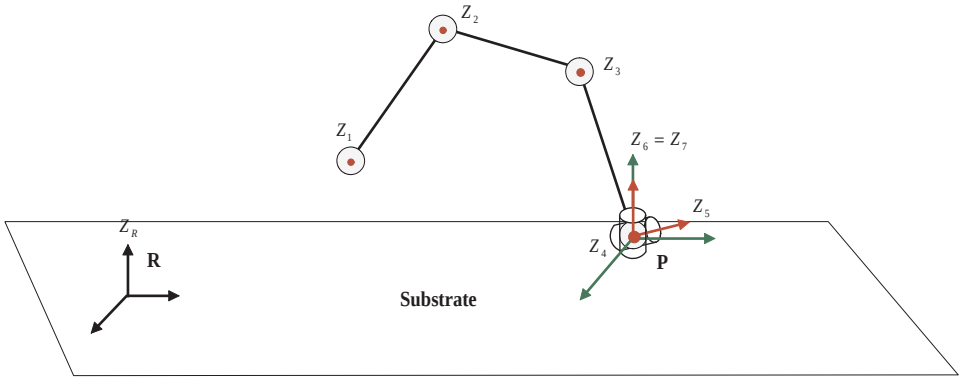

Figure 68: Model of the leg in contact.

Thanks to these assumptions, the dexterity of the spider leg changes and the results are depicted in Fig. 67 where no assumptions are made on the possible collisions with the body. The results confirm the validity of the choices. The working area and the attaching region are larger and these improvements will help the choice of the solution in order to implement a suitable locomotion gait and switch between the attaching and the detaching condition.
The new dexterity of the leg allows to define points at the same height that can be reached both with an angle suitable for the adhesion and for the detaching.

6.3.3 Kinematics of the leg in contact

When a leg touches the substrate the kinematics of the system changes. In such a case an extra spherical joint between the (meta)tarsus and the surface has to be considered. Hence a different kinematic problem appears. In Fig. 68 and in Table 13 the additional DH coordinate systems are imposed and the parameters defined.

The substrate and the center of gravity of the virtual spherical joint become the known elements while the position and orientation of the spider's body (6 DOF) are the target element to control. From the mobility analysis this system has 7

	d_i	θ_i	a_i	α_i
$4 \rightarrow 5$	0	θ_5	0	$-\frac{\pi}{2}$
$5 \rightarrow 6$	0	θ_6	0	$\frac{\pi}{2}$
$6 \rightarrow 7$	0	θ_7	0	0

Table 13: Additional DH parameters.

DOFs and admits ∞^1 solutions for the task to satisfy.

Direct kinematics

The direct kinematics can be expressed as:

$$\mathbf{T}_B^R = \mathbf{T}_6^R \cdot \mathbf{T}_5^6 \cdot \mathbf{T}_4^5 \cdot \mathbf{T}_3^4 \cdot \mathbf{T}_2^3 \cdot \mathbf{T}_1^2 \cdot \mathbf{T}_0^1 \cdot \mathbf{T}_B^0$$

and exploiting the considerations and results of the free-flight kinematics solution:

$$\mathbf{T}_B^R = \mathbf{T}_6^R \cdot \mathbf{T}_5^6 \cdot \mathbf{T}_4^5 \cdot (\mathbf{T}_4^B)^{-1}$$

By defining the values of the angles of the pairs, it is possible to know the position and orientation of the spider's body.

Inverse kinematics

The inverse kinematics problem is more complex because the task is to know the values that must be imposed to the joints in order to bring the body to a wanted position and orientation.
Looking at the overall system and at the DH reference coordinates, it is possible to say that for every leg the distance between the body reference system and the center of gravity of the first revolute joint of every leg is fixed.
By defining the target as:

$$\mathbf{Body} = [\mathbf{B}; \Theta] = [B_x, B_y, B_z, \phi_B, \theta_B, \psi_B]^T$$

the roto-translation matrix between the Reference system and the body can be expressed as:

$$\mathbf{T}_B^R = \left[\begin{array}{ccc|c} c_\phi \cdot c_\theta \cdot c_\psi - s_\phi \cdot s_\psi & c_\phi \cdot c_\theta \cdot s_\psi - s_\phi \cdot c_\psi & c\phi \cdot s_\theta & B_x \\ s_\phi \cdot c_\theta \cdot c\psi + c\phi \cdot s\psi & s_\phi \cdot c_\theta \cdot s_\psi - c_\phi \cdot c_\psi & s_\psi \cdot s_\theta & B_y \\ -s_\theta \cdot c_\psi & s_\theta \cdot s_\psi & c_\theta & B_z \\ \hline 0 & 0 & 0 & 1 \end{array}\right]$$

The rototranslation matrix between the body and the first joint is:

$$\mathbf{T}_0^B = \left[\begin{array}{ccc|c} c_{\theta_0} & -s_{\theta_0} & 0 & X_0 \\ s_{\theta_0} & c_{\theta_0} & 0 & Y_0 \\ 0 & 0 & 1 & 0 \\ \hline 0 & 0 & 0 & 1 \end{array}\right]$$

where θ_0 is directly related to the considered leg (e.g. first leg: $\pm 22.5°$).
The matrix $\mathbf{T}_0^R = \mathbf{T}_B^R \cdot \mathbf{T}_0^B$ is known.
The value of the θ_1 angle is found considering Fig. 68. θ_1 is the rotation that allows to move the reference system 1 on the reference system 0.
The point $\mathbf{P}$ can be expressed in the coordinate system 0 as:

$$\mathbf{P}^0 = (\mathbf{T}_0^R)^{-1} \cdot \mathbf{P} = \mathbf{T}_R^0 \cdot \mathbf{P}$$

and θ_1 can be calculated as in the free flight condition:

$$\theta_1 = atan2(P_y^0, P_x^0)$$

$$\theta_1 = \pi + atan2(P_y^0, P_x^0)$$

The $\mathbf{O}_0 = \mathbf{O}_1$ points, the $\mathbf{Z}_0$ axis and the contact point between the end of the (meta)tarsus link and the surface (i.e. $\mathbf{P} = \mathbf{O}_4 = \mathbf{O}_5 = \mathbf{O}_6 = \mathbf{O}_7$) belong to the same plane π. By exploiting that, the $\mathbf{Z}_4 = \mathbf{Z}_3 = \mathbf{Z}_2 = \mathbf{Z}_1$ axis can be found.
The $\mathbf{Z}_4$ axis is the third column of the rototranslation matrix $\mathbf{T}_1^R$. The spherical joint in $\mathbf{P}$ is a virtual spherical joint that allows to define the rotations that have to be made in order to put the coordinate system 7 on the coordinate system 4. The three unknown angles are the Euler angles (ZYZ) with respect to the coordinate system 4.
In order to move the $\mathbf{Z}_7$ axis to the known $\mathbf{Z}_4$ axis two rotations are required (θ_6 and θ_7).
The spherical joint rototranslation matrix is:

$$\mathbf{T}_7^4 = \mathbf{T}_5^4 \cdot \mathbf{T}_6^5 \cdot \mathbf{T}_7^6 = \left[\begin{array}{ccc|c} c_{\theta_5} \cdot c_{\theta_6} \cdot c_{\theta_7} - s_{\theta_5} \cdot s_{\theta_7} & -c_{\theta_5} \cdot c_{\theta_6} \cdot s_{\theta_7} - s_{\theta_5} \cdot c_{\theta_7} & c_{\theta_5} \cdot s_{\theta_6} & 0 \\ s_{\theta_5} \cdot c_{\theta_6} \cdot c_{\theta_7} + c_{\theta_5} \cdot s_{\theta_7} & -s_{\theta_5} \cdot c_{\theta_6} \cdot s_{\theta_7} + c_{\theta_5} \cdot c_{\theta_7} & s_{\theta_5} \cdot s_{\theta_6} & 0 \\ -s_{\theta_6} \cdot c_{\theta_7} & s_{\theta_6} \cdot s_{\theta_7} & c_{\theta_6} & 0 \\ \hline 0 & 0 & 0 & 1 \end{array}\right]$$

The $\mathbf{Z}_4^7$ axis is:

$$\mathbf{Z}_4^7 = \mathbf{T}_R^7 \cdot \mathbf{Z}_4^R$$

The $\mathbf{T}_4^7$ is equal to the transposed matrix $(\mathbf{T}_7^4)'$ and then the $\mathbf{Z}_4^7$ can be also expressed as:

$$\mathbf{Z}_4^7 = \left[\begin{array}{c} -s_{\theta_6} \cdot c_{\theta_7} \\ s_{\theta_6} \cdot s_{\theta_7} \\ c_{\theta_6} \\ 1 \end{array}\right]$$

By comparing the two expressions for $\mathbf{Z}_4^7$, the angles θ_6 and θ_7 can be found.
The unknown system is now reduced to the four-sided made of the revolute joints defining the angles θ_2, θ_3, θ_4 and θ_5.
All these joints are in the same plane and all the associated reference systems have the same $\mathbf{Z}$ axis. This articulated mechanism has one DOF and admits ∞^1 solutions. This DOF can be used for choosing the best configuration available in order to assure conditions on the overall adhesion of the leg and the system. Hence, being known the points $\mathbf{O}_1$ and $\mathbf{O}_5$, this DOF is used to impose the approaching angle θ_5. Hence, the spherical wrist is defined and the $\mathbf{O}_3$ origin becomes available. The solution of the remaining problem is an inverse kinematics of a dyad, equal to the one solved for the free flight configuration.

6.4 Spider locomotion and gait

Spiders can walk and climb on different terrain types and uneven grounds with their eight legs. In order to understand the spider locomotion efficiently, is necessary to study how each leg is moved, in which direction and which is the stepping pattern. Initially, the movement of each leg and their end point positions with respect to the surface are studied and than the stepping patterns and locomotion are investigated. Legs of different spider species demonstrate similar movements and each pair of legs (L1&R1, L2&R2, L3&R3 and L4&R4; L=left, R=right) have different movements to complete one step. First and fourth leg pairs move in vertical direction (i.e.

extension-retraction), while the second and third pairs of legs have a more complex motion. They move in both vertical and horizontal direction and the latter is dominant. There are also similarities in the movements of these legs as the legs have the same number of limbs and the same number of DOFs. The movements of first and second leg pairs are similar: the legs are lifted, extended in front of the spider, touched down and then flexed to provide the propulsive force. Foelix [60] also agrees on the argument and mentions that first and second pairs of legs are directed forward and pull, whereas third and fourth pairs of legs point backward and push.
When the leg joints make a forward movement the joints of the first two pairs of legs must bend meanwhile the joints of the last leg pairs must stretch. Bending (or flexion) in first leg pair brings the tarsal segments almost under the cephalothorax, according to Ward and Humphreys [66]. Second pair of legs also shows torsion besides bending. This bending movement brings the tarsal segments level with the front of the abdomen. Foelix [60] describes that the third legs are laterally directed, so bending or stretching of their joints hardly contributes to forward movement; however, a torsion of their coxal joints does.
Footprints of the legs tell more about leg movement sequence and walking. The first and second leg pairs seem to touch the substrate only with their tip and the footprints are similar to dots; the third and fourth leg pairs leave long scratch marks, as Foelix quoted from Ehlers [60], that suggests a sliding motion of these feet at the end of the pulling phase. To sum up, contributions of the legs to propulsion are different. The contribution of the first and fourth pairs of legs are dominated by bending and stretching (little contribution of torsion). Second pair legs contribute to the propulsion by both bending and torsion almost equally. The contribution of the third legs is dominated by torsion and there is a little contribution of stretching.
All the studies were carried out on a flat surface in horizontal plane; however lack of information about the vertical climbing patterns and leg movements forced to make the assumptions that walking patterns and leg movements are basically the same in vertical climbing as well. It is very likely that in vertical climbing, the first and second leg pairs are used as hooks and last two pairs of legs are used to create propulsive forces. Plots regarding the movement of legs are shown in Fig. 69 [60]. As Foelix stated, basic stepping pattern of spiders are similar to the patterns of

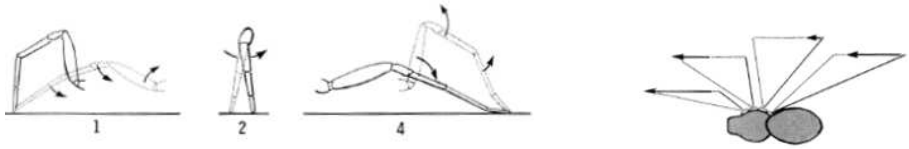

(a) (b)

Figure 69: (a) Contribution of the different legs to the propulsion of the spider. Dotted lines are initial positions of the legs; (b) Working range of the legs of a wolf spider during slow walking (5cm/s), dotted line = propulsion by torsion; vectors=relative contributions to propulsion by bending and stretching [60]

other arthropods, regardless of the number of legs they use.
Mentioned stepping pattern aims to achieve the harmony of diagonal legs. In other words first and third legs on the left move synchronously with second and fourth legs on the right; vice versa for the other four legs in the second half of the step: second and fourth legs on the left move synchronously with first and third legs on the right. Such walking is named *alternating tetrapod*. Basic sketch of the diagonal rhythm is shown in Fig. 70(a). Wilson [64] argued this pattern and stated that

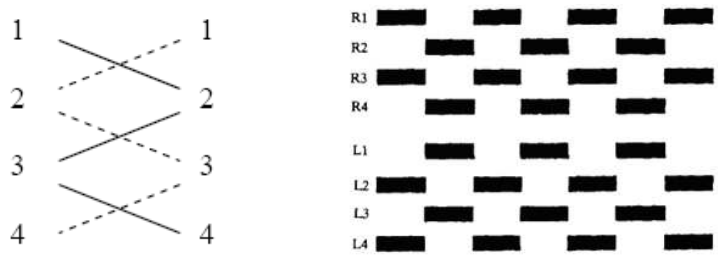

(a) (b)

Figure 70: (a) Walking pattern, solid and dashed lines show legs that move synchronously; (b) Ideal spider stepping pattern

its near variations may be described as that one in which adjacent legs are held in a phase relationship of approximately 180° (or 0.5 in phase-lag) and diagonally opposite legs are held in a phase relationship of approximately 0°. He also argued the presence of other patterns, as in real the legs do not move in perfect synchronism because it would cause a very mechanic way of walking. In other words, all of the legs in L1-R2-L3-R4 (and R1-L2-R3-L4) pattern do not step on the surface perfectly at the same time.
On his studies about tarantulas, he stated that the legs do not necessarily step at exactly the same frequency. Therefore, phase drifts between given legs even during steady locomotion are present; he observed six different types of gait and compared them with his metachronal sequence model. The observed gait types with relative frequencies are in Table 14. As seen from the table, most frequent -most common-

Order	Relative frequency
4-3-2-1	52
4-1-3-2	332
4-2-3-1	157
4-1-2-3	2
3-3-1-2	224
4-2-1-3	31

Table 14: Different stepping orders are shown with relative frequencies in tarantula [64]

stepping orders are 4-1-3-2 and 4-3-1-2. Although other orders have been observed, these two orders are much more common. Typical stepping of metachronal model 4-2-3-1 is rather rare in Wilson's observations but it is also being stated in his metachronal model.
Concentrating on stepping patterns will be the next step of the study on spider locomotion. As mentioned initially, the ideal spider stepping is the perfect harmony of diagonal legs. In such a case, the stepping pattern graph would be as Shultz [59] showed, Fig. 70(b). As the graph shows, ideal stepping pattern achieves a perfect harmony of the legs which would cause a very mechanical way of walking as mentioned. Four legs touch the surface at the same and rise up at the same time. Then, the other four legs touch the surface and walking becomes the continuous flow of the series. However that is not the case of the real life. The phase lags among the legs alter the stepping pattern graph and puts a lot more realistic results.
Phase lag is the generic term that is used to define the time difference between

touch down for specified legs divided by period (period is the time taken for one leg to complete a stepping cycle, from touch down to touch down).
A spider walking speed analysis would also contribute to the current work. Usually, walking speed of a spider on horizontal plane is a few centimeters per second but can be up to 40-50 cm/s depending on the spider size [60]. Vertical speed is generally slower than horizontal speed, the speeds depending on spider size.
It is still not straightforward to argue horizontal and vertical stepping is equally same as the speeds in vertical and horizontal planes differ. The reason why vertical speed is less than horizontal one might be simply caused by the fact that a more accurate control of the adhesion is needed. Indeed the gravity force effect, the changing in the contact surface or the slight sliding down depend on the surfaces and their slope.
Complex phase lag graphs differ for each spider species as expected. Therefore it is not possible to make generalizations that suit every spider species.

6.5 Locomotion of the spider model

The attaching systems and the locomotion patterns of the real spider must be reproduced in a suitable gait in order to allow both the equilibrium control of the system and the correct exploit of the attaching elements.
The control of the adhesion of each leg is directly related to the approaching angle. In order to implement a suitable locomotion strategy, a parametrization of Gao's results [11] is made. The relation between the approaching angle and the legs' adhesion is assumed as in Fig. 71, where different normalized sets of adhesion are defined. In this assumption the maximum adhesion is considered between $25° - 35°$

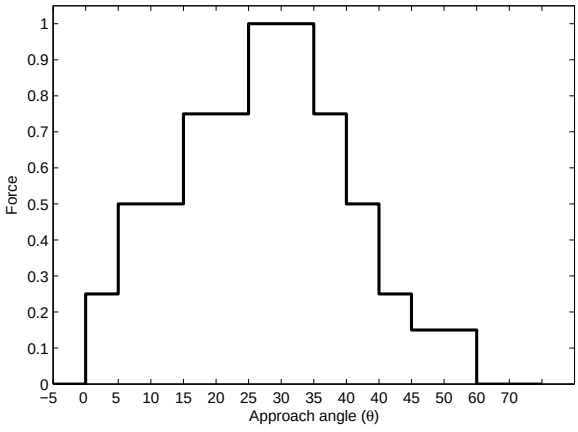

Figure 71: Normalized force of adhesion vs angle: discretized sets.

and for angles bigger than 60° no force is required in order to detach the adhesive elements.
In the implemented model, every leg cooperates with an adhesion factor between 0 and 1 as can be seen in Fig. 71. The sum of the normalized adhesion contributions of all the legs in contact with the substrate is always kept ≥ 2.5. Hence, considering that the safety factor of the spider is 160 in optimal conditions, for a single foot the safety factor is 20 and the implemented rule allows an ideal factor ≥ 50.
Looking at the standard locomotion of the second and third legs' pairs, torsion is

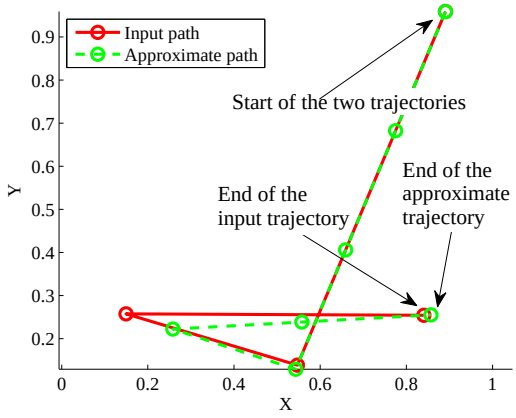

Figure 72: Input trajectory (solid line) and followed trajectory (dashed line).

present and, consequently, considerations about the torsion of the setulae have to be made. In the implemented model, being no experimental data on the relation between torsion and adhesion, the maximum allowable torsion of the (meta)tarsus link with respect to the axis normal to the substrate is upper bounded at 10°. With such a condition the torsion effect on the adhesion is considered irrelevant.

6.5.1 Trajectory definition and discretization

The locomotion is simulated by considering the contact with a flat surface and a constant slope. In such a manner the height of the body system can be kept as fixed and close to the surface, allowing a suitable equilibrium condition of the system.
The ideal trajectory to be followed by the spider-robot is split in *fundamental steps*. The *fundamental step* is the elementary distance that the system can run in a single step and can be suitably chosen with respect to the task to carry out. Hence, the trajectory followed by the spider-robot becomes an approximation of the ideal input trajectory, being the real locomotion path discretized (Fig. 72).

6.5.2 Fundamental step

The stepping gait implemented is the *alternate tetrapod* gait, consisting of four flight legs and four legs in contact with the surface according to an alternate pattern: there are two different conditions switching one to the other at every half-step: the supporting and the motion conditions.
The *fundamental step* is the cycle of actions made by the spider in the time sequence:

- Pattern 1: Support phase;
- Pattern 2: Motion phase (Detaching-Return-Attaching).

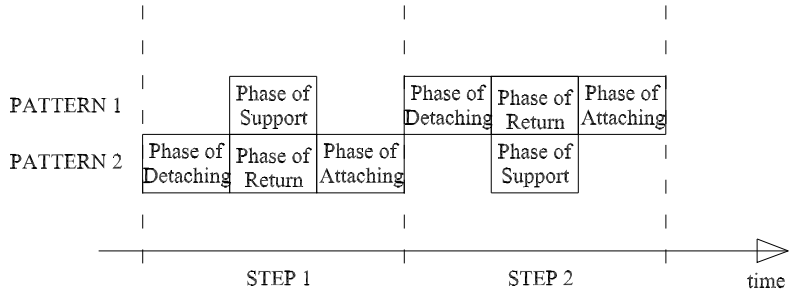

Figure 73: Fundamental step.

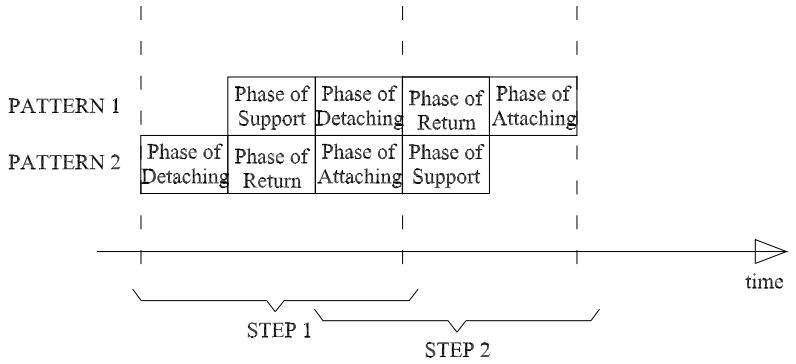

Figure 74: Faster locomotion step.

In Fig. 73 these phases are shown with respect to time. The only phases occurring at the same time are the return phase and the support phase. With such a condition the adhesion force is maximized thanks to the fact that during the step the supporting legs have an approaching angle in the maximum set, corresponding to the maximum force, according to Fig. 71.
Allowing smaller adhesion force, an increase in the maximum velocity of the overall locomotion can be obtained by matching all motion phases with the support phases (Fig. 74). Such a locomotion strategy can be suitably adopted when the slope of the surface is small and a smaller adhesion force is allowed.

By analyzing every phase of the pattern it is possible to better understand the implemented locomotion strategy:

1. Support phase.
   The legs are in the best adhesion condition (approaching angle between 25° and 35°) and support the body during the fundamental translation. The four legs in contact exploit the support phase in different manners:

   - *L1*(fore left leg) or *R1* (fore right leg): the leg moves from an extended to a retracted condition.
     The end point of the leg is considered fixed;

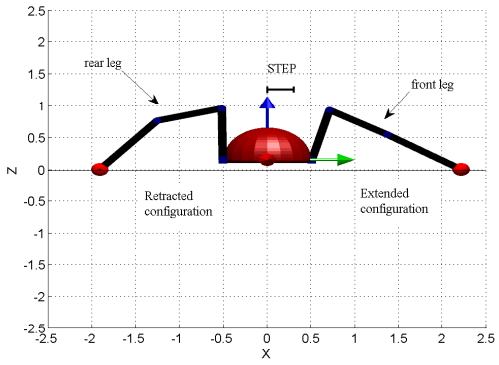

Figure 75: Support phase of the first left and fourth right legs: initial condition.

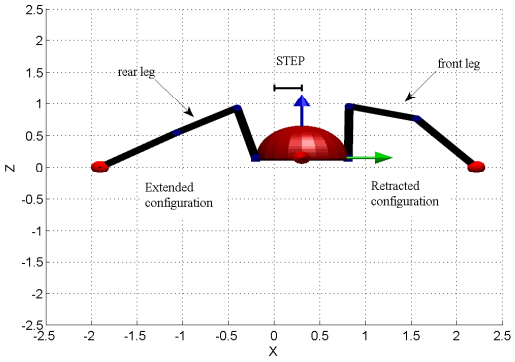

Figure 76: Support phase of the first left and fourth right legs: final condition.

- *L4* (back left leg) or *R4* (back right leg): the leg pushes the body far from the initial position, switching from a retracted condition to an extended one;
- *L3* (lateral back left leg) or *R3* (lateral back right leg): two movements are made. The leg pushes the body switching from a retracted to an extended condition and allows an advancing of the body also with a lateral rowing movement;
- *L2* (lateral front left leg) or *R2* (lateral front right leg): this leg pulls the body switching from an extended to a retracted condition and allows an advancing of the body also with a lateral rowing movement.

In Fig. 75,76 the initial and final posture of a front first leg and a rear fourth leg in the support phase are shown. As described, the two legs swap their positions.

In Fig. 77,78 the initial and final posture of a front second leg and a rear third leg in the support phase are added. As described, the two legs work both with a pushing-pulling action and an oar action.

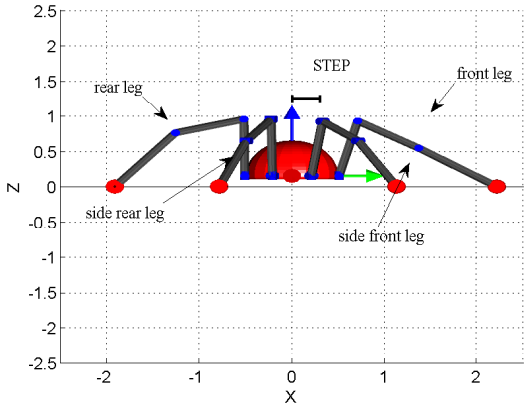

Figure 77: Support phase of all the legs: Initial condition.

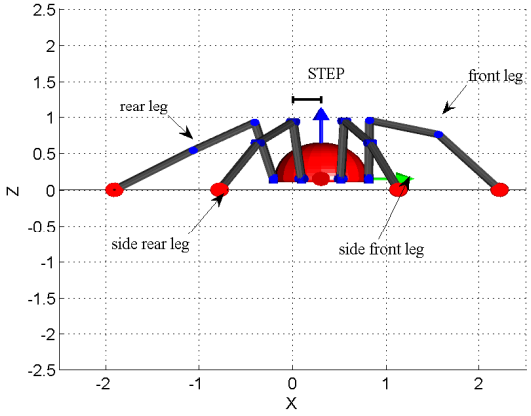

Figure 78: Support phase of all the legs: final condition.

2. Return phase.
   In this phase the legs start from a contact condition but with an angle between the (meta)tarsus and the substrate bigger than 70°. Hence they can be lifted with no efforts. The four legs of the pattern are lifted up from the substrate, retracted near the body, rotated about the first revolute pair of the kinematic chain and finally extended in order to reach the correct position for the subsequent support phase. The next position of each leg is calculated and implemented taking into account the behavior that the leg has to follow and the direction of locomotion. Moreover the next positions are studied in order to allow the inverse kinematic solutions and avoid collisions between the legs.

3. Attaching phase.
   In the starting condition the legs are already in contact with the surface but the approaching angle can be out of the optimal range of adhesion. In this case the system has to maintain the contact and work on the angle between the (meta)tarsus and the surface in order to reach an optimal adhesion. Then, a small proximal movement of 5-10μm in order to adequately activate the attaching elements is implemented.

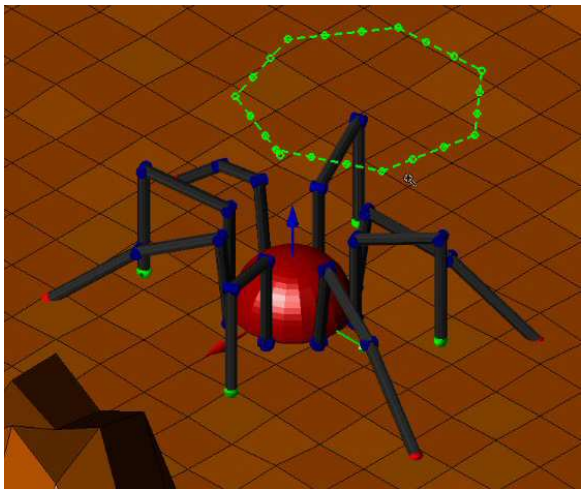

Figure 79: Spider-robot simulator.

4. Detaching phase.
   In this phase the legs start from a contact condition and an approaching angle in the range $20° - 40°$. In order to detach the legs in a correct manner suitable movements must be done, so as to increase the angle up to the detaching threshold.

The spider-robot model, the overall kinematics of the system and the defined locomotion strategy have been implemented in a Matlab simulator. Fig. 79 shows a picture taken during a simulation run.

7 Conclusions

This work studied the spider system in a bio-mimetic perspective.
In particular the mechanisms that allow the spider to climb and overcome most of the existing surfaces and obstacles are evaluated. The attention focused on the spiders' legs in order to search and define both how the spider can climb and walk on different surfaces and how a spider-inspired robotic system can be built in order to assure such abilities.
Taking into account the biological results on the spider system and on the bio-mimesis of the dry adhesion, directives and constraints in order to replicate these natural elements were found. The translation into mechanical and engineering data of the biological studies allowed to define and implement an elastic model of the dry adhesive system. The simulation of the abilities and dimensions of the *E. arcuata* showed that such a spider has a dry adhesive system comparable with the one of the gecko but capable of maintaining a high safety factor in all the scale of roughness thanks to its claws. Moreover, with this simulated model, a first confirmation to the idea that the spider can use the inner pressure of its limbs, in order to easier detach the foot from the surface, has been found.
Once defined the conditions to exploit and activate the attaching systems, the evaluation of the kinematics of the real spider has been done. Then, a new spider-model for a robotic prototype has been developed.
The overall kinematics of the system has been solved starting from the analysis of the simplified leg model. Then, a locomotion strategy inspired by the real pattern of the spider has been studied and evaluated.
The spider-model, the overall kinematics and the locomotion strategy have been implemented in a simulator that confirmed the validity of our choices.

A Appendix

In the following tables are shown the data and the relationships found about the length of the spiders' leg limbs.

Spider type, gender	Species are from Taiwan Dip.Mu.,f	Dip.sp.,f	Ar.Ni.,m	Ar.Ni.,f	Chr.Ful.,m	Chr.Ful.,f	Chr.Tai.,m	The.Xia.,m	Chr.Orc.,m	Chr.Orc.,f	Ach.Iany.,m	Ach.Iany.,f	Ach.Qua.,f	Average
Total length min.	2,74	1,47	1,95	2,21	1,76	2,34	1,97	2,29	2,02	2,48	2,68	5,47	3,16	
Total length max.				4,37	2,05	2,42	2,03		2,53	2,68	3,11	5,51	3,53	
Average				3,29	1,905	2,38	2		2,275	2,58	2,895	5,49	3,345	
Carapace length min.	1,05	0,79	0,79	1,05	0,74	0,87	0,92	1,18	0,98	0,93	1,37	2	1,26	
Carapace length max.				1,21	0,87	1	0,95		1	1,11	1,42	2,16	1,47	
Average				1,13	0,805	0,935	0,935		0,99	1,02	1,395	2,08	1,365	
1st Leg														
Femur	1,05	0,66	1,11	0,92	1,24	1,05	1,58	2,34	2,26	2,84	2,11	3,37	2,16	**1,745**
Patella&tibia	1,21	0,68	1,11	1	1,16	1,11	1,53	2,71	2,47	2,84	2,11	3,21	2,32	**1,805**
Metatarsus	0,87	0,39	0,79	0,66	0,92	0,84	1,34	1,92	2,42	3,16	2,11	3,32	1,84	**1,583**
Tarsus	0,45	0,47	0,5	0,45	0,55	0,55	0,63	0,5	0,79	0,89	0,74	1,11	0,74	**0,644**
Tarsus&Metatarsus	1,32	0,86	1,29	1,11	1,47	1,39	1,97	2,42	3,21	4,05	2,85	4,43	2,58	2,227
2nd patella&tibia	1,05	0,61	0,74	0,76	1,05	0,87	1,03	2,21	2	1,68	1,53	2,26	1,68	**1,344**
3rd patella&tibia	1	0,47	0,45	0,53	0,74	0,82	0,63	1,11	0,84	1	1	1,47	1,21	**0,867**
4th patella&tibia	1,5	0,74	0,63	0,79	0,92	0,95	1,11	1,29	1,32	1,68	1,37	2,74	1,79	**1,295**
Fmr/1st P&T	0,868	0,971	1,000	0,920	1,069	0,946	1,033	0,863	0,915	1,000	1,000	1,050	0,931	**0,967**
Fmr/Mtrs	1,207	1,692	1,405	1,394	1,348	1,250	1,179	1,219	0,934	0,899	1,000	1,015	1,174	**1,209**
Fmr/Trs	2,333	1,404	2,220	2,044	2,255	1,909	2,508	4,680	2,861	3,191	2,851	3,036	2,919	**2,632**
P&T/Mtrs	1,391	1,744	1,405	1,515	1,261	1,321	1,142	1,411	1,021	0,899	1,000	0,967	1,261	**1,257**
P&T/Trs	2,689	1,447	2,220	2,222	2,109	2,018	2,429	5,420	3,127	3,191	2,851	2,892	3,135	**2,750**
Mtrs/Trs	1,933	0,830	1,580	1,467	1,673	1,527	2,127	3,840	3,063	3,551	2,851	2,991	2,486	**2,301**
Fmr/1stT&MT	0,795	0,767	0,860	0,829	0,844	0,755	0,802	0,967	0,704	0,701	0,740	0,761	0,837	**0,797**
1st P&T/2nd P&T	1,152	1,115	1,500	1,316	1,105	1,276	1,485	1,226	1,235	1,690	1,379	1,420	1,381	**1,329**
1st P&T/3rd P&T	1,210	1,447	2,467	1,887	1,568	1,354	2,429	2,441	2,940	2,840	2,110	2,184	1,917	**2,061**
1st P&T/4th P&T	0,807	0,919	1,762	1,266	1,261	1,168	1,378	2,101	1,871	1,690	1,540	1,172	1,296	**1,402**
2nd P&T/3rd P&T	1,050	1,298	1,644	1,434	1,419	1,061	1,635	1,991	2,381	1,680	1,530	1,537	1,388	**1,542**
2nd P&T/4th P&T	0,700	0,824	1,175	0,962	1,141	0,916	0,928	1,713	1,515	1,000	1,117	0,825	0,939	**1,058**
3rd P&T/4th P&T	0,667	0,635	0,714	0,671	0,804	0,863	0,568	0,860	0,636	0,595	0,730	0,536	0,676	**0,689**
Length/Fmr1	2,610	2,227	1,757	2,402	1,419	2,229	1,247	0,979	0,894	0,873	1,270	1,623	1,463	**1,615**
Length/P&T1	2,264	2,162	1,757	2,210	1,517	2,108	1,288	0,845	0,818	0,873	1,270	1,704	1,362	**1,552**
Length/Mtrs1	3,149	3,769	2,468	3,348	1,913	2,786	1,470	1,193	0,835	0,785	1,270	1,648	1,717	**2,027**
Length/Trs1	6,089	3,128	3,900	4,911	3,200	4,255	3,127	4,580	2,557	2,787	3,622	4,928	4,270	**3,950**
	Dipoena mustelina		Argyrodes		Chrosiothes fulvus		Chrosiothes taiwan	Theridion xianfengen	Chrysso orchis, m		Achaearane a		Achaearane a	

Spider type, gender	Neotama corticola male	Neotama corticola female	Prima ansieae, f	Prima syda, f	Murricia uva, f	North America Latrodectus bishopi, f	Latr., Bish, m	Myrmarachne annamita, m	
Total length min.	4,83	6,32	5,25		4,52				
Total length max.	5	7,13	6		5,72				
Average	**4,92**	**6,67**	**5,62**	**4,5**	**5,56**	**8,5**	**4,2**	**4,37**	
Carapace									
length min.	2,16	1,76	1,84		2,08				
length max.	2,33	2,63	2,16		2,18				
Average	**2,25**	**2,28**	**2,06**	**1,88**	**2,13**	**3,4**	**2,1**	**1,87**	
Carapace width	2,02	2,36		1,88	2,22	2,5	1,7	0,89	
Leg Ratio:	1:0,76:0,19:0,67	1:1,1:0,27:0,87	1:1,11:0,34:0,96	1:1,17:0,3:0,9	1:0,45:1,02:0,93				
1st Leg									**Average**
Femur	9,39	6,49	4,73	4,73	3,9	6,9	5,5	1,03	5,334
Patella&tibia	11,82	7,18	5,23	5,25	3,86	6,9	5,9	1,28	5,928
Metatarsus	18,68	8,93	6,54	7,58	2,81	6,8	5,9	0,48	7,215
Tarsus	1,12	0,98	0,81	0,9	0,64	2,3	1,4	0,34	1,061
Total	**37,22**	**21,8**	**16,88**	**17,63**	**13,13**				21,332
MT&T	19,8	9,91	7,35	8,48	3,45	9,1	7,3	0,82	9,798
2nd Leg									0
Femur	7,5	6,01	4,86	5,1	4,01				5,496
Patella&tibia	8,98	6,81	6,12	7	4,14	4,2	3,5		6,61
Metatarsus	10,88	8,09	7,69	7,58	2,81				7,41
Tarsus	0,71	0,98	0,85	0,9	0,6				0,808
Total	**28,58**	**21,07**	**18,79**	**20,58**	**13,35**			**2,33**	20,474
3rd Leg									0
Femur	2,46	2,06	1,66	1,73	1,53				1,888
Patella&tibia	2,44	2,06	1,96	1,73	1,57	2,9	2,2		1,952
Metatarsus	2,1	1,66	1,73	1,43	1,08				1,6
Tarsus	0,6	0,64	0,7	0,45	0,55				0,588
Total	**7,25**	**5,95**	**5,71**	**5,34**	**4,77**			**2,29**	5,804
4th Leg									0
Femur	6,75	5,47	4,69	4,43	3,57				4,982
Patella&tibia	7,25	5,74	3,78	4,88	3,39	5,5	4,4		5,008
Metatarsus	11,07	7,8	5,4	6,83	2,89				6,798
Tarsus	0,75	0,86	0,9	0,83	0,56				0,78
Total	**25,05**	**19,16**	**14,31**	**16,97**	**12,19**			**3,42**	17,536

Ratios									
Leg1									
Fmr/P&T	0,794	0,904	0,904	0,901	1,010	1,000	0,932	0,805	**0,906**
Fmr/Mtrs	0,503	0,727	0,723	0,624	1,388	1,015	0,932	2,146	**1,007**
Fmr/Trs	8,384	6,622	5,840	5,256	6,094	3,000	3,929	3,029	**5,269**
P&T/Mtrs	0,633	0,804	0,800	0,693	1,374	1,015	1,000	2,667	**1,123**
P&T/Trs	10,554	7,327	6,457	5,833	6,031	3,000	4,214	3,765	**5,898**
Mtrs/Trs	16,679	9,112	8,074	8,422	4,391	2,957	4,214	1,412	**6,908**
	0,474	0,655	0,644	0,558	1,130	0,758	0,753	1,256	**0,779**
Leg2									
Fmr/P&T	0,835	0,883	0,794	0,729	0,969				**0,842**
Fmr/Mtrs	0,689	0,743	0,632	0,673	1,427				**0,833**
Fmr/Trs	10,563	6,133	5,718	5,667	6,683				**6,953**
P&T/Mtrs	0,825	0,842	0,796	0,923	1,473				**0,972**
P&T/Trs	12,648	6,949	7,200	7,778	6,900				**8,295**
Mtrs/Trs	15,324	8,255	9,047	8,422	4,683				**9,146**
Leg3									
Fmr/P&T	1,008	1,000	0,847	1,000	0,975				**0,966**
Fmr/Mtrs	1,171	1,241	0,960	1,210	1,417				**1,200**
Fmr/Trs	4,100	3,219	2,371	3,844	2,782				**3,263**
P&T/Mtrs	1,162	1,241	1,133	1,210	1,454				**1,240**
P&T/Trs	4,067	3,219	2,800	3,844	2,855				**3,357**
Mtrs/Trs	15,324	8,255	9,047	8,422	4,683				**9,146**
Leg4									
Fmr/P&T	0,931	0,953	1,241	0,908	1,053				**1,017**
Fmr/Mtrs	0,610	0,701	0,869	0,649	1,235				**0,813**
Fmr/Trs	9,000	6,360	5,211	5,337	6,375				**6,457**
P&T/Mtrs	0,655	0,736	0,700	0,714	1,173				**0,796**
P&T/Trs	9,667	6,674	4,200	5,880	6,054				**6,495**
Mtrs/Trs	14,760	9,070	6,000	8,229	5,161				**8,644**
Ratios									
Length/Leg1	0,132	0,306	0,333	0,255	0,423				**0,290**
Length/Leg2	0,172	0,317	0,299	0,219	0,416				**0,285**
Length/Leg3	0,679	1,121	0,984	0,843	1,166				**0,958**
Length/Leg4	0,196	0,348	0,393	0,265	0,456				**0,332**
Length/Fmr1	0,524	1,028	1,188	0,951	1,426	1,232	0,764	4,243	**1,023**
Length/P&T1	0,416	0,929	1,075	0,857	1,440	1,232	0,712	3,414	**0,943**
Length/Mtrs1	0,263	0,747	0,859	0,594	1,979	1,250	0,712	9,104	**0,888**
Length/Trs1	4,393	6,806	6,938	5,000	8,688	3,696	3,000	12,853	**6,365**

Length/Fmr2	0,656	1,110	1,156	0,882	1,387	**1,038**
Length/P&T2	0,548	0,979	0,918	0,643	1,343	**0,886**
Length/Mtrs2	0,452	0,824	0,731	0,594	1,979	**0,916**
Length/Trs2	6,930	6,806	6,612	5,000	9,267	**6,923**
Length/Fmr3	2,000	3,238	3,386	2,601	3,634	**2,972**
Length/P&T3	2,016	3,238	2,867	2,601	3,541	**2,853**
Length/Mtrs3	2,343	4,018	3,249	3,147	5,148	**3,581**
Length/Trs3	8,200	10,422	8,029	10,000	10,109	**9,352**
Length/Fmr4	0,729	1,219	1,198	1,016	1,557	**1,144**
Length/P&T4	0,679	1,162	1,487	0,922	1,640	**1,178**
Length/Mtrs4	0,444	0,855	1,041	0,659	1,924	**0,985**
Length/Trs4	6,560	7,756	6,244	5,422	9,929	**7,182**

Aver. of all legs	Fmr/P&T	Fmr/Mtrs	Fmr/Trs	P&T/Mtrs	P&T/Trs	Mtrs/Trs	
	0,933	0,963	5,485	1,033	6,011	8,461	

References

[1] J. C. Spagna, D. I. Goldman, P-C. Lin, D. E. Koditschek and R. J. Full, *Distributed mechanical feedback in arthropods and robots simplifies control of rapid running on challenging terrain*, Bioinspir. Biomim., vol. 2, n.1, 2007.

[2] J-N. Huang, *Taxonomic study of Myrmarachne (Araneae: Salticidae) from Taiwan*. Thesis submitted to National Sun Yat-sen University, 2004.

[3] A.B. Kesel, A. Martin and T. Seidl,, *Adhesion measurements on the attachment devices of the jumping spider Evarcha arcuata*, J. Exp. Biol. 206 (2003), pp. 2733–2738.

[4] A. B. Kesel et al., *Getting a grip on spider attachment: an AFM approach to microstructure adhesion in arthropods*, Smart Mater. Struct., 13, 512-518, 2004

[5] G. Huber, S. N. Gorb, R. Spolenak and E. Arzt, *Resolving the nanoscale adhesion of individual gecko spatulae by atomic force microscopy*, Biol. Lett. 1, 2-4, 2005.2.

[6] S. Niederegger, S. Gorb, *Friction and adhesion in the tarsal and metatarsal scopulae of spiders*, Journal of Comp. Physiology 192, 1223-1232, 2006.

[7] *www.calacademy.org/research/entomology/Entomology_Resources/Arachnida/images_atlas/Griswold_139_Feet_5.jpg*

[8] K. Autumn, Y. A. Liang, S. T. Hsieh, W. Zesch, Wai Pang Chan, T. W. Kenny, R. Fearing and R. J. Full, *Adhesive force of a single gecko foot-hair*, Nature 405, 681-685, 8 June 2000.

[9] S. Niederegger, S. Gorb, *Tarsal movements in flies during leg attachment and detachment on a smooth substrate*, Journal of Insect Physiology 49, 611-620, 2003.

[10] M. Sitti and R. S. Fearing, *Synthetic Gecko Foot-Hair Micro/Nano-Structures for Future Wall-Climbing Robots*,Proc. of IEEE International Conference on Robotics and Automation (ICRA '03), 1, 1164- 1170, 14-19 Sept. 2003.

[11] Huajian Gao, Xiang Wang, Haimin Yao, Stanislav Gorb, Eduard Arzt, *Mechanics of hierarchical adhesion structures of geckos*, Mechanics of Materials, 37, 2-3, 275-285, February-March 2005.

[12] K. Autumn, C. Majidi, R. E. Groff, A. Dittmore and R. Fearing, *Effective elastic modulus of isolated gecko setal arrays*, The Journal of Experimental Biology 209, 3558-3568, 2006

[13] R. Ruibal. and V. Ernst, *The structure of the digital setae of lizards*, J. Morph., 117, 271-294, 1965.

[14] K. Autumn and A.M. Peattie, *Mechanisms of Adhesion in Geckos*, INTEGR. COMP. BIOL., 42:1081–1090, 2002.

[15] Arzt, E., Gorb, S. and Spolenak, R., *From micro to nano contacts in biological attachment devices*, Proc. Natl. Acad. Sci. 100, 10603-10606, 2003.

[16] G. Huber, H. Mantz, R. Spolenak, K. Mecke,K. Jacobs, S.N. Gorb and E. Arzt, *Evidence for capillarity contributions to gecko adhesion from single spatula and nanomechanical measurements*, Proc. Natl. Acad. Sci. 102, 16293-16296, 2005(1).

[17] W. R. Hansen and K. Autumn, *Evidence for self-cleaning in gecko setae*, PNAS, 102, 385 - 389, Jan 2005.

[18] P. Bergmann, DJ. Irschick, *Effects of temperature on maximum clinging ability in a diurnal gecko: Evidence for a passive clinging mechanism?*, Journal of Experimental Zoology. 303A:785-791, 2005.

[19] A. Peressadko, S. N. Gorb, *WHEN LESS IS MORE: EXPERIMENTAL EVIDENCE FOR TENACITY ENHANCEMENT BY DIVISION OF CONTACT AREA*, Journal of Adhesion, 80, 4, 247-261(15), April 2004.

[20] Gaurav J. Shah and Metin Sitti, *Modeling and Design of Biomimetic Adhesives Inspired by Gecko Foot-Hairs*, IEEE Proc. of the 2004 IEEE International Conference on Robotics and Biomimetics, Shenyang, China, August 22 - 26, 2004.

[21] B.N.J. Persson, *Biological Adhesion for Locomotion on Rough Surfaces: Basic Principles and A Theorist's View*, MRS bulletin, vol.37, June 2007

[22] N.M. Pugno, *Towards a Spiderman suit: large invisible cables and self-cleaning releasable superadhesive materials*, Journal of Physics:Condensed Matter, 19, 395001, 2007

[23] K. Autumn, M. Sitti, Y.A. Liang, A.M. Peattie, W.R. Hansen, S. Sponberg, T. Kenny, R. Fearing, J.N. Israelachvili and R.J. Full, *Evidence for van der Waals adhesion in gecko setae*, Proc. National Academy of Sciences, 99, 19, 12252-12256, September 17, 2002.

[24] Wanxin Sun, Pavel Neuzil, Tanu Suryadi Kustandi, Sharon Oh and Victor D. Camper, *The Nature of the Gecko Lizard Adhesive Force*, Biophysical Journal: Biophysical Letters 6 June 2005

[25] M. Sitti and R.S. Fearing, *Nanomodeling based fabrication of synthetic gecko foot-hairs*, Proc. IEEE Conf. Nanotechnology, 137-140, August 26-28, 2002.

[26] M. Sitti and R.S. Fearing, *Synthetic gecko foot-hair for micro/nano structures as dry adhesives*, J. Adhesion Sci. Technol. 18, 1055-1074, 2003a.

[27] Betul Yurdumakan, Nachiket R. Raravikar, Pulickel M. Ajayanb and Ali Dhinojwala, *Synthetic gecko foot-hairs from multiwalled carbon nanotubes*, Chem. Commun., 3799–3801, 2005.

[28] Paul Holister, Tim E. Harper, Cristina Román Vas, *NANOTUBES*.

[29] Philip G. Collins and Phaedon Avouris, *Nanotubes Electronics*.

[30] bdml.stanford.edu

[31] H. Lee, B. P. Lee and P. B. Messersmith, *A reversible wet/dry adhesive inspired by mussels and geckos*, Nature, vol.448, 19 July 2007.

[32] C. Menon and C. Lira, *Active articulation for future space applications inspired by the hydraulic system of spiders*, Bioinspiration and Biomimetics., 1, 2006.

[33] C. Menon, M. Murphy, F. Angrilli, and M. Sitti, *WaalBots for Space Applications*,

[34] M. P. Murphy, W. Tso, M. Tanzini, M. Sitti, *Waalbot: An Agile Small-Scale Wall Climbing Robot Utilizing Pressure Sensitive Adhesives*, Proc. of the 2006 IEEE/RSJ Int. Conf. on Intelligent Robots and Systems, Beijing, China, October 9 - 15, 2006

[35] Terence E. Wei, Kathryn A. Daltorio, Stanislav N. Gorb, Lori Southard, Roy E. Ritzmann and Roger D. Quinn, *A Small Climbing Robot with Compliant Ankles and Multiple Attachment Mechanisms*, CLAWAR 2006

[36] Kathry A. Daltorio, Stanislav Gorb, Andrei Peressadko, Andrew D. Horchler, Roy E. Ritzmann, and Roger D. Quinn, *A Robot that Climbs Walls using Micro-structured Polymer Feet*, Proceedings of the 8th International Conference on Climbing and Walking Robots and the Support Technologies for Mobile Machines, pg.131-138, London (UK), 2005.

[37] Kathryn A. Daltorio, Andrew D. Horchler, Stanislav Gorb, Roy E. Ritzmann, and Roger D. Quinn, *A Small Wall-Walking Robot with Compliant, Adhesive Feet*, IEEE/RSJ International Conference on Intelligent Robots and Systems, 2005.

[38] Carlo Menon, Michael Murphy, and Metin Sitti, *Gecko Inspired Surface Climbing Robots*, Robotics and Biomimetics, 2004. ROBIO 2004, 431 - 436, 22-26 Aug. 2004.

[39] G. Caprari, T. Estier, R. Siegwart, *Fascination of Down Scaling : "Alice the Sugar Cube Robot"*, J. of Micro-Mechatronics, VSP, 1, 3, 177-18, 2002.

[40] Ozgur Unver, Ali Uneri, Alper Aydemir, Metin Sitti, *Geckobot: A Gecko Inspired Climbing Robot Using Elastomer Adhesives*, Proc. of Robotics and Automation, ICRA 2006, 2329- 2335, 2006

[41] Ozgur Unver, Michael P. Murphy, Metin Sitti, *Geckobot and Waalbot: Small-Scale Wall Climbing Robots*,

[42] Carlo Menon, Metin Sitti, *Biologically Inspired Adhesion based Surface Climbing Robots*, Proc. of the 2005 IEEE Int. Conf. on Robotics and Automation Barcelona, Spain, April 2005.

[43] Alan T. Asbeck, Sangbae Kim, M.R. Cutkosky, William R. Provancher, Michele Lanzetta, *Scaling hard vertical surfaces with compliant microspine arrays*

[44] Alan T. Asbeck, Sangbae Kim, Arthur McClung, Aaron Parness, and Mark R. Cutkosky, *Climbing Walls with Microspines*

[45] Sangbae Kim, Matthew Spenko, Salomon Trujillo, Barrett Heyneman, Virgilio Mattoli, Mark R. Cutkosky, Whole body adhesion: hierarchical, directional and distributed control of adhesive forces for a climbing robot, 2007 IEEE International Conference on Robotics and Automation, Roma, Italy, 10-14 April 2007.

[46] K. Autumn, A. Dittmore, D. Santos, M. Spenko, and M. Cutkosky, *Frictional adhesion: a new angle on gecko attachment*, J. Exp. Biol., 209(18):3569-3579, 2006.

[47] A. Saunders, D.I. Goldman, R.J. Full, M. Buehler, *The RiSE Climbing Robot: Body and Leg Design*, Proc. of SPIE Vol. 6230, 623017, 2006.

[48] Matthew Spenko, Mark Cutkosky, Carmel Majidi, Ronald Fearing, Richard Groff, Kellar Autumn, *Foot design and integration for bioinspired climbing robots*, Proc. of SPIE Vol. 6230, 623019, 2006.

[49] Krishnan Ramaswami, *PROCESS PLANNING FOR SHAPE DEPOSITION MANUFACTURING*, Ph.D. thesis, Department of Mechanical Engineering, Stanford University, Stanford, California, 1997.

[50] Mark Cutkosky and the SU-RiSE team, *SDM Forms & Materials for Manufacturable Robotics*, Feb 20, 2004.

[51] Sean A. Bailey, Jorge G. Cham, Mark R. Cutkosky and Robert J. Full, *Biomimetic Robotic Mechanisms via Shape Deposition Manufacturing*, Robotics Research: the Ninth International Symposium, John Hollerbach and Dan Koditschek (Eds), Springer-Verlag, London, 2000.

[52] A.K. Geim, S.V. Dubonos, I.V. Grigorieva, K.S. Novoselov, A.A. Zhukov, S.Yu. Shapoval, *Microfabricated adhesive mimicking gecko foot-hair*, Nature Mater. 2, 461–463, 2003.

[53] Ralph Spolenak, Stanislav Gorb and Eduard Arzt, *Adhesion design maps for bio-inspired attachment systems*, Acta Biomaterialia, 1, 5–13, 2005

[54] Tae Wan Kim and Bharat Bhushan, *Adhesion analysis of multi-level hierarchical attachment system contacting with a rough surface*, Journal of Adhesion Science and Technology, 21, 1, 1-20(20), 2006.

[55] B. Bhushan, T.W. Peressadko and A.G. Kim, *Adhesion analysis of two-level hierarchical morphology in natural attachment systems for "smart adhesion"*, Journal of Adhesion Science and Technology, 20, 13, 1475-1491(17), 2006

[56] D. A. Parry, *Spider Leg-muscles and the Autotomy Mechanism*, Quarterly Journal of Microscopical Science, 98, 331-340, 1957.

[57] A.T. Sensenig and J. W. Shultz, *Mechanics of cuticular elastic energy storage in leg joints lacking extensor muscles in arachnids*, The Journal of Experimental Biology, 206, 771-783, 2002.

[58] A.T. Sensenig and J.W. Shultz, *Elastic Energy Storage in the Pedipalpal Joints of Scorpions and Sun-Spiders (Arachnida, Scorpiones, Solifugae)*, The Journal of Arachnology, 32, 1-10, 2004.

[59] J.W. Shultz, *Walking and Surface Film Locomotion in Terrestrial and Semi-Aquatic Spiders*, The Journal of Experimental Biology, 128, 427-444, 1987.

[60] Rainer F. Foelix, *Biology of Spiders*, Oxford University Press. 2 edition, September 1996.

[61] E. F. Fichter and B.L. Fichter, *A Survey of Legs of Insects and Spiders From a Kinematics Perspective*, Proc. of the 1988 IEEE International Conference on Robotics and Automation, vol.2, 984 - 986, 24-29 Apr 1988.

[62] C. H. Ellis, *The Mechanism of Extension in the Legs of Spiders*, Thesis submitted to the Faculty of the Gradute School of California Institute of Technology, 1943.

[63] M. Karner, *Volumenverschiebungen beim Sprung der Jagdspinne Cupiennius salei*, 1999.

[64] D. M. Wilson, *Stepping Patterns in Tarantula Spiders*, Journal of Experimental Biology, 47, 133-151, 1967.

[65] Lorenzo Sciavicco and Bruno Siciliano, *Modelling and Control of Robot Manipulators (Advanced Textbooks in Control and Signal Processing)*, Feb 17, 2001

[66] T.M. Ward and W.F. Humphreys, *Locomotion in burrowing and vagrant wolf spiders*, Journal of Experimental Biology, 47, 133-151, 1980.